UNIVERSITAT POLITÈCNICA DE VALÈNCIA

Tesis Doctoral

Optimización teórico-experimental de sondas de calor para intercambio geotérmico (SGE) según condiciones hidrogeológicas, características geométricas y propiedades de sus materiales

Theoretical and experimental optimization of borehole heat exchangers (BHEs) according to hydraulic and geological conditions, geometric characteristics and material properties

Autor: Borja Badenes Badenes

Directores: Dr. Javier F. Urchueguía Schölzel
Dr. Javier Soriano Olivares

Diciembre 2020

Acknowledgements

I would first like to thank my supervisors, Prof. Dr. Javier F. Urchueguia and Pr. Dr. Javier Soriano, whose experience and support was invaluable in the research methodology and achievement of results. Thank you for your time dedicated to improving my background.

I would also like to thank the external reviewers for their personal time spent on the review of the thesis and for their valuable comments that have improved the quality of the thesis.

I would like to acknowledge my all colleagues from ICT against Climate Change research group, mainly the people who have collaborated with this research, Miguel Á., José M., Bruno, Teresa, Lourdes, but also Edgar, Begoña, Juanan, José V., Lenin, Pep, Vicky, Juanan, David, Pau, David, Jimena, Jorge, Olga, Jimena, Jordi, Eloina, Nereida, Salva.., you guys are great!

In addition, I would like to thank the Department of Hydraulic Engineering and Environment and the Doctoral Program in Water and Environmental Engineering for all their support.

To conclude, I would like to thank my girlfriend Amparo for all the time this Thesis has been taking from her. Parents, sisters and family.., thanks for always being there for me.

This research has received funding from the European Union's Horizon 2020 Research and Innovation program under grant agreement No [657982], [727583] and [792355].

Abstract

One of the biggest challenges for the ground source heat pump market is the high cost associated with drilling geothermal borehole heat exchangers. Achieving more efficient geothermal heat exchangers would reduce this cost, since a shorter exchanger length would be required to obtain the same working temperatures in it (same efficiency of the heat pump).

The thermal efficiency of a geothermal heat exchanger is characterized by its borehole thermal resistance. This borehole thermal resistance depends on a number of parameters, mainly: properties and flow rate of the working fluid that flows through the borehole heat exchanger, diameter of the geothermal borehole, geometry and materials of the heat exchanger pipe and the properties of the borehole grouting material.

The higher thermal resistance of the heat exchanger, the less heat is transferred between the heat carrier fluid and the ground, resulting in an increased requirement for the length of the buried heat exchanger. Consequently, it is essential to reduce this parameter to the minimum possible.

Therefore, the main objective of this Ph. Doctoral Thesis is to carry out, based on a comprehensive analytical model of quantification of the impact of the above mentioned parameters, a detailed study to analyze their combined influence on the thermal resistance of the geothermal borehole, but also exploring this effect in other less researched areas, such as economic costs of running the exchanger and operating it (electricity consumption of the heat pump and associated pumping costs).

Resumen

Uno de los mayores retos para el mercado de bombas de calor geotérmicas es el alto coste asociado a la perforación de los intercambiadores de calor geotérmicos. Conseguir unos intercambiadores de calor geotérmicos más eficientes reduciría dicho coste, ya que sería necesaria una menor longitud de intercambiador para obtener las mismas temperaturas de trabajo en él (misma eficiencia de la bomba de calor).

La eficiencia térmica de un intercambiador de calor geotérmico está caracterizada por su resistencia térmica. Dicha resistencia térmica depende de una serie de elementos entre los que se encuentran: propiedades y caudal del fluido que recorre el intercambiador de calor, diámetro de la perforación geotérmica, geometría y materiales de la tubería del intercambiador de calor y las propiedades del material de relleno de la perforación (grouting).

Cuanto mayor sea la resistencia térmica del intercambiador de calor, menor será el calor transferido entre el fluido caloportador y el terreno, traduciéndose en una necesidad mayor de longitud de intercambiador enterrado. Por lo tanto, es necesario una reducción de este parámetro al mínimo posible.

En consecuencia, el objetivo principal de esta Tesis Doctoral consiste en, a partir de un modelo analítico comprensivo de cuantificación del impacto de los parámetros anteriores, realizar un estudio detallado para analizar su influencia combinada en la resistencia térmica del intercambiador geotérmico, pero también examinando dicho efecto en otros planos, como costes económicos de ejecución del intercambiador y de explotación (consumo eléctrico de la bomba de calor y costes de bombeo asociados).

Resum

Un dels majors reptes per al mercat de bombes de calor geotèrmiques és l'alt cost associat a la perforació dels bescanviadors de calor geotèrmics. Aconseguir uns bescanviadors de calor geotèrmics més eficients reduiria aquest cost, ja que seria necessària una menor longitud de bescanviador per a obtenir les mateixes temperatures de treball en ell (mateixa eficiència de la bomba de calor).

L'eficiència tèrmica d'un bescanviador de calor geotèrmic està caracteritzada per la seva resistència tèrmica. Aquesta resistència tèrmica depèn d'una sèrie d'elements entre els quals es troben: propietats i cabal del fluid que recorre el bescanviador de calor, diàmetre de la perforació geotèrmica, geometria i materials de la canonada del bescanviador de calor i les propietats del material de farciment de la perforació (grouting).

Com més gran sigui la resistència tèrmica del bescanviador de calor, menor serà la calor transferida entre el fluid termòfor i el terreny, traduint-se en una necessitat major de longitud de bescanviador enterrat. Per tant, és necessari una reducció d'aquest paràmetre al mínim possible.

En conseqüència, l'objectiu principal d'aquesta Tesi Doctoral consisteix en, a partir d'un model analític comprensiu de quantificació de l'impacte dels paràmetres anteriors, realitzar un estudi detallat per a analitzar la seva influència combinada en la resistència tèrmica del bescanviador geotèrmic, però també examinant aquest efecte en altres plans, com a costos econòmics d'execució del bescanviador i d'explotació (consum elèctric de la bomba de calor i costos de bombament).

Contents

List of Figures

List of Tables

Chapter 1

Introduction

Recent data from European Heating Industry (EHI) [1] indicates that the EU space heating market represents roughly 105 million installed appliances, supplied at 80% by fossil fuels [2]. Moreover, around 60% of these heat appliances are over 15 years old, demonstrating the low energy efficiency performance of most of the installed heating stock and the urgency to act upon its conscious replacement. And in this critical turnaround, the shallow geothermal market is key to help decarbonize the heating and cooling sector. The current trend from 1 million units in 2010 to 2 million units of shallow geothermal in 2020 is not fast enough to answer this challenge.

Shallow geothermal represents a competitive, clean, local and long-term stable technology to provide heating, cooling, hot water and heat storage for buildings (domestic and tertiary) and commercial low temperature heating and cooling utilisation (process energy for industry and services). Shallow geothermal benefits from the heat stored in the uppermost meters to hundreds of meters on the subsurface – the technology can be applied anywhere in Europe. Shallow geothermal energy is based on the capacity of the underground to keep a constant temperature regardless of external conditions. The principle is quite simple: what the system does is transfer the heat from the building to the ground in summer and transfer the heat from the ground to the building in winter.

Unlike other renewable energies, the geothermal heat pump works at any time of the year and at any time, not depending on outdoor weather conditions or whether it is day or night. The reason for this has already been explained: our heat exchange medium, the ground, maintains a stable and constant temperature below a certain depth.

However, green energies should not be in competition with each other. Another aspect is that ground source heat pump systems (GSHPs) are easily combined and hybridised with other renewable technologies, resulting in an exponential improvement in their benefits, for example, geothermal-solar photovoltaic hybridisation, thanks to which a significant reduction in the electricity bill can be achieved by covering a large part of the heat pump's electricity demand with solar energy. Another example is geothermal-solar thermal hybridisation, which is highly recommended for cases where there is a significant demand for heat (or hot water) throughout the year. And hybrid geothermal-aerothermal systems (areothermal systems are conventional heat pumps that exchange heat with the outside air), which are ideal for systems with unbalanced thermal load. As a surplus, cooling can be efficiently provided by the same equipment with the capability to cover the increasing cooling demand in urban areas. Supplementary by using shallow geothermal technologies, heat can be stored in the underground making it interesting for sector coupling.

Renewable heating and cooling (RHC) sources play a key role in many scenarios for a CO_2-free building sector in the future. However, shallow geothermal energy is still a niche inside the European heating and cooling market covering around 2% of the end-user heating consumption. A significant increase of aerothermal heat pumps can be observed at the European renewable heating market, at which ground source heat pumps, supplied by shallow geothermal energy, participate in a very limited way only. The lower efficiency of aerothermal heat pumps leads to higher peak electricity demand requiring even more investments into electrical grids. In comparison with ground source heat pumps, aerothermal heat pumps have also not the capability of cooling, heat storage and of sector coupling, contributing to the transition to a more flexible electricity market. By raising the share of ground source heat pumps inside the European heat pump market from currently 21% to 50% would lead to an efficiency increase of +10% at an EU level regarding the smart integration of electricity in the heat markets [3].

According to the last report from International Energy Agency (IEA) [4], ground source heat pumps annual sales are of around 400,000 units. More than half of the installations are in the United States, where shipments and installations have more than doubled since 2010, partly owing to a 30% federal

tax credit available during 2008-16 and 2018-21. Sweden and Germany are the two main European markets, with 20,000 to 30,000 sold every year in each country. In fact, Sweden has the highest installation rate per capita globally. Currently, geothermal energy has an installed capacity of about 24,3 GW_{th} for heating and cooling in the European Union [5].

Shallow geothermal development in Europe dates back to more than thirty years, but the market is still at the infancy stage, although its potential is indeed promising. For example, regional source-sink matching studies in Germany[1] and Austria[2] indicate that up to 60% of the residential and low-temperature heating demand can be covered by geothermal energy. In the last years, there has been a resurgence of interest in shallow geothermal, after four years (2008-2012) of only small development in shallow geothermal market development, mainly due to the financial and economic crisis. A substantial number of projects[3] (nearly 1 million units between 2010 and 2019) have been developed throughout Europe, and shallow geothermal energy is on its way to becoming a key player in the European energy market.

In Spain, the market for geothermal heat pumps is still immature[4]. The Spanish geothermal sector is performing unevenly over the last few years. At present, there is no electricity generation by geothermal plants in Spain. However, some business initiatives have shown interest in undertaking this type of project in the short and medium term, mainly in the Canary Islands or the south of Spain, where the geological setting is suitable for the implementation of this kind of technology (see [6] for further details). However, the ongoing development of these projects has been blocked due to the situation of the Spanish electricity sector and the lack of regulations. As for shallow geothermal energy used for cooling and heating by heat pumps coupled to the ground, the first domestic installation was carried out in 2007, 30 years behind other European countries. According to a recent report [6], it is estimated that there is currently an installed power capacity of about 300 MW_{th} in about 8,000 installations. The forecast is that in 2025 it will triple [7]. Cities like Madrid, with 2,000 installations, is the community that leads this expansion, with a growth of 100% every year.

But the current market conditions do not allow this development; many technical and non-technical barriers still need to be removed. A new generation of geothermal technologies is also needed for addressing the challenges of the next decade for the European energy system.

[1] `https://www.egec.org/wp-content/uploads/2019/11/Country-Fiches-DE-final_.pdf`
[2] `https://www.egec.org/wp-content/uploads/2019/11/Country-Fiches-AT.pdf`
[3] See list of main projects at `https://www.geothermalresearch.eu/`
[4] `https://www.egec.org/wp-content/uploads/2019/11/Country-Fiches-ES.pdf`

Among the technical barriers, to identify the most suitable potential improvements, the Roadmap of the RHC-Platform [8] can be followed, where some key performance indicators for shallow geothermal installations were stated:

- *SG1.* An increase of the Seasonal Performance Factor of the Geothermal Heat Pump to values greater than 5.
- *SG2.* A reduction of the thermal borehole resistance to values less than 0.05 $K/(Wm)$.
- *SG3.* A further decrease in energy input and reduced costs for operating the geothermal heat pump system.

Specifically on "SG2" is the main goal of this Ph.D. Thesis, a holistic assessment on the simultaneous impact of different factors on the borehole thermal resistance in order to reduce this value in the most optimal way.

The heat transfer in a geothermal borehole can be summarized in the Figure 1.1, which shows the temperature evolution from the heat carrier fluid to the ground.

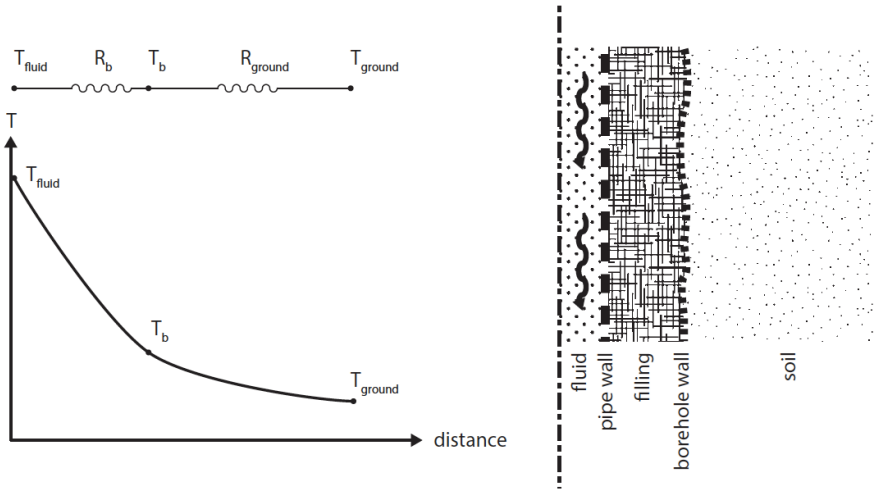

Figure 1.1: Temperature and thermal resistances of borehole heat exchanger [from [9]]

In general terms, the total thermal resistance (R_{tot}) between the water in the pipe and the ground lies in the relation between the heat flow q (W/m) and the

temperature difference between the working fluid inside the pipe of the borehole (T_{fluid}) and the average temperature in the surrounding ground (T_{ground}):

$$R_{tot} = \frac{(T_{fluid} - T_{ground})}{q}, \tag{1.1}$$

When the steady conditions are established, the total thermal resistance can be split up into two terms:

$$R_{tot} = R_{ground} + R_b, \tag{1.2}$$

where R_{ground} is the ground resistance (mainly related to the ground thermal conductivity (λ) and other soil-related factors) and R_b is the – constant – (effective) borehole thermal resistance, given mainly by borehole characteristic parameters (detailed below). Therefore, this approach will focus on the aspects or parameters affecting the specific borehole thermal resistance (R_b).

This borehole thermal resistance should be the lowest possible since, as explained above, it has a direct relationship with the thermal efficiency of the borehole heat exchanger (BHE). Lower borehole thermal efficiency means less heat exchange from the working fluid to the ground. Therefore, increasing borehole thermal efficiency (lower borehole thermal resistance, R_b) decreases the average working fluid temperature in the borehole field under the same conditions. Improving the thermal efficiency of the borehole can either reduce the number of drilling meters required (keeping the thermal efficiency of the heat pump) or improve the average fluid temperature in the borehole field (increasing the thermal efficiency of the heat pump). Thus, the borehole thermal resistance should be reduced to the lowest possible value.

The borehole thermal resistance is mainly influenced by the following key parameters [10, 11]:

- Properties and flow rate of the fluid through the borehole,
- Diameter of the geothermal borehole,
- Geometry and materials of the pipe inside the borehole, and,
- Grouting material.

Several studies have been carried out concerning borehole thermal resistance [12] either employing finite element numerical techniques [13, 14] or based on analytical solutions of the borehole heat transfer process with more or less realistic assumptions [15, 16, 17]. The analytical methods are

easy to implement, but can only be applied on a limited type of geometries and under certain conditions. These works conclude that factors like an increase in thermal conductivity of the pipe material or in the grout material would improve the borehole thermal performance. In [18], theses statements were subsequently validated in several field thermal experiments. Other researchers have investigated the impact of the flow rate of the working fluid on the borehole thermal resistance (revealing a strong decrease with at low flow rates [19]), on the thermo-hydraulic performance of a specific BHE geometry [20] or of a particular installation [21]. Even [22] proposes an analytical solution based on an entropy minimisation technique to calculate the optimal flow rate but this approach does not include the operation of the heat pump. There are parametric studies on parameters affecting the thermal resistance [23, 24] but in these cases the influence of the conductivity of the borehole materials is not taken into account.

As far as different geometries, this research has focused on studying the influence of the different parameters on standard geothermal borehole geometries: Single-U pipe and coaxial heat exchanger. Different geometries have been suggested (Muovitech with rifled pipes for U-loop[5], Geothex coaxial heat exchanger [25], Geokoax heat exchanger[6]) to enhance heat transfer but the scope of this thesis is not to develop new borehole geometries.

Regarding experimental validation using thermal tests (TRT), there is a huge body of literature [26, 27, 28, 29] and although advanced implementation using PID control in the control of energy injection has been developed since 1997 [30], the thermal injection is not controlled at the head of the borehole, as is the case at the geothermal laboratory of the Universitat Politècnica de València.

Despite the background described, no studies have been found on an analysis of global effect of all the above mentioned parameters on the borehole thermal resistance and its reflection in the pumping energy cost. The object of this research is not to develop any new methodology or to develop new innovate models but to carry out an extensive detailed optimisation and sensitivity assessment on the thermal efficiency of a geothermal heat exchanger under different simultaneous conditions, with two main objectives: to obtain the optimum specifications for the development of new advanced products and to analyse the influence of the water flow rate in the borehole heat exchanger, in therms of both thermal efficiency and pumping energy costs. Both the analytical models and the computer applications employed to archive these

[5] https://www.muovitech.com/group/?page=products&id=4251

[6] https://geokoax.com/us/our-products/geokoax-heat-exchanger/

results are well known (and therefore, with proven efficiency). The main objectives of this Ph. D. Thesis are structured as shown in Figure 1.2.

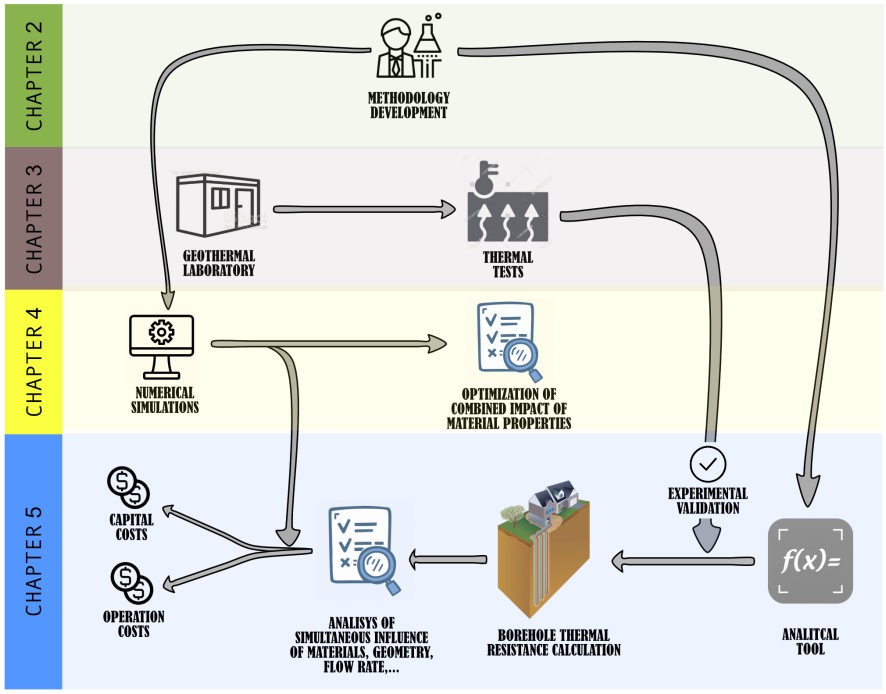

Figure 1.2: Diagram of the structure of the Doctoral Thesis

In the first place, *Chapter 2* provides an introduction to the methodology originally planned to be followed during this research.

In order to validate all the analytical research developed and therefore be able to conclude that the results are consistent and reliable, several experimental thermal tests were designed to be able to compare its results with those obtained by the analytical tool. This is what is collected in *Chapter 3*, where the laboratory for shallow geothermal is described. The laboratory has been designed for Thermal Response Tests purposes, but the final facility is flexible to develop other typologies of experiments. The operation and methodology employed in the thermal tests are detailed, and will be applied for experimental validation of the analytical tool, as will be seen in *Chapter 5*. To conclude the chapter, several examples of the first thermal tests carried out are presented.

Following *Chapter 4* includes the first results of the Doctoral Thesis. Through extensive simulations by numerical software, a sensitivity analysis to highlight

the influence of some of the most critical parameters that affect the overall performance of a GSHP system is carried out. This detailed assessment has allowed guiding the real development of more efficient new advanced materials. At the end of the chapter, the new developed materials and their properties are discussed, including a comparative assessment about their compliance with reference material properties as currently seen in the market.

This first contact allowed to observe the combined influence of the materials that conform a geothermal borehole, but it was required something more robust to assess the influence of all the parameters that by means of the computer program. For this reason, an analytical tool was developed to calculate the borehole thermal resistance and subsequently to carry out a sensitivity study of these input parameters.

And to close the Ph. Doctoral Thesis, *Chapter 5* gathers the main results of this research work. This chapter describes, thanks to the support of the analytical tool, not only the influence on the thermal efficiency of the working fluid borehole, materials and geometry, but also its impact on the energy cost of pumping. In the first subchapter, the study is centered in a Single-U tube borehole configuration, where beyond the study of sensitivity of the impact these parameters on the borehole thermal resistance and the pressure losses, a quantification of the impact of the flow rate on drilling and operation costs in a borehole field of 9 single U-tube in two scenarios (constant length and constant thermal efficiency) is performed. In the other subchapter, the study is focus on a coaxial borehole configuration.

The Doctoral Thesis concludes with *Chapter 6* where the main results obtained are discussed and *Chapter 7* where the conclusions are detailed (both already detailed in previous chapters).

Chapter 2

Optimization methodology of Borehole Heat Exchangers

Through this chapter, the methodology to be followed during the development of this research work is detailed as an initiation to Doctoral Thesis work.

This chapter contains the short article entitled "Optimization methodology of borehole heat exchangers (BHE) according geometric characteristics, material properties and installation and operating cost" presented to "Alternative Energy Sources, Materials & Technologies (AESMT'19) Congress", 3 - 4 June, 2019, Sofia (Bulgaria), and published in Proceedings of short papers, Volume 1, pp.37-38, 2019.

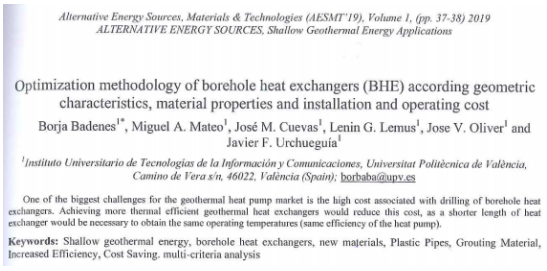

Alternative Energy Sources, Materials & Technologies (AESMT'19), Volume 1, (pp. 37-38) 2019
ALTERNATIVE ENERGY SOURCES, Shallow Geothermal Energy Applications

Optimization methodology of borehole heat exchangers (BHE) according geometric characteristics, material properties and installation and operating cost

Borja Badenes[1*], Miguel A. Mateo[1], José M. Cuevas[1], Lenin G. Lemus[1], Jose V. Oliver[1] and Javier F. Urchueguía[1]

[1]*Instituto Universitario de Tecnologías de la Información y Comunicaciones, Universitat Politècnica de València, Camino de Vera s/n, 46022, València (Spain);* borbaba@upv.es

One of the biggest challenges for the geothermal heat pump market is the high cost associated with drilling of borehole heat exchangers. Achieving more thermal efficient geothermal heat exchangers would reduce this cost, as a shorter length of heat exchanger would be necessary to obtain the same operating temperatures (same efficiency of the heat pump).

Keywords: Shallow geothermal energy, borehole heat exchangers, new materials, Plastic Pipes, Grouting Material, Increased Efficiency, Cost Saving. multi-criteria analysis

2.1 Introduction

The thermal efficiency of a borehole heat exchanger is characterised by its thermal resistance. This parameter originally comes from the works of [10] and [11] where the thermal behaviour of geothermal heat exchangers is modelled on the basis of the following key parameters:

i the conductivity of the ground,

ii the thermal resistance of the borehole heat exchanger,

iii the undisturbed ground temperature and,

iv the injection (or extraction) of heat ratio (thermal power input).

Therefore, the thermal efficiency of a borehole heat exchanger is determined by its thermal resistance. This parameter is modelled from the following key parameters:

- Properties and flow of the fluid through the heat exchanger,
- Diameter of the geothermal borehole,
- Geometry and materials of the heat exchanger pipe, and,
- Grouting material.

The higher the thermal resistance of the heat exchanger, the lower the heat transferred between the heat carrier fluid and the ground, resulting in a greater need for buried heat exchanger length. This parameter should consequently be optimised as minimally as possible. The article describes, within the framework of this project, the work carried out in order to obtain the optimal design characteristics of the materials that conform the geothermal exchangers (pipes, grouting) from a detailed analysis that obtains the optimal values of the different parameters that minimize the value of the thermal resistance. This study has been conducted from analytical expressions and tools that model the thermal resistance of the heat exchanger, several scenarios have been simulated in order to unravel the best possible configurations in terms of performance of the installations. The effect of the combination of the different enhancements project is evaluated here by means of sensitivity analysis of the main properties of the materials.

The results have been compared with the current state of the art to calculate the impact in economic terms and evaluate the benefits associated to the expected enhancements. In the tested scenarios, it was possible to corroborate that the enhancement of the thermal conductivity of the pipelines and the grouting products in combination may trigger important reduction of the total

BHE length required for a certain installation. Those savings could achieve values up to 22% of the total installation costs. Moreover, the results have demonstrated that the optimal combination of thermal conductivity for pipes and grouting not always should be the highest possible value but should be in concordance with the thermal characteristics of the ground. In this way, it has been demonstrated that the thermal properties of the grouting products should be adapted to the ground conditions (geological setting) of the place where the geothermal installation will be located. The obtained results will then be confronted with experimental thermal tests to validate the thermal efficiency of the borehole with the new developed products and configurations through the development of a state-of-the-art geothermal laboratory that provides controlled and detailed heat injection, gathering in detail the variables involved in the heat exchange process of the borehole heat exchanger.

2.2 Background

Based on the thermal transfer model in a geothermal borehole exchanger [10], there are numerous publications on the resistance of a geothermal borehole. Some studies have used finite element numerical techniques, but rigorous, they have also proven cumbersome to use. Others have proposed analytical solutions [15, 16] that are easily applied but can only be applied to a limited type of pipe geometries, under certain conditions. These studies showed that increased thermal conductivity of grouting and the placement of piping close to the wall of the geothermal borehole improve the thermal performance, and [18] subsequently demonstrated this fact in experimental field thermal tests. A finite element model has also been published for the case of a two-loop (double U) probe in a geothermal borehole [31], following the work of [32]. Finally, there is also a comparative study of helicoidal and triple U probes in foundation piles [33]. In spite of the described antecedents, no studies have been found that analyse in a global way the impact of each one of the parameters that influence in the final result of the thermal resistance of the geothermal heat exchanger including an analysis that also considers economic restrictions and costs, both in execution (CAPEX) and exploitation (OPEX).

2.3 Methodology

Based on the different analytical expressions that model the thermal resistance of the geothermal heat exchanger, an analysis will be carried out in order to obtain the optimum values of the different parameters. To this end, analytical models will be compiled describing the influence of the factors on the thermal transfer of the heat exchanger with the ground, obtaining the relationship of the thermal resistance and, therefore, of its thermal efficiency. With all these

expressions, the different criteria to be considered will be defined (maximising the thermal efficiency of the exchanger (i.e. minimising the thermal resistance value of the exchanger) and minimising the total cost associated with the exchanger).

In the case of the total costs associated with the geothermal heat exchanger, the installation costs of the borehole will be analysed (drilling, geothermal probe, grouting, ..) and the operating costs (the electricity consumption of the heat pump during its operating time and the electricity consumption of the circulation pump necessary to overcome hydraulic losses, which will require a hydraulic study of the installation).

On the other hand, experimental thermal tests will also be carried out to validate the conclusions obtained from the analytical study described above. In order to achieve this objective, a series of thermal tests (called Thermal Response Test, or TRT) will be carried out with a constant and controlled thermal power injection that will allow the thermal transfer in the borehole to be evaluated and, therefore, the main thermal characteristics of the heat exchanger to be extracted, thus enabling its thermal behaviour to be evaluated (for example, the thermal study evaluated at a foundation pile used as a borehole heat exchanger [34]).

The methodology to be used in these tests is described in [35] and highlights the importance of thermal heat injection control (by means of a PID) and evaluating it at the borehole, since in this way more precise results are obtained than in the traditional methodology, where no control of thermal injection is carried out, limiting itself to the generation of a constant heat pulse that does not take into account, for example, the thermal losses of the pipes or the thermal influence of the external temperature.

Therefore, verification of analytical optimisation results by means of experimental thermal tests will allow firm, coherent and robust conclusions to be drawn.

2.4 Conclusions

The obtained results will then be confronted with experimental thermal tests to validate the thermal efficiency of the borehole with the new developed products and configurations through the development of a state-of-the-art geothermal laboratory that provides controlled and detailed heat injection, gathering in detail the variables involved in the heat exchanger.

Chapter 3

Assessing of Shallow Geothermal Laboratory

After the theoretical analysis of the previous chapter, this chapter describes the innovative laboratory for shallow geothermal research built at the Universitat Politècnica de València (Spain). The laboratory has been designed for Thermal Response Tests purposes, but the final facility is flexible to develop other typologies of experiments. The operation and methodology employed in the thermal tests are detailed, and will be applied for experimental validation of the analytical tool, as will be seen in the next chapter. Finally, several examples of the first thermal tests carried out are presented.

This chapter contains the article entitled "Assessing the Shallow Geothermal Laboratory at Universitat Politècnica de València" presented to "European Geothermal Congress 2019", Den Haag (The Netherlands), 11-14 June 2019 and published in Proceedings of the European Geothermal Congress 2019, article 343, 4.H. Science – Exploration (S-EX) Section. ISBN code 978-2-9601946-1-6.

http://europeangeothermalcongress.eu/wp-content/uploads/2019/07/343.pdf

3.1 Introduction

Thermal Response Test (TRT) was designed as a tool for investigate the ground parameters before a full design of air-conditioning systems based on ground source heat pump (GSHP) [36, 37]. Although its wide use, the improvement of TRT evaluation techniques is still an active area of research. Our research group in the Universitat Politècnica de València (UPV) have a wide and long expertise on this area [38, 39, 35].

As a partner of the European Union's Horizon 2020 project "Cheap and Efficient Application of Reliable Ground Source Heat Exchangers and Pumps (Cheaps-GSHPs)", one of tasks of our research group has been the design, construction and exploitation of an installation able to evaluate the developed technologies. This installation will serve as a demo site for results and technology dissemination. In fact, there is a total of six demo sites in Cheaps-GSHPn project:

i the UPV test site at Valencia (Spain),

ii a test site at Erlangen-Eltersdorf (Germany),

iii a residential home at Putte (Belgium),

iv an office building at Pikermi (Greece),

v an office building at Dublin (Ireland) and

vi the Nikola Tesla Technical Museum at Zagreb (Croatia).

The Valencia and Erlangen sites are experimental test laboratories, while the other ones are demonstrators of geothermal technologies by means of monitored air-conditioning systems. The Nicola Tesla Technical Museum site have been designed with special attention to improve the visibility of geothermal green energy use, because both the number of visitors and the popularity of the museum.

The UPV test site has been designed as a shallow geothermal research facility, but also for use in popularizing geothermal energy, educational purposes and training specialists. For this reason, the final installation was performed to make the more visible possible all components, arranging them in a wall of the room to easier the explanation of their function (Figure 3.1).

Figure 3.1: General view of the test site room

The geothermal laboratory at UPV allows a very precise comparative study of the thermal performance between different boreholes heat exchangers (BHEs), as well very detailed studies of the thermal behaviour of BHE in different operation modes (heating and cooling). A special operation mode is added to allow the simulation of any thermal load of a building (thermal profiles). For this purpose, an air source heat pump operates as heating and cooling source under controlled conditions.

3.2 Material and methods

3.2.1 Site environment

The geographical location of the test site is at 39º 29' north and 0º 20' west, inside the campus of the Universitat Politècnica de València at the city of Valencia, in the Spanish mediterranean coast. The geology of the site is an estuarine-deltaic sedimentary environment related to the river Turia and other minor ravines. It is not expected to find a real "bedrock" at least in the first 150-200 meters; therefore, the stratigraphy can be assumed as mainly composed of fine unconsolidated deposits from ground level to 100 meters of depth.

Figure 3.2 presents the vertical section of the ground with the description of the different layers. These descriptions are based on the samples obtained while drilling the boreholes. Figure 3.3 shows the results of the analysis of these samples, detailing the geological and geothermal properties. Groundwater table is observed at shallow depth, around 2 m.

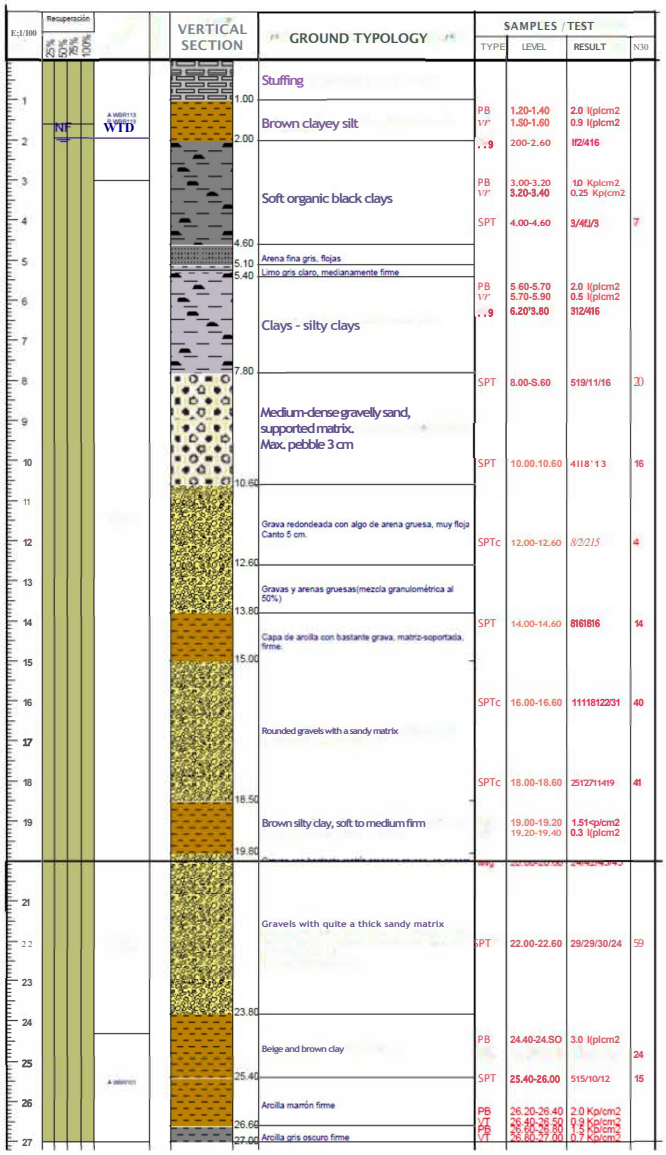

Figure 3.2: Litholigical column and layers

Deep	Lithology	Geotechnical properties	Thermal properties
0 – 1,00	**Stuffing**	ρ ap 1,80 t/m³ C' = 0 kPa φ= 28°	--
1,00 – 2,00 N.F. ▽	**Brown clayey silt** dried	ρ ap natural 2,0 t/m³ ρ ap dried 1,70 t/m³ Cohesion: C' = 1 kPa Internal friction angle: φ= 26° Simple compression: q_u = 60 kPa Non-drainage shear strength: c_u = 30 kPa Elastic modulus E = 5000 kPa Poisson's coefficient ν = 0,30 Permeability: K = 10^{-5} m/s Bearing resistance q_b – Shaft resistance: τ_b = 25 kPa	**λ = 0,59 – 1,86 (1,60) W/m·K** **Cv = 1,27 – 2,97 (2,42) MJ/(m³·K)** **Dif. = 0,46 – 0,82 (0,65) mm²/s**
2,00 – 7,80	**Clays – silty clays** saturated	ρ ap natural 1,90 t/m³ ρ ap dried 1,50 t/m³ C' = 5 kPa φ= 26° q_u = 40 kPa c_u = 20 kPa E = 3000 kPa ν = 0,30 K = 10^{-5} m/s q_b – τ_b = 15 kPa	**λ = 0,55 – 1,86 (1,43) W/m·K** **Cv = 0,64 – 3,34 (2,30) MJ/(m³·K)** **Dif. = 0,45 – 0,82 (0,63) mm²/s**
7,80 – 26,0	**Gravel and sand** (sandstone, variable matrix)	ρ ap natural 2,20 t/m³ ρ ap dried 2,00 t/m³ Cohesion: 0 - 20 kPa (depending on the matrix) φ= 35° q_u = 100 kPa c_u = 30 - 50 kPa E = 50.000 – 100.000 kPa ν = 0,25 - 0,30 K = 10^{-4} m/s q_b : 5500 kPa τ_b = 75 kPa	**λ = 0,44 – 2,94 (1,29) W/m·K** **Cv = 0,92 – 2,15 (1,59) MJ/(m³·K)** **Dif. = 0,21 – 1,91 (0,84) mm²/s**
Levels 13,80 – 15,00 18,50 – 19,80 23,80 – 26,60	**Silty clays** firm consistency	ρ ap natural 1,90 t/m³ ρ ap dried1,65 t/m³ Cohesion: C' = 28 kPa φ= 26° q_u: 60 kPa c_u = 20 – 30 kPa E = 5000 kPa ν = 0,30 K = 10^{-5} m/s q_b : 450 kPa τ_b = 20 - 35 kPa	**λ = 0,68 – 2,35 (1,77) W/m·K** **Cv = 1,37 – 3,50 (2,37) MJ/(m³·K)** **Dif. = 0,46 – 1,14 (0,75) mm²/s**

Figure 3.3: Geotechnical and thermal properties

3.2.2 BHEs description

The geothermal elements of our test site are three different typologies of boreholes: helicoidal BHE (helix), coaxial BHE and single-U BHE. The last one is used as a reference of the conventional technology.

The installed BHEs are separated 6m from each one. The pipe path from the control cabin to each BHE was designed with the same length in order to balance hydraulic losses (Figure 3.4).

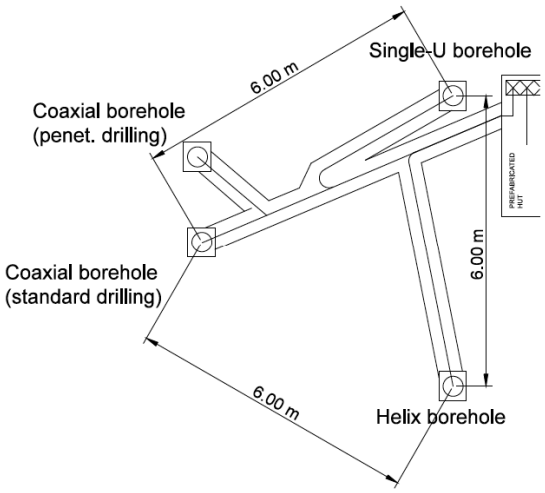

Figure 3.4: Connection layout

The installed probe in the single-U BHE is the RAUGEO PE-Xa from REHAU (see Figure 3.5). The cross-linked polyethylene (PE-Xa) type probe is a continuous pipe. The 'U' bend at the probe is achieved by innovative bending technology with no joint, and a glass fibre reinforced polyester resin protects it.

Figure 3.5: RAUGEO PE-Xa single-U tube

The main reason for the choice of this area is due to valuable information on the geotechnical and geological characteristics of the ground available from other projects at that location [40] or nearby [41]. That information was very useful during the drilling planning of the geothermal heat exchangers. The main geometric characteristics of the single-U tube BHE are:

- External diameter of the pipe: 32 mm
- Internal diameter of the pipe: 26.2 mm
- Drilling depth: 15m
- BHE effective depth: 14.6 m

The Helix or helicoidal heat exchanger is a technology improved within the project. These systems with spiral piping have considerable advantages both from a technical and economical point of view; in fact, for an equal heat exchange surface, they can be installed at depths of a few tens of meters, meaning lower depth than the classical U-tubes. The installed probe is the REHAU Helix PE-Xa. The main geometric characteristics of the helix BHE are:

- External diameter of the pipe: 25 mm
- Internal diameter of the pipe: 20.4 mm
- Drilling depth: 10 m
- Drilling diameter (casing): 450 mm
- BHE effective depth: 9.4 m
- Helix diameter: 360 mm
- Pitch helix: 63 cm

The coaxial BHE were installed using rotopercussion drilling. It is composed of an external stainless-steel case and an internal plastic pipe. Its main geometric characteristics of the coaxial BHE are:

- Int. diameter external pipe: 68.1 mm
- Ext. diameter internal pipe: 40 mm
- Drilling depth: 15 m
- Drilling diameter: 126 mm
- Effective borehole depth: 14.2 m

The grouting used for single-u and coaxial BHE was the high thermal conductivity grouting EnerGrout HD 2.1. For the helix BHE, silica sand was used for grouting.

3.2.3 Demo Site Layout and Specification

Figure 3.6 (at the end of the chapter) shows the hydraulic system and components of the test site. The different sensors and actuators are shown in the same figure as well.

To better explain the sensors, they have been divided into seven subsystems. Table 3.1 describes these subsystems, the signal names and the description of the physical magnitudes that each sensor measures.

Table 3.1: Subsystems and names of signals to measure

Subsystem	Signal names	Description
3-way valve	3V1 3V2 3V3 3V4	The three input temperatures to the 3-way valve and the internal temperature of the storage tank.
Borehole *n*	BHE*n*.1 BHE*n*.2 BHE*n*.3 BHE*n*.4	*n* can be 1, 2, 3 or 4 depending on the borehole. BHE*n*.2 and BHE*n*.3 are the inlet and outlet temperatures. for the borehole BHE*n*.1 and BHE*n*.4 are the manifolds temperatures.
Main pipes	FLOW.1	Flow in the collector pipe. The sensor is installed after the circulating pump.
Main pipes	PRES.1	Pressure in the system. The sensor is installed in inlet collector.
Heat pump	T_HP.1 T_HP.2	Temperatures in inlet (T_HP.1) and return (T_HP.2) of hydraulic circuit between Heat Pump and storage tank
Ambient	T_AMB.1	External temperature
Soil	T_GR.1	Ground temperature. This sensor was buried equidistant to boreholes 1, 2 and 3 at a 100 cm deep.

In addition to the sensors, there are the following actuators to control the system:

1. Heat Pump. A heating and cooling air-water heat pump that will be used to generate the power used in the TRT experiments.

2. Auxiliary Resistance. There is an auxiliary heating resistance inside the tank. This resistance is 1.8kW and allows performing TRT with heat injection without the need to use the heat pump.
3. K-Flows. There is one K-Flow valve for each of the BHE (4 in the current configuration). Each k-flow valve has an associated control signal. In this way, the BHE selection can be done remotely. Experiments on several BHEs could be performed by activating more than one of these valves. They also work to balance the flow through each pipe.
4. Circulating Pump. A Modbus interface connects the integrated controller of the circulating pump to PLC. Multiple operating parameters can be read and written using this interface. This allows the flow rate to be regulated.
5. 3-way valve. The 3-way valve includes an opening/closing motor and a position control system. The "close" position is the one that makes that the output is not connected at with the energy tank. The "open" position is when all the output comes from the tank.

A Siemens S7-1200 PLC is being used to implement the control algorithms, the user interface and the data acquisition and logging. The PLC implements specific control algorithm for the 3-way valve, the circulating pump and the auxiliary resistance. The test site operating modes are:

1. STOPPED. The water pump is off and the 3-way valve is closed.
2. RECIRCULATING CLOSED. The water pump is ON, with a PID controlling the flow, and the valve is in closed position.
3. RECIRCULATING OPEN. The circulating pump is ON, with a PID controlling the flow, and the valve is in open position.
4. HEAT INJECTION. The water pump and the 3-way valve are controlled. The reference is thermal injection constant. The main objective is to control the 3-way valve in order to maintain constant the temperature jump in BHE head with inlet borehole temperature higher than outlet temperature.
5. HEAT EXTRACTION. The water pump and the 3-way valve are controlled. The reference is thermal extraction constant. The main objective is to control the 3-way valve in order to maintain the temperature jump in BHE head constant with inlet borehole temperature lower than outlet temperature.

6. THERMAL PROFILE (Heating mode). A version of (5) with parameters for power and flow taken from a table describing the 24-hour profile of a building.
7. THERMAL PROFILE (Cooling mode). A version of (4) with parameters for power and flow taken from a table describing the 24-hour profile of a building.

A complex control algorithm is responsible for constant thermal power injection at the head of BHE by controlling the 3-way valve position (see Figure 3.7). The main difficulties solved in the design of this control have been the great delay of the system (due to the distance from the 3-way valve to the head of the borehole) and the non-linearity issues that the 3-way valve causes.

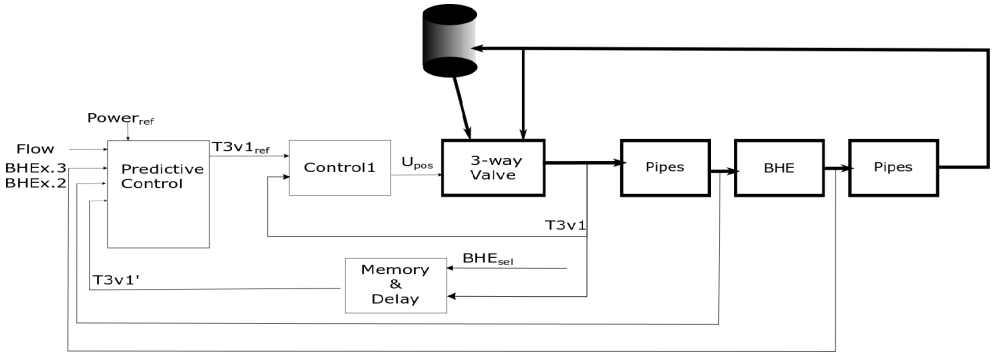

Figure 3.7: Control system blocks

3.2.4 Experiment setup

This section presents the results of Thermal Response Tests carried out with constant and controlled thermal power injection at each of the borehole heat exchangers.

The main purpose of any TRT is to perform an analysis of the obtained data in order to derive the main parameters that characterized the ground (ground thermal conductivity or λ and the undisturbed underground temperature or T_0) and the borehole thermal resistance (or R_b) [42]. These parameters are necessary when designing a shallow geothermal installation in order to properly size the length of buried heat exchanger.

The data obtained from these tests has been analysed with three different BHE analytical models: Infinite Line Source Model (ILSM), Cylindrical Source

Model (CSM) and Finite Line Source Model (FLSM). For these analysis the methodology used is described in [35].

In order to compare the results from different BHEs, the parameters of the TRT were fixed with the values presented in Table 3.2. The Reynolds values were selected to ensure turbulent flow (indeed this is transitional regime but due to the elements of the installation (elbows, valves, borehole foot, ..) forced turbulent flow can be ensured) but low enough to minimize pressure losses.

Table 3.2: Parameters used to perform all TRT

Parameter	Value
Injected heat rate	80 W/m
Reynolds	≈ 2300
Duration of TRT	5 days
Logging interval	180s

Therefore, according to these guidelines, the parameters of each of the tests performed are presented in Table 3.3. In this table, ΔT represents the calculated temperature jump in BHE head.

Table 3.3: TRT parameters for each borehole

	Single-U	Helix	Coaxial
Depth (m)	14.6	9.4	14.6
Heat Ratio (W/m)	80	80	80
Heat injected (W)	1168	752	1136
Flow rate (l/h)	187	146	680
Reynolds	2294	2391	2022
$\boldsymbol{\Delta T(C)}$	5.4	4.4	1.4

3.3 Results

The measured typical parameters during a TRT are the fluid flow rate and the temperatures in the inlet and outlet of the borehole (T_{in} and T_{out}). In some cases, the ambient temperature is also monitored in order to detect malfunctions or thermal interference.

Although our system monitors more variables, this example focuses on the evaluation and comparison of the three boreholes as if a standard TRT has been used.

Figure 3.8 shows the results of the TRT on the single-u BHE. The thermal power injected (yellow line in the figure) was calculated using the measures from the flow sensor and the two temperatures sensors located in the head of the borehole. The values are raw data, no filtered. The error between the set point (see Table 3.3) and the measured value is always inside a 5-10% tolerance and it seems not related to ambient temperature, which is a common problem during a standard TRT. Figure 3.9 and Figure 3.10 show the data plots for the TRTs performed on coaxial and helicoidal BHEs.

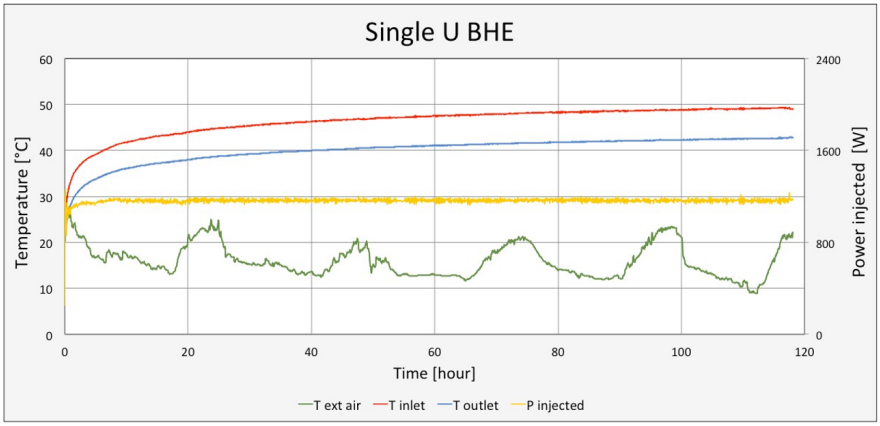

Figure 3.8: TRT measurements of the Single U BHE

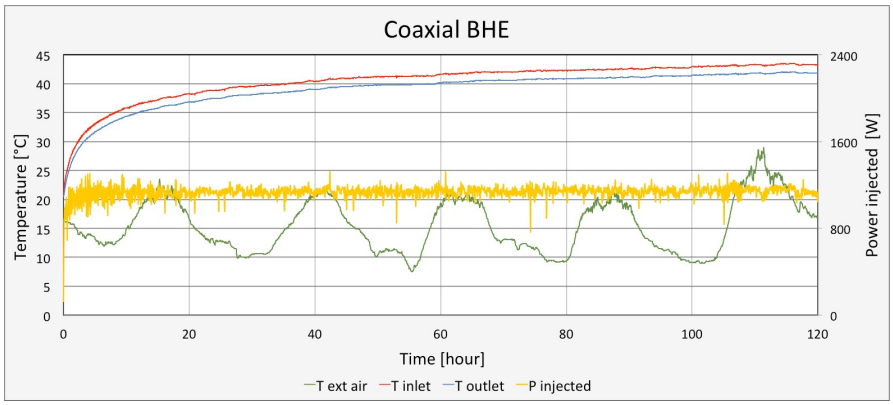

Figure 3.9: TRT measurements of the Coaxial BHE

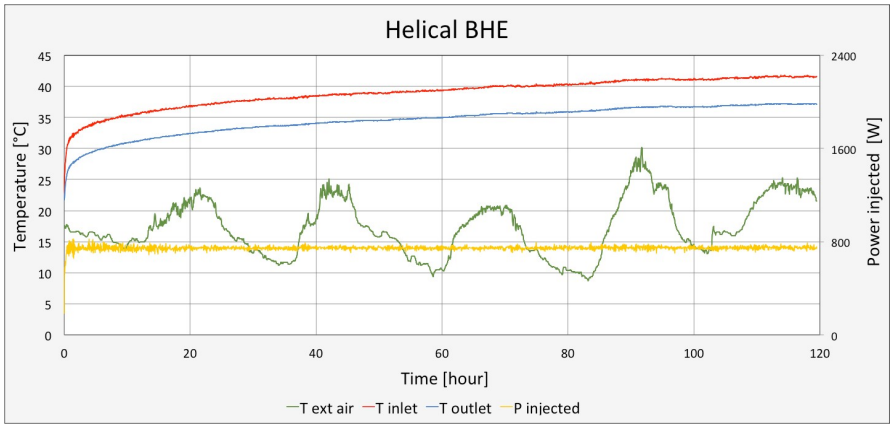

Figure 3.10: TRT measurements of the Helicoidal BHE

In these figures, it can be seen that in the TRT experiments with thermal power injection the typical influence of ambient temperature is not observed.

From these data, the mean temperature of the BHE is defined by Equation 3.1. Figure 3.11 shows the T_m for each BHE for the five days of the test.

$$T_m = \frac{(T_{in} + T_{out})}{2} \tag{3.1}$$

With the values of T_m, time and flow, there are different models that can be used to determine the thermal characteristics of the ground and the borehole.

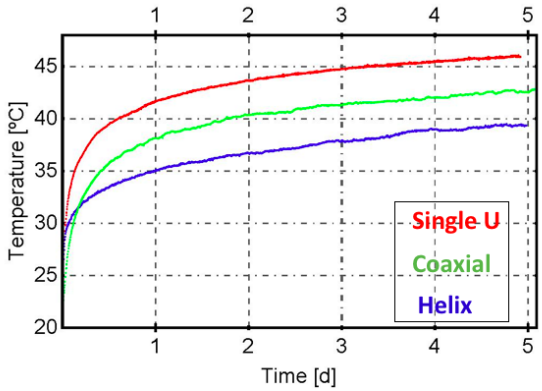

Figure 3.11: T_m evolution in each type of BHE

The main parameters to be identified by the models are λ and R_b. Other parameters, such as undisturbed underground temperature (T_0) and soil thermal diffusivity (α), are estimated. The ground thermal diffusivity is the thermal conductivity divided by density and specific heat capacity at constant pressure, and it represents the ability of the ground to conduct thermal energy in relation to its ability to store thermal energy. For example, a value of $6 \times 10^{-7}\,\mathrm{m^2\,s^{-1}}$ for the thermal diffusivity and, for T_0, the average temperature in the borehole obtained during a test without thermal injection and without thermal effect from the circulation pump.

Using a modified version of the analytical methods discussed in [42], the borehole thermal resistance fixing the other parameters of the model is calculated, including ground thermal conductivity.

As the three BHE been studied are installed in the same location, the surrounding soil can reasonably be expected to have similar characteristics. Taking this into account, a study was performed about how the soil thermal conductivity influences the calculated borehole resistance using three analytical models. The ground thermal conductivity values were from 1.5 to 3 W/mK. These values comes from of our knowledge of the geology of the UPV test site and from previous experiments [35].

Figures 3.12, 3.13 and 3.14 show the results of this study according to the main models (Infinite Line Source Model -ILS-, Finite Line Source Model -FLS- and Finite Cylindric Source Model -CLS-). The R_b obtained in the nine plots are around 0.1 – 0.2 mK/W, which are values inside the expected range.

The coaxial BHE gets the minimum value and the single-U tube BHE is the one with higher values.

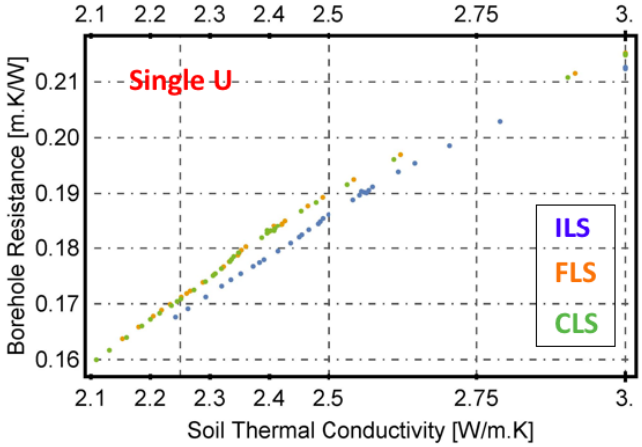

Figure 3.12: R_b model parameter identification for single-U

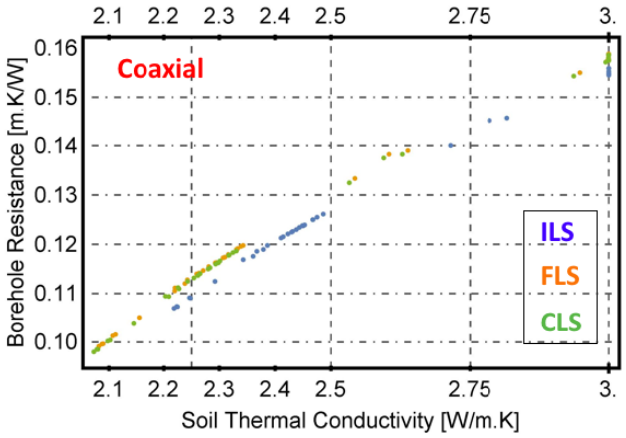

Figure 3.13: R_b model parameter identification for Coaxial BHE

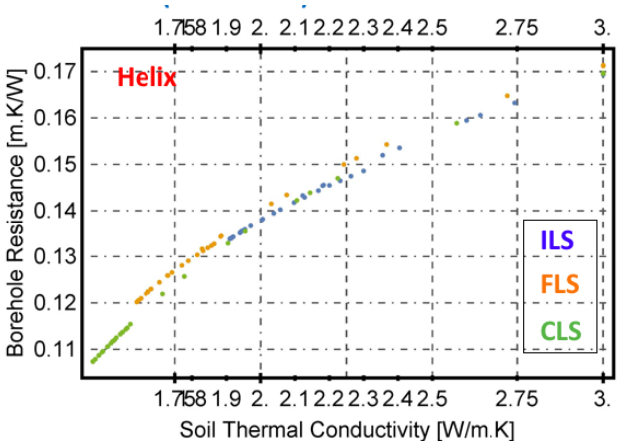

Figure 3.14: R_b model parameter identification for Helicoidal BHE

3.4 Discussion

The main objective these experiments carried out in the UPV geothermal laboratory is the comparison of these BHE.

After applying numerical methods to fit different model, a picture of the R_b of three BHE can be outlined. Figure 3.15 summarizes the results shown in Figures 3.12, 3.13 and 3.14 using only the ILS model.

Figure 3.15 shows that, after a five-day TRT, the coaxial BHE tested presents the better R_b, independently of the λ of the ground. Single-U, the standard typology for BHE, presents the worst value. These results are only valid from the point of view of thermal performance. Taking into account the installation costs (the main costs of installation are the cost of the borehole probe, the cost of drilling (depending on the drilling technique) and the grouting cost. the Figure 3.16 shows the cost of drilling (vertical axis in euros) related to the length of the BHE.

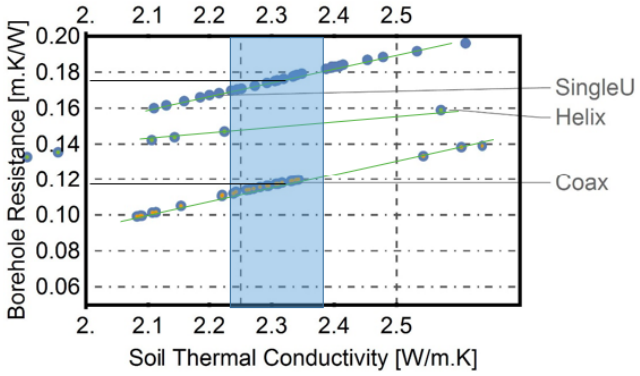

Figure 3.15: R_b ILS model parameter identification

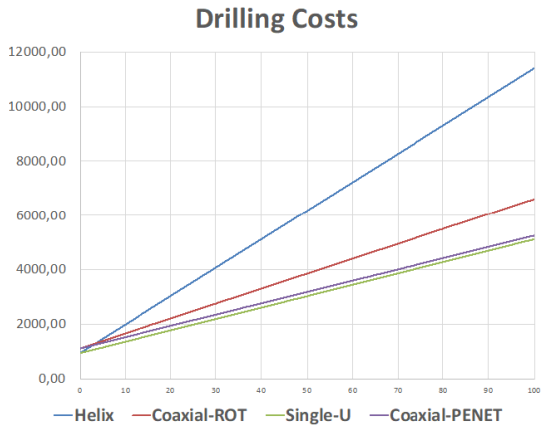

Figure 3.16: Drilling costs (€) vs BHE depth (m)

Single-U BHE are the cheapest one but is the technology that presents the higher R_b. On the other hand, helicoidal BHE are the most expensive to install and our tests also shows that its Rb is higher than R_b of coaxial BHE.

The coaxial BHE installed with standard drilling and grouting has shown the better R_b, but it is a bit more expensive to install than single-U tube.

3.5 Conclusions

The UPV geothermal test site has been described in this paper. This installations aims to be a reference in shallow geothermal research and it has been initially developed as part of CHEAP-GSHPs project.

The presented results are based on standard TRT performed to the three installed BHE. These three borehole heat exchangers are compared because two of them are experimentally developed BHEs and the other one that represents the standard technology. Although they have different characteristics, what is valued is their thermal behaviour per metre of drilling to be able to compare them. The results show that coaxial BHE presents the better borehole thermal resistance. Single-U, the cheaper and most popular type of BHE, show a R_b higher than the other two types.

New drilling technologies, like penetrometer-type installed coaxial, are promising that the performance of the coaxial could be obtained with the cost of installing the single-U tube (see Figure 3.16).

Regarding to the laboratory facility, the geothermal laboratory is flexible enough to implement new experiment setups. But there also some points for improvement. First of all, the control algorithm is sensitive to reference noise and to the lack of linearity of the 3-way valve actuator. More thorough controls have to be designed and validated.

Another restriction of the actual facility is that switching from cooling to heating injection is not possible due to the thermal inertia of storage tank. The installation of a second storage tank will solve this problem, as one can be used for storing cold water while the other one stores hot water.

In fact, the installation will be expanded in the next months as part of the H2020 European project GEOCOND. At least 6 new BHEs will be added to the test site in order to evaluate the new products developed within the project.

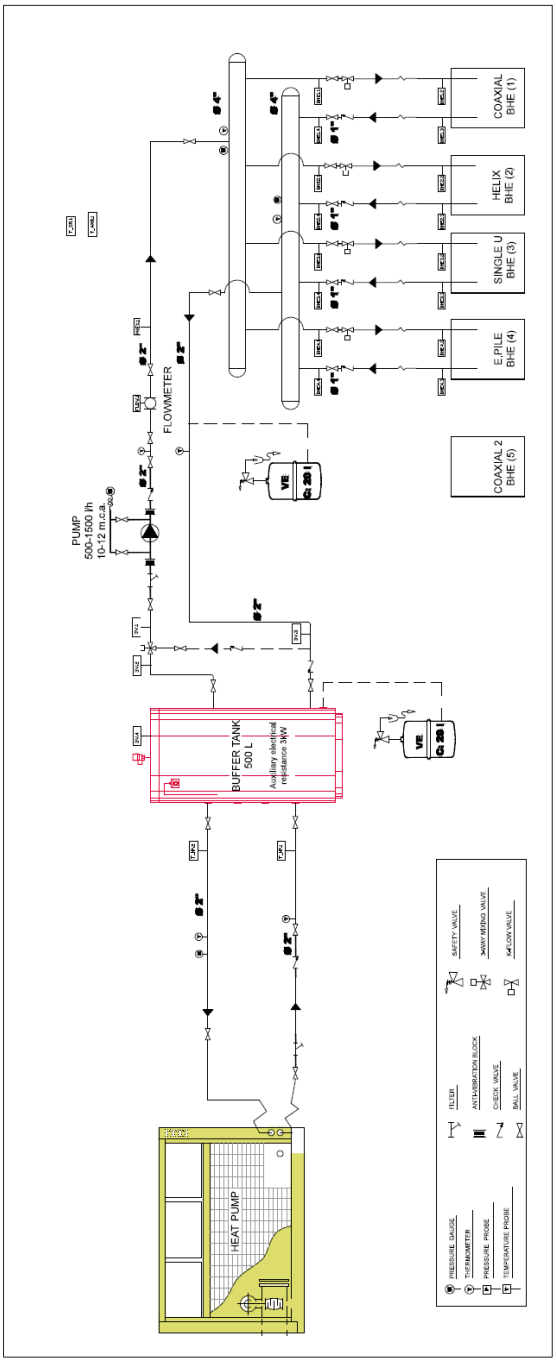

Figure 3.6: Hydraulic system diagram

Chapter 4

Numerical simulations to improve performance and cost-efficiency of Borehole Heat Exchangers

In this chapter, the first results of the Doctoral Thesis are presented. Through extensive numerical simulations, a sensitivity analysis to highlight the influence of some of the most critical parameters that affect the overall performance of a GSHP system is carried out. The results have allowed guiding the real development of more efficient new advanced materials. Finally, the developed materials and their properties are discussed, including a comparative assessment about their compliance with reference material properties as currently seen in the BHE market.

This chapter contains the article entitled "Development of advanced materials guided by numerical simulations to improve performance and cost-efficiency of borehole heat exchangers (BHEs)" published in "ENERGY" journal (9.9 CiteScore, 6.082 Impact Factor), Volume 201, 15 June 2020, 117628.

https://doi.org/10.1016/j.energy.2020.117628

4.1 Introduction

Shallow geothermal energy systems, comprising Ground Source Heat Pumps (GSHPs) and Underground Thermal Energy Storage (UTES) [43], are being exploited as a stable, reliable and renewable energy source for all types of buildings (including nearly zero energy buildings [44]), district heating networks [45] or solar assisted systems [46]. Implementing it on a large scale, though, presents some setbacks, given the high initial capital required compared to other alternatives such as gas or other fossil fuels, low consciousness, and lack or changing standards.

In this paper, the methodology and results of a sensitivity analysis performed in simulated scenarios are presented, in the framework of the European project GEOCOND. This H2020 research project aims at overcoming different challenges, especially cost reduction, increase in efficiency, reliability and security, longer lifetime, better environmental friendliness and increased acceptance. This sensitivity analysis is aimed at understanding and demonstrating the potential impact that the optimization of new materials may trigger in real installations. It is shown how the combination of optimized products (pipes and grouting materials), adapted to the geological setting and specific locations, can trigger significant reductions in the total length of the installations by reducing drastically the effective borehole thermal resistance. This optimization assessment has further been used in the development of real products that will be tested and evaluated in real environments and installations. In Section 4, the finally developed materials and products are described in comparison with some of the most representative standard reference materials, such as PE100 and well-known grouting formulations. As well, other mechanical and rheological properties are discussed that have been taken into account throughout the product development stages.

4.2 State of the art

The history of ground source heat pumps has recently been summarized in [47]. The first idea to use the ground as a source for a heat pump was published already in 1912 in a patent filed by Heinrich Zoelly. He envisaged a closed system, where the heat transfer fluid is circulated in pipes in the underground; the patent shows a helicoidal heat exchanger in a large-diameter hole (Figure 4.1(a)). The first practical application of a ground heat exchanger recorded in literature was in 1945 in Indianapolis, USA, using horizontal pipes in the ground (3 circuits totalling 152 m) to supply heat to a compressor with 2.2 kW electric power input [48]. This was a direct-expansion system, i.e. the refrigerant of the heat pump circuit circulated directly in the buried heat

exchanger pipes. Only two years later, a paper [49] presented a collection of ground-coupling technologies available at that time, among them three types of borehole heat exchangers (Figure 4.1(b)); they comprise the basic geometries to which the BHE in use today can be ascribed to, i.e. co-axial, U-tube and helicoidal ("spiral").

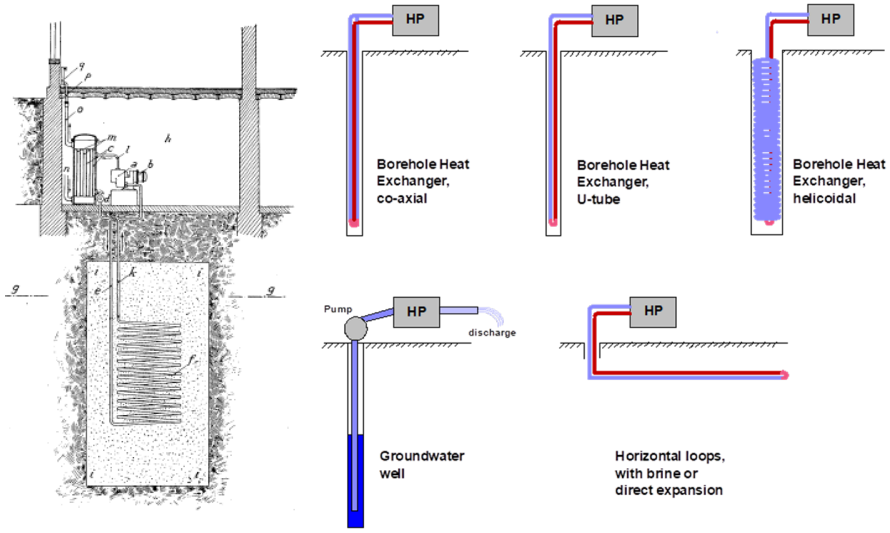

Figure 4.1: At left (a) Ground Source Heat Pump in Swiss Patent 59350 of 1912 (inventor H. Zoelly); at the right (b) Ground-coupling methods listed by [49], re-drawn and harmonized as in [50]

The concern for increasing heat exchange efficiency in ground heat exchangers was soon addressed. The first German BHE installation in 1974 [51] used steel tubes, and attempts then were made to combine the advantage of high thermal conductivity of metal with a continuous pipe that can be coiled and does not need the connection of individual, rigid tubes. A German company brochure [52] shows photos of drilling and installation for a coaxial BHE, made from corrugated stainless steel for the outer pipe, and a rubber hose for the inner pipe. This design was improved by another company (Helmut Hund GmbH) using a thin PE-coating extruded under vacuum to the outer pipe wall, in order to provide corrosion protection with as little temperature drop as possible (Figure 4.2). In Switzerland, where Double-U-BHE made from PE are the norm since the early 1980s, an improved coaxial design (Figure 4.3)

was successfully tested and used for some years. Alas, the higher cost of the bespoke extrusion compared to standard PE-pipes in U-tube designs were not set off by the better performance, at least not at that time.

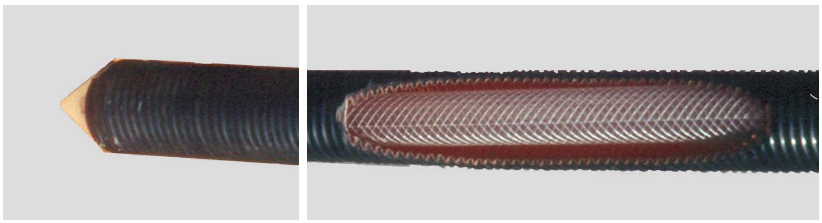

(a) (b)

Figure 4.2: Footpiece (a) and cut-out section (b) of coaxial BHE as tested in Schwalbach GSHP research station [53], consisting of corrugated metal outer tube (usually stainless steel, but copper in this sample for exhibitions), protected against corrosion by a PE-coating

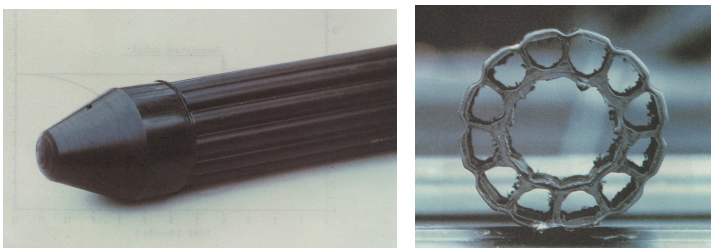

(a) (b)

Figure 4.3: Footpiece (a) and cross-section (b) of coaxial BHE used formerly in Switzerland, made of PE with multi-chamber outer channel for turbulent flow and increased heat exchange (photos from [54])

The most efficient BHE of the 1980/90s probably was a type of coaxial BHE used e.g. in a BTES-experiment in Luleå in Northern Sweden [55], where the borehole wall in solid rock provided the outer boundary and only an inner pipe had to be inserted (Figure 4.4). This technology of course only works in very stable rocks and with water as heat carrier fluid, that can be in exchange with groundwater in fissures and fractures. This technology thus has not found much replication, and experiments with hoses made of plastic foil used to tighten the borehole walls ("liner" in Figure 4.4) in another Swedish BTES in Anneberg near Stockholm [56] in 2002 were not quite successful.

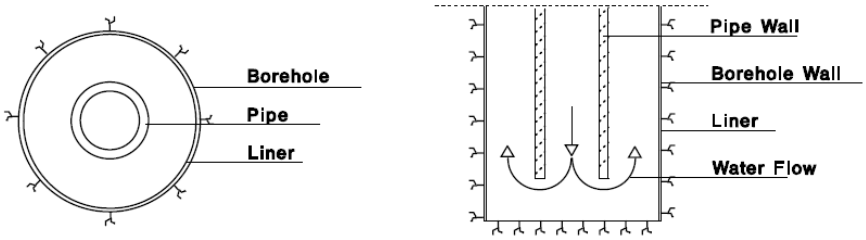

Figure 4.4: Coaxial BHE in open borehole (with or without liner, depending on rock quality) as used in Luleå BTES, constructed 1982/83 (graph from [55])

4.2.1 State-of-the-art in materials for pipes

After the early period of experimentation with various metal and plastic materials, and with the emergence of factory-made BHE coils on the market in the late 1980s, high-density polyethylene (HDPE) became the preferred material for decades. The main advantages were cost, easy handling incl. welding, and longevity.

A list of the pipe materials recommended for use with BHE (Table 4.1) is indicated in the draft version of the new edition of guideline VDI 4640-2[1], published in May 2015.

Metallic pipes for BHEs have been considered since long because of the significantly higher thermal conductivity compared to the plastic pipes and have been employed in several situations. However, the corrosion problems and of the cost of non-corrosive metals were considered an barrier. In situ corrosion tests conducted in 1986-1988 in a groundwater well at Schwalbach GSHP research station [57] showed that a useful life of 30 to 40 years could be expected with plain steel and copper and that short-term corrosion could not be measured with stainless steel. This is compatible with [58], showing service life for galvanized steel tubes of about 50 years. For metals in general, [58] concludes: "*In geologic formations characterized by low to moderate corrosive potential, stainless steel, aluminum and copper are good metallic alternatives to HDPE ... Galvanized steel pipes may also provide competitive alternatives to HDPE in such environments*".

[1] VDI 4640 is a widely respected industry standard in Germany and neighbouring countries, first published in 1998, and now comprising 5 parts for different aspects of shallow geothermal energy.

Table 4.1: Pipe material properties, selected values from [59]

Material	Thermal Conductivity	Maximum operating temperature for 50 years pipe lifespan[7]	Maximum operating temperature for 1 year pipe lifespan[7]
PE100 [1]	0.42 $W/(mK)$	40 ºC	70 ºC [8]
PE100-RC [2]	0.42 $W/(mK)$	40 ºC	70 ºC [8]
PE-RT [3]	0.42 $W/(mK)$	70 ºC	95 ºC
PE-X [4]	0.41 $W/(mK)$	70 ºC	95 ºC
PA [5]	0.24 $W/(mK)$	40 ºC	70 ºC
PB [6]	0.22 $W/(mK)$	70 ºC	95 ºC

[1] Polyethyne with minimum required strength (MRS) 10MPa
[2] Polyethyne with minimum required strength (MRS) 10MPa with Resistance to Crack (RC)
[3] Polyethyne for Raised Temperature (RT)
[4] Cross-linked polyethylene
[5] Polyamide
[6] Polybutylene
[7] at given maximum pressure conditions ranging from 0.6-1.2 MPa
[8] even short-time excess temperatures can damage pipes

In conclusion, HDPE-pipes dominate the market in Europe due to their cost, corrosion resistance and handling. For the most common design of BHE, the U-tube design (single, double,..), it is very improbable that metallic pipes will have a market share. But looking at mainly coaxial designs, there may be room for non-plastic alternatives in boreholes of limited depth.

4.2.1.1 Considerations on pipe materials

After HDPE proved to be an easy-to-use and reliable material, development focused mainly on improving the resistance of the material to pressure, temperature, damage (like from scratching), corrosion, etc., resulting in the materials listed in Table 4.1. The thermal conductivity on the order of 0.4 W/(mK) was accepted as suitable, albeit not being ideal. Considering the thermal efficiency of the whole BHE-system, from surrounding ground to the fluid inside the pipes, thermal conductivity is only one factor of many. Furthermore, for the whole GSHP or UTES facility, the efficiency of BHE again is just one factor, with the physical properties of the ground being likewise important and ground thermal conductivity typically is in a range of 0.5-4.0 W/(mK), and not one or two orders of magnitude higher as most metals exhibit. The overall efficiency of a BHE usually is given by the borehole thermal resistance R_b, expressed in K/(Wm) and comprising the individual resistances from borehole wall to fluid.

Parameter studies observed the influence of thermal conductivity of the pipe material on the overall efficiency of the borehole. Such modelling was made e.g. in 2003 within project Groundhit [60], funded by the EU in FP6 [61]. The results in Figure 4.5 show clearly that an increase in thermal conductivity of the pipes from about 0.2 $W/(mK)$ to 1 $W/(mK)$ can reduce R_b substantially, and a reduction on a smaller scale can be seen up to 4-5 $W/(mK)$; for further increase of thermal conductivity into the realm of metals, the reduction of R_b is only marginal.

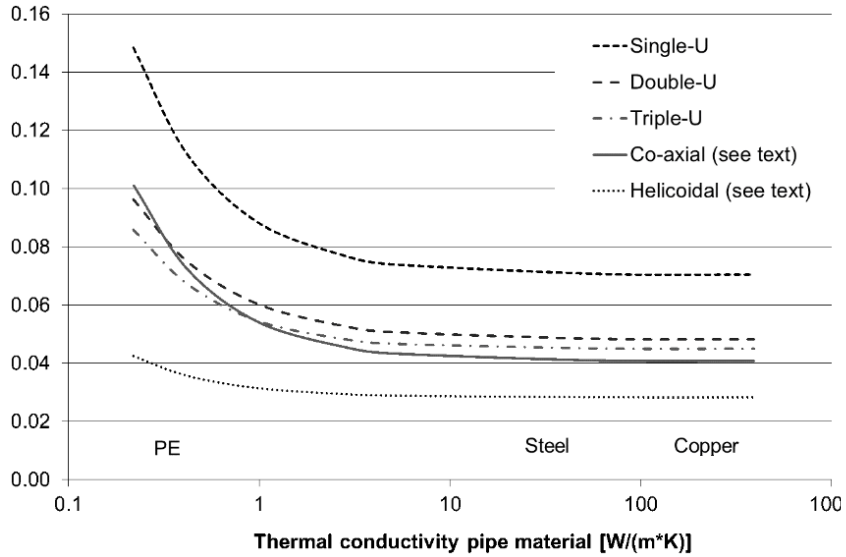

Figure 4.5: Borehole Thermal Resistance R_b for different configurations versus thermal conductivity of pipe material, see text for details; helicoidal by approximation only. Data from European project Groundhit

4.2.2 State-of-the-art in materials for grouting

The early BHE had no grouting, they were either immersed in groundwater in open holes, or filled by gravity from top (often using the drill cuttings as filling material). In softer geological layers, the ground was allowed to collapse around the pipes after installation, and in other cases steel pipes were driven directly into the ground, with no annulus. Inserting BHE-pipes into open, water-filled boreholes in hard rock, with just the softer overburden stabilized by a steel tube, still is the norm in most of Scandinavia.

Grouting of BHE by pumping a mixture down a tremie pipe and filling the annulus from bottom to top was presumably first done in Switzerland and in USA in the late 1980s. The first standard to require grouting from bottom to top of the borehole was [62] in Switzerland. The first German standard on GSHP, [63], also recommended grouting, but still left room for some exceptions for shallow boreholes. The grout mixtures originally consisted of bentonite, cement and water; [64] gave an example with 25% bentonite, 25% cement and 50% water, resulting in a thermal conductivity of about 0.7-0.8 $W/(mK)$.

The supposedly first publication on the idea of grout with enhanced thermal conductivity is [65]. In the mid-1990s, a thermally enhanced grout came on the market in the USA, with a thermal conductivity of almost 1.5 $W/(mK)$; in American units, this means $0.85 Btu/(hr ft^{\circ} F)$, leading to the name of thermal grout 85. The increase in thermal conductivity was achieved by adding siliceous sand. Experiments in 1996-1999 at Brookhaven National Laboratory in USA targeted different additives for increased thermal conductivity, beside siliceous sand also steel grit, steel microfibers and aluminium oxide; siliceous sand was found the only viable option [66]. Developments in Germany around 2000 resulted in grout mixtures with addition of either quartz powder or graphite, under the brand names Stüwatherm and Thermocem, respectively. Also in [64] the addition of quartz sand was suggested to improve thermal properties. Currently, numerous brands of grout ready for use are on the market.

4.2.2.1 Considerations on grouting material

Similar parameter studies as with pipe material can be made for the grout. The handy range of thermal conductivity for grout is much smaller, extending from around 0.6 $W/(mK)$ with some plain bentonite-cement mixtures to slightly above 2 $W/(mK)$ in currently available materials [67]. A further increase would require new concepts, and considering the other material constraints for sealing properties and cost, more than a doubling of the current achievement seems out of reach. Thus for the calculations resulting in the curves in Figure 4.6, the thermal conductivity of the grout was varied from 0.5-8.0 $W/(mK)$, and the pipe thermal conductivity fixed at the value for HDPE, 0.42 $W/(mK)$.

Like for pipe material, a substantial improvement (decrease of R_b) can be seen for grout thermal conductivity increasing to about 2 $W/(mK)$. A further reduction of R_b is visible towards values of 4 $W/(mK)$ for most configurations; the effect is highest for single-U and lowest for the already very low R_b of helicoidal BHEs. Additional increase in grout thermal conductivity has little visible effect only.

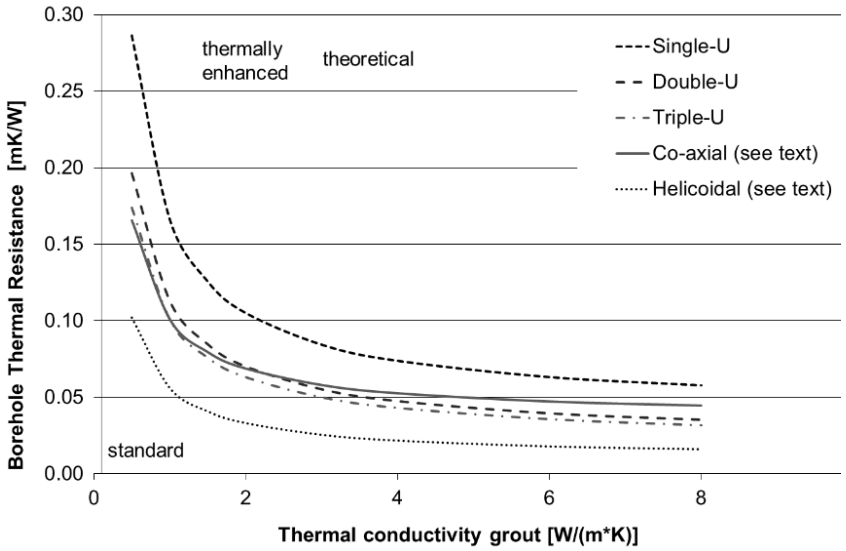

Figure 4.6: Borehole Thermal Resistance R_b for different configurations versus thermal conductivity of grout (backfilling); helicoidal by approximation only. Data from European project Groundhit

These basic findings were experimentally confirmed in [68], with the conclusion: "*The grout thermal conductivity has a great influence on the borehole thermal resistance. However, when the thermal conductivity of the grout becomes considerably higher, the borehole thermal resistance will assume a constant value, ...*".

4.3 Parameter sensitivity analysis implementation

4.3.1 Tools and procedure

Several previous studies have been carried out to analyze the influence on thermal performance of the various geometrical and material parameters of a BHE, including ground thermal profile [69, 70]. Yet, the cooperative effect of grout and pipe conductivity has been so far not considered, as pipe material properties were usually regarded as given. In our case, more than 17,000 simulations were carried out to obtain the best specifications, i.e., the best efficiency, for the products to be developed. The core of the simulations was performed using "Earth Energy Designer" (EED) [71], a PC based software (Windows platform) for designing borehole heat exchangers based on analytical solutions for the heat exchange process between the

borehole and the surrounding ground. This design software has proven to be able to predict borehole fluid temperatures, as can be found in [72] where the mean brine temperature was monitored from July 1995 - July 1996 in UBEG (Wetzlar, Germany) and compared with the predicted brine temperature. Also in [73] a comparison of monitored with forecast values was made, to assess the suitability of the tool for borehole design. Finally, [74] describes the comparison of the monitored data from three buildings (Building GEW (Gelsenkirchen), Building FAS (Dortmund) and building HSZ (Salzgitter)) with the data calculated by EED, showing a reasonable match with predicted fluid temperatures.

The simulation process comprised five main steps: defining simulation parameters, generating simulation models, executing the models, filtering the results and, finally, analyzing the obtained values.

The simulations are configured by means of plain text files with self-descriptive elements. The lines of the model file contain the name and value of each of the required parameters. Once the parameter values are decided, a dedicated script creates a set of base model files, each with different values of those parameters.

Since EED has only a Graphical User Interface (GUI) without scripting capabilities or an alternative Command Line Interface (CLI), our team decided to create a robot program simulating an interactive user to enable the automatic execution of hundreds or even thousands of simulation without human intervention.

The procedure produces a result file for each simulation with a similar structure than the model files: plain text files with self-descriptive entries. By means of *shell* and *awk* scripts, results are filtered to extract the desired performance indicators: total installed BHE length and equivalent BHE thermal resistance. The final results of this stage is a comma separated value (CSV) file including the input parameters and its associated performance indicators.

As a further step, it is necessary to define a series of variables or parameters that must be necessarily established for the simulations. Some of the input variables are considered as *fixed variables* according to the defined scenarios. Other variables, coinciding with those variables that will be presumable modified and enhanced are considered as *open variables*. Those *open variables* are varying in the simulations to perform the sensitivity analysis.

4.3.1.1 Fixed Variables

Fixed variable are determined by our so–called *scenario setting*. There are three main categories for the configuration of the different scenarios that will constitute the initial conditions for the simulations of the sensitivity study. Those major categories are named as Ground, Location and Building as defined below.

Ground

The typology of the ground will be defined by two variables:

1. The thermal conductivity of the ground: (expressed in W/(mK) and often denoted k, λ or κ) is the property of a material to conduct heat according to the Fourier's Law for heat conduction.
2. The volumetric heat capacity of the ground: (expressed in MJ/(m^3K) describes the ability of a given volume of a substance to store internal energy while undergoing a given temperature change without phase transition.

The above parameters depend on the geological characteristics and the lithologies that are found in each specific location. Three different types of ground have been distinguished: low conductivity ground, medium conductivity ground and high conductivity ground, with the properties listed in Table 4.2 [63].

Table 4.2: Characteristics of three different typologies of ground conditions attending to the main geological settings around Europe

Thermal Conductivity	**Density**	**Heat Capacity**	**Volum. Heat Capacity**	**Ground Thermal Conduct.**	**Thermal Diffusivity**
	kg/m^3 x 10^3	$kJ/(kg{\cdot}K)$	$MJ/(m^3{\cdot}K)$	$W/(m{\cdot}K)$	m^2/s x 10^{-7}
Low	1.45	0.88	1.28	1.2	9.4
Medium	2.3	0.91	2.1	2.3	11
High	2.7	0.93	2.5	3.5	14

Those values represent a generic value for different types of associated lithologies (sandy sediments and conglomerates for low conductivity, well-cemented limestones for medium conductivity and granite and metamorphic gneiss for high thermal conductivity). All those typologies could be found in different European regions and could be generally grouped into non-consolidated sediments, carbonatic rocks, and igneous and metamorphic rocks.

Location
The location of the building will provide us with several important input data for the simulations. On one hand, the location of the building is directly related to its climate typology. On the other hand it is closely related to the undisturbed temperature of the ground and the geothermal heat flux value, which can be directly extracted from the EED libraries. Indirectly, the location affects the thermal loads that would be needed to achieve the comfort requirements of different types of buildings.

Two European cities with different climatic regimes were selected. Representing areas dominated by warm/mild climate, Madrid (Classified as Csa according to the Koeppen-Geiger classification), and hot climate, Seville, (Classified as Csa with extremely high temperatures according to the Koeppen-Geiger classification). No city has been selected for a cold climate since it would imply a different method of design (different fluid temperature constraints). In cold regions, the design of the heat exchanger length is carried out, due to the low ground temperature, fixing lower the fluid temperature in the heat exchanger (several degrees below zero) and using glycol water as the fluid heat carrier. Therefore, by using different design conditions, it would not be possible to compare the results obtained, which is why this type of climate has been excluded.

The EED software contains libraries allowing extraction of the most significant values (temperature of the ground and geothermal heat flux) for the modeling. Those values have been established for hot and mild climate with values of ground temperature of 18 ^{o}C and 14 ^{o}C and values of geothermal heat flux of 0.07 W/m^2 and 0.08 W/m^2 respectively.

Building
The building typologies have been reduced to two main types: residential house and office building. Each typology has totally different thermal demands according to the constructive characteristics and the expected uses. The thermal profile, which will vary according to the type of building, together with the climate associated to the specific locations (explained in the previous section) is analyzed in order to provide the monthly thermal loads.

In order to obtain the thermal loads of the selected building typologies, results from the European project “Policies to enforce the transition to nearly zero energy buildings in the EU-27 (ENTRANZE)” were consulted. Specifically, the results of deliverable 2.3 of Work Package 2 of the Project: "Data from Heating and cooling energy demand and loads for building types in different countries

of the EU" [2], regarding the energy needs for Heating, Cooling and Domestic Hot Water were used for: a single-family house of 120 m^2 and an office building of 500 m^2 in the climatological conditions described in the previous section.

The energy data demands used in the simulations, depending on the type of building and climate, has been established as follow:

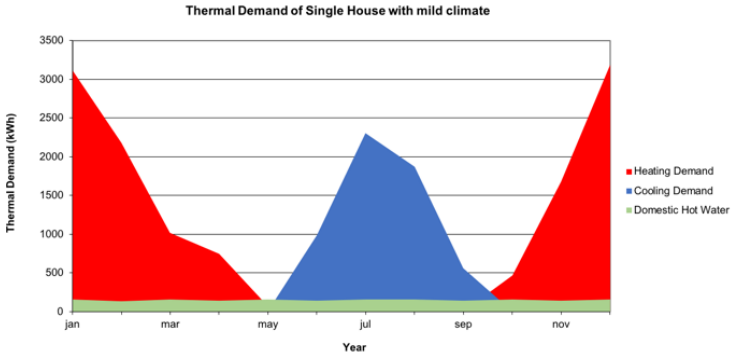

	Heating Mode	Cooling Mode
Power Capacity (kW)	13.6	12
SPF	3.8	3.5
Peak Hours (h)	8	6.5

Figure 4.7: Thermal loads for a single house in a mild climatic region

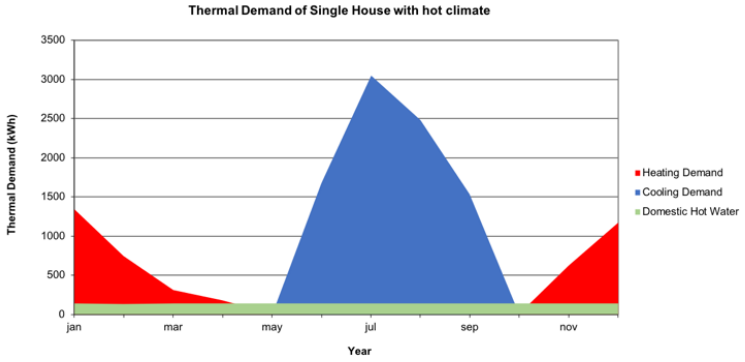

	Heating Mode	Cooling Mode
Power Capacity (kW)	12	10
SPF	3.8	3.5
Peak Hours (h)	4	10

Figure 4.8: Thermal loads for a single house in a hot climatic region

[2] https://www.entranze.eu/files/downloads/D2_3/Heating_and_cooling_energy_demand_and_loads_for_building_types_in_different_countries_of_the_EU.pdf

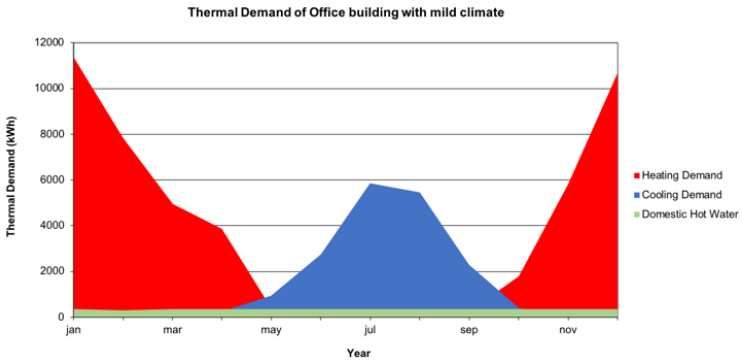

	Heating Mode	Cooling Mode
Power Capacity (kW)	32	30
SPF	3.8	3.5
Peak Hours (h)	12	6.5

Figure 4.9: Thermal loads for an office building in a mild climatic region

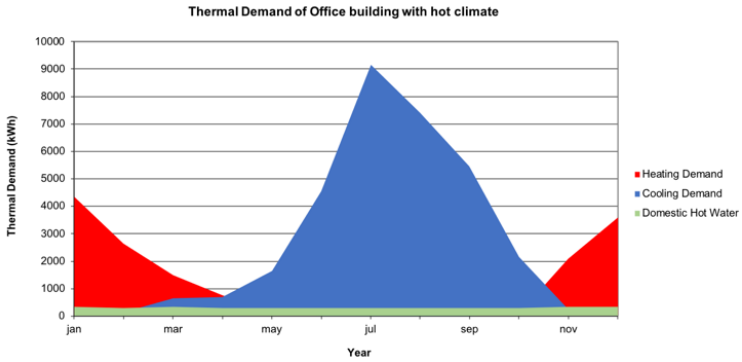

	Heating Mode	Cooling Mode
Power Capacity (kW)	32	30
SPF	3.8	3.5
Peak Hours (h)	5	10

Figure 4.10: Thermal loads for an office building in a hot climatic region

Borehole Heat Exchanger

Two types of borehole heat exchangers have been considered for the simulations. One system is the single –U typology which is the most generally used solution in SGES around the world. The second solution is a standard coaxial geometry, which is currently much less introduced in the market but posses a high potential for introducing enhancements due to the associated reduction of total length of the installations. Whilst being significantly more expensive and slightly more difficult to install, coaxial BHEs are now in the focus of different European projects (e.g. CHEAPs-GSHP [3] and GEO4CIVHIC [4]) and initiatives to improve its installation time, performances and cost. The data used in the simulations concerning the heat exchangers are listed in Table 4.3.

[3] See more information about this project at https://cheap-gshp.eu/
[4] See more information about this project at https://geo4civhic.eu/

Table 4.3: Main characteristics of simulated BHE

Borehole Heat Exchanger (BHE)		
	Single-U	**Coaxial**
Number of Boreholes	Depending on the thermal load	
Depth	Determined by simulation outputs	
Spacing	10 m	
Diameter of the borehole	110 mm	63 mm
Flow rate [1]	0.00011 m^3/s	0.000273 m^3/s
Contact Res. Pipe/Filling	0 m^2K/W	
Filling Thermal Conductivity	From 1 to 4 $W/(mK)$	2.1 $W/(mK)$ (when applicable)
Pipe outer diameters	32 mm	63mm (outer pipe) and 32mm (inner pipe)
Wall thickness	3 mm	5.8 (outer pipe) and 2.9 mm (inner pipe)
Shank spacing	0.07 m	Not Applicable
Pipe Thermal Conductivity	From 0.4 to 2 $W/(mK)$	Inner: From 0.1 to 0.5 $W/(mK)$ Outer: From 0.4 to 2 $W/(mK)$

[1] The water flow has been chosen according to the thermal power dissipation according to the load balance of the building. It has remained constant at a convenient value because the objective of the simulations was to asses the influence of other parameters (i.e., the conductivity of pipes and grouting) on the thermal resistance of the borehole

Heat carrier fluid

The heat carrier fluid in the simulations is water. Water is generally used as heat carrier fluid in a wide range of applications in particular from hot climate to moderately mild climates. In moderate to cold climates, systems often are designed for temperatures dropping down to negative values, and anti-freeze additives such as glycol may be added to the water. The heat carrier fluid used for the simulations at this stage is plain water.

Fluid temperature constraints
The fluid temperatures are constrained by the generally used design values for the defined locations according to the thermal loads demanded by the buildings. The temperature of the fluid in the heat exchanger is limited to the generally used design values in systems with plain water as heat carrier fluid (including peaks) as given in Table 4.4.

Table 4.4: Fluid temperatures constraints

Minimum Mean Fluid Temperature	5 ^oC
Maximum Mean Fluid Temperature	32.5 ^oC

The minimum and maximum mean fluid temperatures shown in Table 4.4 have been selected as a common choice for GSHP heating and cooling operation respectively. The actual value would depend on the given location, due to the ground influence. The BHE average water temperature is obtained by means of simulation since it depends on the thermal building thermal loads. For the purpose of our study, the minimum temperature in the exchanger was limited to about 5 ^oC because of the use of water without antifreeze. The maximum temperature is usually limited to around 32.5 ^oC, as higher temperatures would impact considerably heat pump efficiency and reduce pipe's lifespan.

Simulation period
For all the scenarios contemplated an effective performance period of 25 years was established.

4.3.1.2 Open Variables
Open variables are those input variables necessary for doing the simulations which values are going to be modified. Our goal is to determine the optimal values for those variables in the different scenarios in order to provide the guidelines and specifications for the product developers. The main considered *open variables* are:

Thermal conductivity of the filling grout
This variable considers the thermal conductivity of the grouting products. As highlighted in the introduction, currently the thermal conductivity of standard grouts could vary from 0.8 $W/(mK)$ to 2 $W/(mK)$ depending on the different solutions available in the geothermal product market. Our objective is to increase the range of values in order to optimize the performance of the SGES with lower total BHE length. In the simulation procedure designed, a range of 0.1 $W/(mK)$ to 4.0 $W/(mK)$ is being simulated with steps of 0.1 $W/(mK)$.

Thermal conductivity of the pipe
This variable considers the thermal conductivity of the pipes used as heat exchanger. Currently the thermal conductivity of standard PE pipes is 0.42 $W/(mK)$. Our objective is to increase the range of values in order to optimize the performance of the SGES. In the simulation procedure designed, a range of 0.1 $W/(mK)$ to 2 $W/(mK)$ is being simulated with steps of 0.1 $W/(mK)$.

Diameter ratio between inner and outer pipe in coaxial borehole
Simulations have also been performed to obtain the outer and inner pipe diameter ratios for coaxial borehole pipes that maximize efficiency.

4.3.1.3 Simulation output values

In order to evaluate the effects produced by the enhancements, a detailed analysis of the simulation results has been done, paying attention to two output values: total length of the heat exchangers for covering the energy demands and borehole thermal resistance. Result show that both parameters respond in the same way to the introduced simulations as it was initially expected.

Total length of the heat exchangers
This output parameter shows the final total length of heat exchanger that will be required to cover the energy demands of the buildings while limiting the overall temperature increase around the BHE area to a certain value within the operational period of the system under the input conditions described in the Section 4.3.1.2. Hence, the different solutions that will be discussed in the next sections are equivalent from the point of view of heat pump efficiency and can serve as a basis for a comparative cost analysis.

Borehole thermal resistance
According to the general accepted definition, the borehole thermal resistance (R_b) is the thermal resistance between the pipe fluid and the borehole wall. It is the main efficiency characteristic of a geothermal heat exchanger. Lower thermal resistance of the borehole leads to better efficiency of the geothermal system per borehole unit length and higher Hellström efficiency. Since its original definition by Mogensen [75], there have been several methods proposed for its calculation. EED offers one possible methodology which, inter alia, takes into account short-circuiting thermal flow between the upstream and downstream pipes of the BHE. As will be seen later these effects are critical to explain some of the features observed in our study when varying the open parameters.

As expected, simulations show that the response of R_b when other input variables are modified (thermal conductivity of the pipe or thermal conductivity of the ground together with different geometrical configurations of the pipes) is identical to the response observed in the total length of the heat exchangers. Nevertheless it is important to consider R_b separately in order to be able to compare BHE efficiency regardless of the considered scenario and geometry, since it constitutes an intrinsic system parameter.

4.3.2 Simulations to evaluate the sensitivity analysis of parameters

4.3.2.1 Sensitivity analysis of combination of pipe and grouting thermal conductivity in a single-U borehole

The aim of this assessment is to analyze the combined effect of varying the thermal conductivity of the pipe materials and the grouting materials at the same time. This sensitivity analysis was done varying the previously described parameters simultaneously, in order to decipher the combined effect that both modifications trigger in the total length of the borehole field and the effective borehole thermal resistance. The total length of the borehole field is directly proportional to the borehole resistance (R_b). Those parameters are going to be realistically modified by means of producing new typologies of piping materials, including new materials and new geometrical configurations; and new thermally enhanced grouting adapted to the ground conditions, in order to optimize the efficiency of the systems.

The interval of modeling were defined as follows:

λ_{PIPE} values varying from 0.4 W/(mK) to 2 W/(mK) (step: 0.1 W/(mK))
λ_{GROUT} values varying from 1 W/(mK) to 4 W/(mK) (step: 0.1 W/(mK))

To obtain the surface graphs for each defined scenario, it was necessary to perform 480 simulations according to the procedure defined above. The results are highly valuable to guideline and set practical limits to the development of the new pipes and grouts.

For illustration the combined effect of modifying both parameters, the graphic corresponding to an office building, in a hot climatic region and with a medium value of thermal conductivity of the ground has been selected as representative of the results (Figure 4.11). The heat exchanger used for the simulation is a single-U heat exchanger.

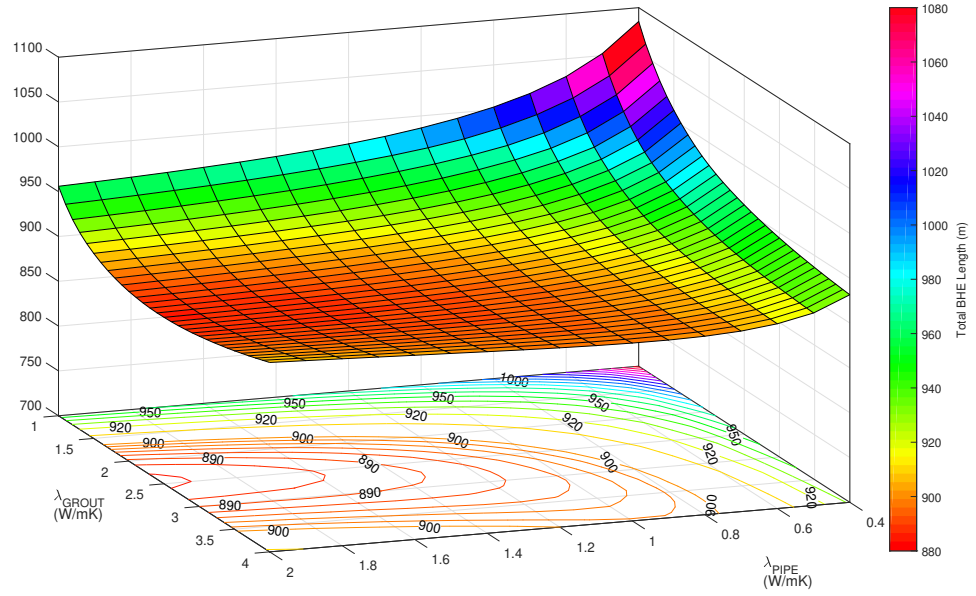

Figure 4.11: Simultaneous effect of varying the λ_{PIPE} and λ_{GROUT} in the total length of a designed system for an office building in a hot region with medium thermal conductivity of the ground. Isolines are spaced at 2 m until 900 m and 10 m from that value to 1100 m

The obtained results demonstrate that the optimal area, in terms of total length of the borehole field, corresponds to λ_{PIPE} between 1.2-1.5 W/(mK) and λ_{GROUT} between 2.1 and 2.9 W/(mK). The reason why higher values of the thermal conductivity of the grouting material are counterproductive in this

scenario is related with the increase in thermal short-circuiting between supply and return pipes.

The results of the simulations show that a significant reduction of the total length may be achieved by means of using a optimal configuration (λ_{PIPE} = 2 W/(mK), λ_{GROUT} = 2.4 W/(mK), required length = 885.5 m) instead of a standard PE geothermal pipe with a standard grouting (λ_{PIPE} = 0.42 W/(mK), λ_{GROUT} = 2.0 W/(mK), required length = 1003.7 m). Figure 4.12 shows the corresponding borehole thermal resistance values for the same scenario, where the trend is identical.

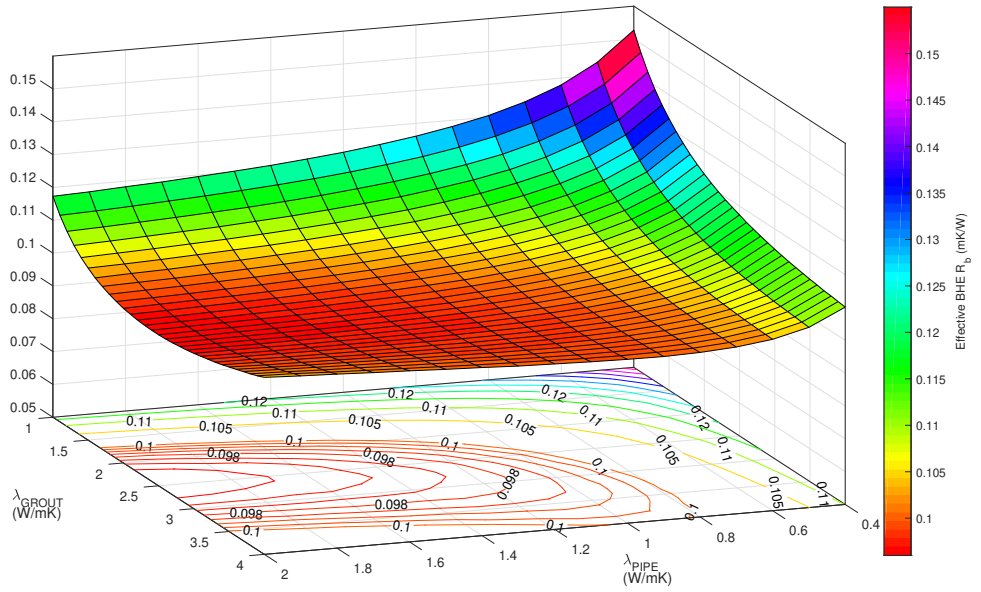

Figure 4.12: Simultaneous effect of varying the λ_{PIPE} and λ_{GROUT} in the R_b of a designed system for an office building in a hot region with medium thermal conductivity of the ground. Isolines are spaced 0.0005 mK/W until 0.1 mK/W and 0.005 mK/W from that value to 0.15 mK/W

Results of this study were done for several possible scenarios considering two different typologies of buildings, the climatic conditions and finally the ground characteristics related to the thermal conductivity.

4.3.2.2 Sensitivity analysis of combination of inner pipe and external pipe conductivity in a borehole coaxial without grouting

In this second part, the effect of a coaxial heat exchanger is analyzed following the sensitivity approach related to the thermal conductivity of the inner and outer pipes. This sensitivity analysis is done to unravel the influence of installing a coaxial heat exchanger instead a conventionally used U-pipe. In this case, the simulations were done by modifying systematically the thermal conductivity of the inner and outer pipes. The assumptions that have been considered for the simulations are that:

1. The conductivity range shall be of the order of coaxial pipes manufactured in plastic.
2. Thermal isolation of the inner pipe will produce an enhancement of the efficiency of the system avoiding thermal loss.
3. The outer pipe should have higher thermal conductivity in order to facilitate the heat exchange with the ground.
4. The simulations consider no need for external grouting between the ground and the external pipe of the coaxial BHE.

The configuration of the coaxial heat exchanger used in the simulations is:

a. Outer pipe: external diameter 63 mm; thickness wall: 5.8 mm; thermal conductivity from 0.4 (standard PE-100) to 2 W/(mK). (Step: 0.1).
b. Inner pipe: external diameter 32 mm; thickness wall: 3 mm; thermal conductivity from 0.1 to 0.5 W/(mK).(Step: 0.1).

A basic scenario, described as office building in a mild climatic region and with a medium value of ground thermal conductivity has been chosen for illustrating the results of the effect of the typology and geometries of the heat exchanger in the design of the SGE systems (Figure 4.13). The results of the simulations show that a significant reduction of the total length may be achieved by means of using coaxial systems with different thermal conductivities in the outer and inner pipes. This reduction is highly significant and might have a considerable impact on costs, passing from a total length of 917 m. in a standard PE coaxial system to a total length of 670 m. in a coaxial system with values of thermal conductivity of 0.1 W/(mK) for the inner pipe and 2 W/(mK) for the outer pipe.

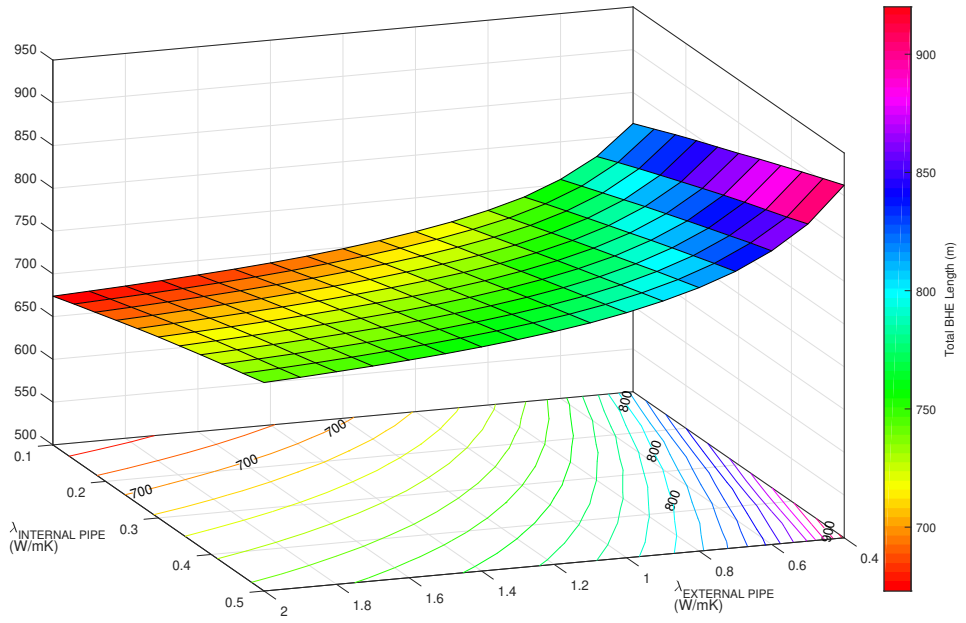

Figure 4.13: Simultaneous effect in the total length of a borehole field of varying the λ_{PIPE} in the outer and inner pipes of a coaxial system for an office building in a mild region with medium thermal conductivity of the ground. Isolines every 10m

Finally, the effective borehole thermal resistance calculated for the different configurations shows the same pattern indicating that the optimal configuration corresponds to higher differences in the thermal conductivity of the inner and outer pipes used in the coaxial heat exchanger (Figure 4.14).

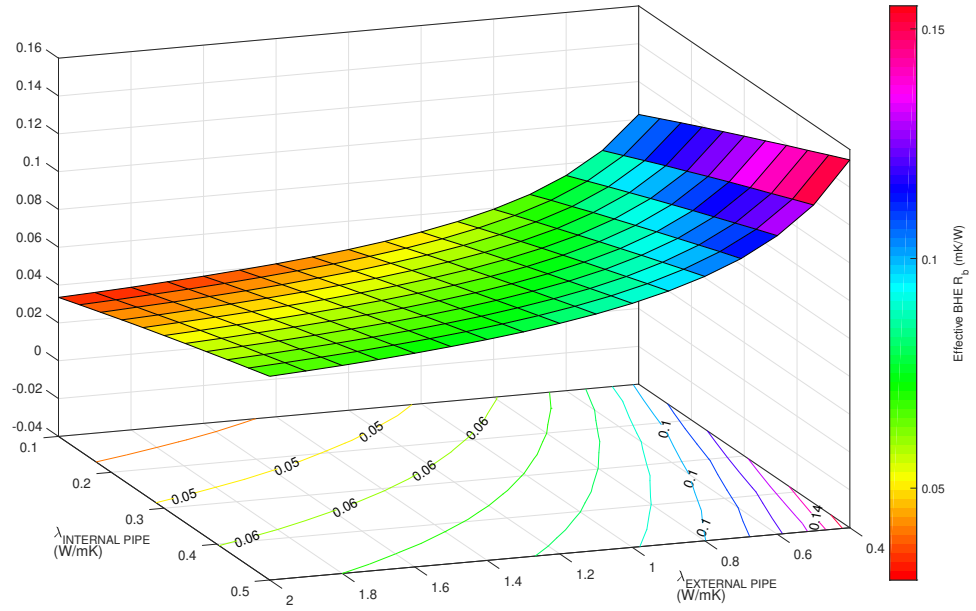

Figure 4.14: Simultaneous effect in the effective borehole thermal resistance of varying the λ_{PIPE} in the outer and inner pipes of a coaxial system for an office building in a mild region with medium thermal conductivity of the ground. Isolines every 0.01 mK/W

4.3.2.3 Sensitivity analysis of influence of the ground typology

The influence of the ground typology for the scenario of a single-U geothermal system for a house in a mild climate region is be studied below. In the following Figure 4.15 shows the surfaces obtained for a high conductivity ground (upper graph), a medium conductivity ground (middle graph) and a low conductivity ground (lower graph). The contour shape correlates to the same shape as that obtained in Figure 4.12, although less accentuated as the system (house) has a lower thermal load than that obtained in Figure 4.12 (office). As is to be expected, there is less need for geothermal exchanger length in the case of high conductivity ground and greater length of geothermal exchanger required in the case of low thermal conductivity ground. In higher ground thermal conductivity environments, the maximum allowable grouting conductivity values would be higher. The three surfaces follow the same pattern without significant differences.

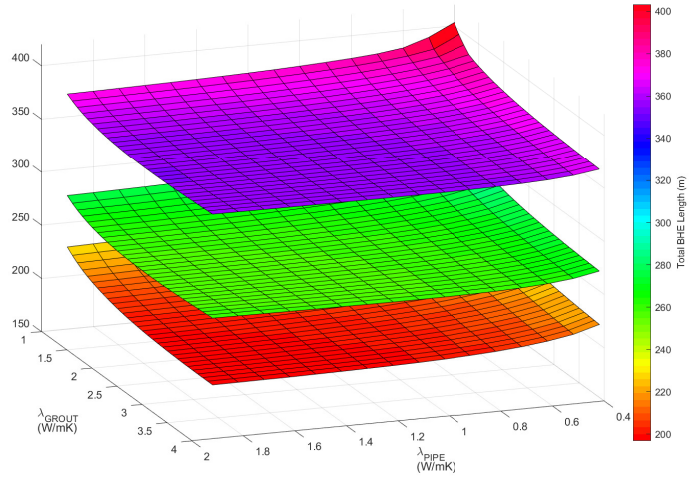

Figure 4.15: Simultaneous effect of varying the λ_{PIPE} and λ_{GROUT} in the total length of a designed system for a house in a mild region with high (bottom), medium (middle) and low (upper) thermal conductivity of the ground

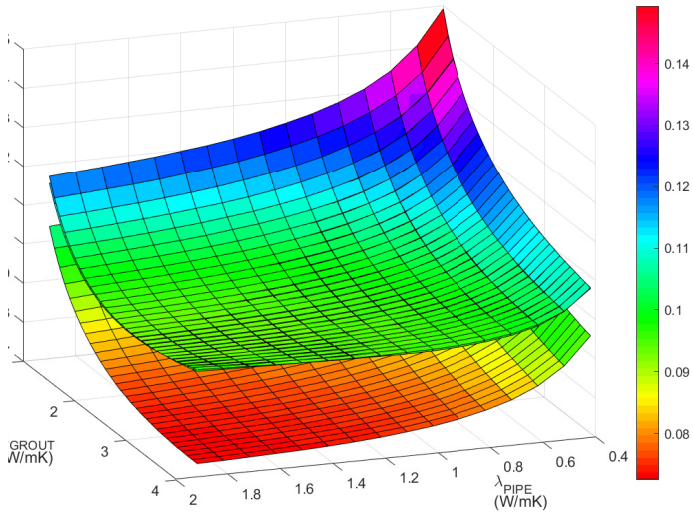

Figure 4.16: Simultaneous effect of varying the λ_{PIPE} and λ_{GROUT} in the R_b of a designed system for a house in a mild region with high (bottom), medium (middle) and low (upper) thermal conductivity of the ground

As for the influence the ground typology on R_b (Figure 4.16), the pattern of the shape of the three surfaces is the identical, although in the case of the surface generated in the case of high conductive ground, a higher influence on R_b is shown.

4.3.2.4 Sensitivity analysis of influence of the climatic conditions

The influence of the climate for the scenario of a single-U geothermal system for a office located in an area of medium ground thermal conductivity is studied below. In the following Figure 4.17 shows the surfaces obtained for a hot region (upper graph) and a mild region (lower graph). As is to be expected, there is less need for geothermal exchanger length in the case of high conductivity ground and more length of geothermal exchanger required in the case of low thermal conductivity ground. The shaping of the two surfaces is similar, although in the case of hot climates, the influence of the "thermal short-circuit" previously explained for high grout conductivities is greater.

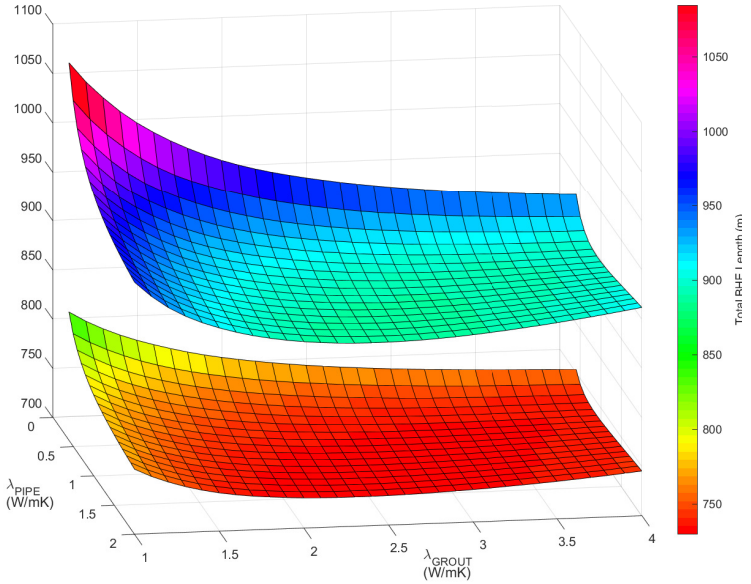

Figure 4.17: Simultaneous effect of varying the λ_{PIPE} and λ_{GROUT} in the total length of a designed system for an office building in a hot (upper) and mild (bottom) region with medium thermal conductivity of the ground

As for the influence of the climate on R_b (Figure 4.18), almost the same thermal resistance surface as the borehole for both climates is obtained, although in the case of the hot climate surface, the highest sensitivity to "thermal short-circuit" is observed, as in the previous case.

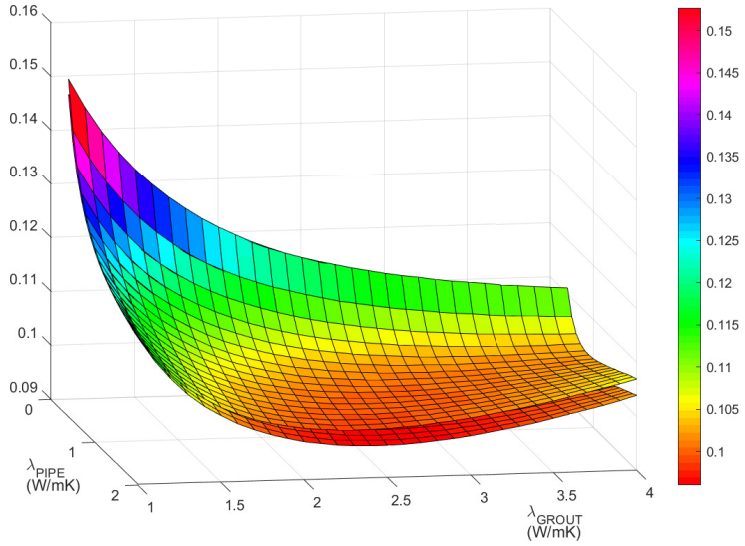

Figure 4.18: Simultaneous effect of varying the λ_{PIPE} and λ_{GROUT} in the R_b of a designed system for an office building in a hot (upper) and mild (bottom) region with medium thermal conductivity of the ground

4.3.2.5 Sensitivity analysis of the different scenarios

All the previously described considerations have allowed the definition of different scenarios where the influence of variations on the thermal conductivity of the pipes and the grouting products could be measured. Considering the three major parameters referred as building typology, location and geological setting, Table 4.5 shows the scenarios were set up for the simulations and Table 4.6 summarizes the obtained results.

Table 4.5: Definition of the scenarios for simulations

	Ground Thermal Conductivity	Climate	Building Typology
SCENARIO 1	HIGH	MILD	HOUSE
SCENARIO 2	HIGH	HOT	HOUSE
SCENARIO 3	MEDIUM	MILD	HOUSE
SCENARIO 4	MEDIUM	HOT	HOUSE
SCENARIO 5	LOW	MILD	HOUSE
SCENARIO 6	LOW	HOT	HOUSE
SCENARIO 7	HIGH	MILD	OFFICE
SCENARIO 8	HIGH	HOT	OFFICE
SCENARIO 9	MEDIUM	MILD	OFFICE
SCENARIO 10	MEDIUM	HOT	OFFICE
SCENARIO 11	LOW	MILD	OFFICE
SCENARIO 12	LOW	HOT	OFFICE

Table 4.6: Results of the optimal configuration for each scenario

	Total Length (m) (State of the art)[1]	**Total length (m) (Minimum value)**	**Reduction**
SCENARIO 1	240.6	196.8 $\lambda_{pipe} = 1.9 W/(mK)$ $\lambda_{grout} = 3.6 W/(mK)$	18%
SCENARIO 2	229.3	178.5 $\lambda_{pipe} = 1.9 W/(mK)$ $\lambda_{grout} = 3.9 W/(mK)$	22%
SCENARIO 3	287.4	256.0 $\lambda_{pipe} = 1.9 W/(mK)$ $\lambda_{grout} = 2.6 W/(mK)$	11%
SCENARIO 4	294.7	238.4 $\lambda_{pipe} = 1.9 W/(mK)$ $\lambda_{grout} = 3.9 W/(mK)$	19%
SCENARIO 5	377.8	354.7 $\lambda_{pipe} = 1.8 W/(mK)$ $\lambda_{grout} = 2.7 W/(mK)$	6%
SCENARIO 6	519.4	462.9 $\lambda_{pipe} = 1.9 W/(mK)$ $\lambda_{grout} = 2.2 W/(mK)$	11%
SCENARIO 7	660.5	584.8 $\lambda_{pipe} = 2.0 W/(mK)$ $\lambda_{grout} = 1.8 W/(mK)$	11%
SCENARIO 8	390.4	333.4 $\lambda_{pipe} = 2.0 W/(mK)$ $\lambda_{grout} = 3.8 W/(mK)$	15%
SCENARIO 9	790.9	729.7 $\lambda_{pipe} = 2.0 W/(mK)$ $\lambda_{grout} = 2.4 W/(mK)$	8%
SCENARIO 10	1003.7	885.6 $\lambda_{pipe} = 2.0 W/(mK)$ $\lambda_{grout} = 2.4 W/(mK)$	15%
SCENARIO 11	1078.7	1030.7 $\lambda_{pipe} = 2.0 W/(mK)$ $\lambda_{grout} = 2.4 W/(mK)$	4%
SCENARIO 12	1754	1591.7 $\lambda_{pipe} = 2.0 W/(mK)$ $\lambda_{grout} = 2.4 W/(mK)$	9%

[1] Standard PE geothermal pipe with a standard grouting ($\lambda_{PIPE} = 0.42$ W/(mK), $\lambda_{GROUT} = 2.0$ W/(mK))

4.4 Material development[5]

The comprehensive numerical analysis by simulations described in the previous section have been a valuable design guideline tool for the specification range of the improved materials for later composing and manufacturing. It has shown that pipe thermal conductivity values above 1.5 - 2 W/(mK) do not provide a significant improvement in the thermal efficiency of the borehole, compared to the increase of the manufacturing cost and complexity of the formulations. As for the thermal conductivity of the grout, too high values have been shown to be possibly counterproductive depending on ground condition and distance between the U-tube legs and therefore a compromise value must be reached.

4.4.1 Development of the new plastic material for improved geothermal pipes

This section describes the preparation of different polyethylene (PE) formulations based on carbonous particles, together with the effect achieved over thermal, physical and mechanical properties of the new material. The objective was to develop a PE formulation with high thermal conductive properties, in order to increase the efficiency of geothermal systems, while keeping the material suitability for pipes production in conventional pipe extrusion lines as well as the mechanical performance of the pipes necessary for their installation and during its lifespan. The challenge was to match the thermal and mechanical properties showed by the compounds with the results from the simulations carried. The work carried out for the complete development of the final pipes includes a first stage of selection of basic raw materials for the plastic pipes, the design and testing of master-batches and compounds; then a laboratory production of pipes for testing mechanical and physical properties and finally the up-scaling of the results into a real factory where the real pipes to be installed in relevant environment was achieved.

4.4.1.1 Selection of the most suitable raw materials: List of additives

Expanded Graphite: Considering all the available data of the recommended graphite grades, it was decided to work with expanded graphites due to their expected higher effect on thermal conductivity, as well as with natural graphite for being the most economical alternative in case that the modulation of the content in the final compounds leads to satisfactory thermal conductivity values. In addition, it is provided in flakes, which will improve handling during compounding compared to graphites in powder form.

[5]Due to intellectual property (IPR) issues, the indication of specific additives and exact formulations has been omitted.

A **grafted maleic anhydride polyolefin** which is an efficient compatibilizer of polyolefins with different polar polymers and fillers. Indeed the paraffin backbone grants useful interaction with the HDPE matrix while the grafted maleic anhydride groups give adhesion to the aromatic rings of the graphite to promote the dispersion in the polyolefin matrix.

Graphene is a filler reported to have a very high thermal conductivity. Therefore its higher cost could be compensated by the need of minor amounts compared to graphite, with important advantages of polymer compound processability during pipe extrusion and a larger flexibility of the pipe which helps during storage and application.

A **polyolefin elastomer** as a very flexible polyethylene to recover the IZOD impact reduced by the addition of significant amounts of the rigid filler (graphite).

A **copolymer** which with its polyolefin flexible blocks can help the IZOD impact value of the composite, while the aromatic rings in its molecular structure can help the dispersion of the graphite and the graphene thanks to the interaction between the aromatic groups of both components.

An **elastomeric polyolefin grafted with epoxy groups** as compatibilizer. This product was tested at laboratory scale to get information about the role of the innovative epoxy group in assisting the dispersion of the graphite into the polyethylene and to stabilize the ultimate properties of the final blend in terms of structure morphology and thermal conductivity.

4.4.1.2 Preparation of masterbatches and compounds

Lab-scale compounds were prepared by SPIN-PET laboratory [76] using a mechanical mixer (Brabender mixer) and the successive scaling up in extruders was carried out by SILMA [77]. Brabender mixer is the tool used for the preparation of polymeric compounds by batch mixing in the molten state. This tool allows to simulate at the laboratory scale the processes of mixing and compounding. Experiments performed in the Brabender allow to test the processability of thermoplastic and elastomer polymer in the presence of fillers and evaluate the dynamic of changes occurring in the compounds as consequence of dispersion of the different phases. These effects are easily evidenced thanks to the possibility of recording the torque curve as a function of processing time. The mixer can also be used as a reactor in the molten state for the production of molecular modified polymer samples through reactive processes between two or more different species.

From different proportions of the raw materials previously described, several preliminary formulations were produced and prepared for a detailed physical-mechanical characterization and comparison against standard PE-100, the benchmarking product. Characterization tests over the graphite PE compounds have been performed by AIMPLAS [78]. The characterization included all the standard testing procedures that are currently used for the characterization of the PE-100 pipes because the final produced pipes must fulfill with the basic requirements of those products in shallow geothermal applications.

In those comparisons, the thermal conductivity values and the mechanical properties (including flexural modulus, flexural strength and deflection) were carefully analyzed because those could be the main properties determining the feasibility of the compound for production plastic pipes. From all those tests, two final composition were selected named as COMPOUND 1 and COMPOUND 2. Table 4.7 shows the main properties and the comparison with the standard PE 100 properties.

Table 4.7: Results derived from the characterization tests

	Thermal Conduct.	**Flexural properties**			**MFI**[1]
	$(W/(mK))$	**Modulus** (MPa)	**Flexural strength** (MPa)	**Deflection** (mm)	$(g/10min)$ $190^oC, 2.16kg$
Standard PE100	0.421	826	21.1	7.2	6.7
Compound 1	1.183	1080	21.0	7.1	7.7
Compound 2	1.021	758	18.0	8.2	4.9

[1] Melt Flow Index (MFI)

From characterization tests performed to the compounds, the following conclusions are drawn:

- Addition of expanded graphite in PE100 increases thermal conductivity significantly. These values are in the range of the required theoretical values of thermal conductivity from the simulations.
- Graphite increases rigidity of PE compounds, which can be reduced with the incorporation of compatibilizers and fluidificants, although the use of these additives results in a decrease in thermal conductivity of the pipe.
- The use of compatibilizer and fluidificant, combined with the preparation of the compound in two steps, led to a compound with balanced

mechanical and thermal properties compared to the rest of formulations assessed.

Mechanical properties of the developed compounds are very similar to the properties of the PE-100 (and consequently to those required in a geothermal installation) and hence these compounds are suitable for the production of high efficient pipes for heat exchangers. Therefore, these two final compositions were selected for the production of pipes at full scale.

4.4.1.3 Full scale production of plastic pipes

Last step of validation of the optimized compound was the use of the compound as a raw material for producing standard 32mm (2.9mm wall thickness) pipes. The manufacture was carried out at CAUDAL facilities [79]. The setting of the production line for pipes is totally standard and ready to produce PE-100 pipes including feeders, silos, extruders, cooling baths, etc. In our process, the plasticizing process of the material takes place in the extruder, where the material, once in the hopper, it is picked up and transported by the screw along the barrel, being melted progressively by means of heat provided by the external resistances and the shearing forces caused by the compression of the material between itself and the cylinder, until its plasticization.

The temperature profiles set for pipes production were the same for standard PE100, showing to be optimum for the conductive compounds. The production of pipes proceeded without major difficulties and the final appearance of the pipes was similar to the standards PE-100 pipes. Finally, the CAUDAL quality department performed their own control to the product following their protocols and summarising the following conclusions about the pipe:

- From the production point of view, pipe are uniform but with a slight excentricity in thickness. MFI (Melt Flow Index) is also adequate for standard pipe extrusion processes.
- It is estimated an internal pressure resistance at 23^{o}C of 15-16 bar for 100 hours. This is similar to internal pressure resistance of PE100 pipes 32 mm x 2 mm (tube 32x10 bar) which withstands 16 bar. However, internal pressure resistance is below PE100 pipes 32 mm x 3 mm (tube 32-16 bar), withstanding 25 bar.
- Tensile strength is slightly lower than that for standard PE100 pipes, but it is enough for the service time and conditions of the pipe for geothermal shallow applications.

- While the presence of some micropores has been observed, attempts are currently being undertaken to eliminate them since the existance of pores limits both mechanical properties and internal pressure resistance.
- Butt welding between pipes from developed compounds and PE100 pipes is compatible.

The rest of parameters determined like OIT (Oxidative Induction Time), longitudinal shrink, black carbon and ash content and black carbon dispersion are suitable for the application.

4.4.2 Development of the new grout material

Analogously to the production of thermally enhanced pipes, a new generation of thermally enhanced grouts has also been developed. The target properties of the grout has been defined according to the results of the modeling and numerical simulations that shown that optimal values of thermal conductivity could oscillate between 2.5-3.3 W/(mK). Nevertheless, the final properties of the grouts for shallow geothermal applications must fulfill a vast series of standards and rules according to the normative of different countries. After analyzing the different standards, recommendations guides and in force documents (inter alia, [80, 81, 82, 83, 84, 85, 86, 67, 59, 87]), the Table 4.8 is summarizing the required values for the grout development based on the different regulations analyzed.

The critical issue is the formulation of a grouting mixture that achieves the range of thermal conductivity defined by the simulations and that complies with the viscosity, flow, bleeding, permeability and compressive strength specifications so essential in this type of grout when used by filling geothermal boreholes. With those premises, the selection of the different raw materials for the grouting included different silica-rich sands with a good granular selection and sizes between 0-1 mm; expanded graphite and a filler with a high potential for increasing the thermal conductivity; standard Portland and SR (Sulphate Resisting) cement and finally some additives (superplasticizers and stabilizers) to enhanced the rheology of the mixture. Water content was also calculated for cover the fluidicity parameters.

The formulation, preparation and characterization of the samples was performed at RISE [88]. Several hundreds of formulations were performed and tested in order to achieve: in one hand, the expected conductivity values and, at the same time, fulfill the technical requirements stated by the standards. Furthermore, during the development, it was observed that the mixing parameters played also a relevant role in the final properties of the admixtures including not only the experimental values but also the

benchmarking studies. In this sense, a deficient mixture procedure may trigger that grouts with declared thermal conductivity of 2 W/(mK) showed values slightly higher than 1.2 W/(mK).

With all those considerations, final grout ready to use after the addition of water in site was prepared and characterized (see Table 4.8 for final properties). This grout fulfill all the in force standards and show a thermal conductivity value of 2.93 W/(mK) after mixing according to specifications (colloidal mixer for 4-6 minutes).

Table 4.8: Required and achieved grout properties

Grout Properties	Required range of values	Achieved range of values
Viscosity (Marsh cone time)	50-100s	92-98s
Flow	26-30 cm	27.0-30.2 cm
Bleeding (water seperation)	<2%	<1%
Thermal conductivity	2.0-3.0 W/(mK)	2.73-2.91 W/(mK)
Compressive strength	>1 N/mm^2	4.5-7.0 N/mm^2
Density	>1300 kg/m^3	1950-1970 kg/m^3
Heat of hydration (fresh grout temperature)	< 30°C	< 30°C
Permeability	< $1x10^{10}$	< $1x10^{10}$ m/s
Freezing-thawing (increase of permeability)	< 1 order of magnitude	Achieved according to the German Standard VDI 4640
Resistance against aggressive groundwater	Required	Achieved

4.5 Conclusions

Improving substantially the operational efficiency of BHE systems by optimizing the materials for individual components (pipes, grout) and the overall setup has a direct impact on cost savings in installation and operation, allowing for a leap in economic benefits of shallow geothermal technology. Furthermore, a significant reduction of the drilled meters and the amount of pipes used to fulfill the same heating and cooling needs enables a decrease of environmental impact.

As for the parameter sensitivity analysis performed, the results of the simulations that were carried out in the different scenarios are now available for the product developer in order to manufacture the new products under the optimal configurations. Those new product specifications produce reductions of the total length of the boreholes and, subsequently, a reduction of the total costs (CAPEX costs) with the same efficiency of the systems. Furthermore, the correct performance of the installation with a higher coefficient of performance is guaranteed since the conditions of performance have been identical for all the scenarios.

These results have been compared with the current state of the art to calculate the impact in economic terms and evaluate the benefits associated to the expected enhancements. In the tested scenarios (combining different types of buildings, types of ground and types of climates), it was possible to corroborate that the enhancement of the thermal conductivity of the pipelines and the grouting products in combination may trigger important reduction of the total BHE length required for the installation, obtaining in simulations of certain cases a reduction in the length required of the borehole heat exchanger of up to 22%.

Moreover, the results have demonstrated that the optimal combination of thermal conductivity for pipes and grouting not always should be the highest possible value, but should be in concordance with the thermal characteristics of the ground. In this way, it has been demonstrated that the thermal properties of the grouting products should be adapted to the ground conditions (geological setting) of the place where the geothermal installation will be located. The results show that the implementation of the enhanced products in real installation could produce either a reduction of the total length of the borehole field or an increment of the efficiency of the geothermal system in case that the total length is maintained.

The results achieved in this research therefore constitute a guidance document for the product developers. Finally, for production, technological, economic and optimization reasons, it was decided to manufacture a geothermal plastic pipe with a conductivity of 1.1 W/(mK) and a grout with a conductivity of 2.9 W/(mK). If the results of the thermal tests are satisfactory, these products could soon be on the market, achieving important reductions in the total length to be drilled, resulting in more economical and competitive geothermal installations.

Chapter 5

Theoretical and experimental optimization of Borehole Heat Exchangers (BHEs) according to hydraulic conditions, geometric characteristics and properties

In ground source heat pump systems, the heat exchange rate is influenced by various design and operational parameters that condition the thermal performance of the system and the operating costs during exploitation. One less studied area is the relationship between the working fluid flow rate in a given system and the heat exchange rate and pumping costs. In this chapter, the investment and operating costs of borehole heat exchanger are analysed with varying circulating flow rate by means of a combination of analytical formulas and case study simulations to allow a precise quantification of the capital and operational costs in typical scenario. As a conclusion, an optimal flow rate minimising either of both costs can be determined. Furthermore, it is concluded that, in terms of operating costs, there is an operational pumping rate above which performance of geothermal systems is energetically strongly penalised.

5.1 Thermal performance assessment of single-U tube borehole according to working fluid flow rate

This subchapter contains the article entitled "Theoretical and experimental cost-benefit assessment of borehole heat exchangers (BHEs) according to working fluid flow rate" published in "Energies" journal (3.8 CiteScore, 2.702 Impact Factor), Volume 13(18), 4925, 19 September 2020.

https://doi.org/10.3390/en13184925

5.1.1 Introduction

The thermal efficiency of a borehole heat exchanger is characterised by its thermal resistance, that is the thermal resistance between the circulating fluid and the borehole wall. This parameter originally was defined by Mogenson [75] and widely analysed by Eskilson [10] and Hellström [11] where the thermal behaviour of geothermal heat exchangers is modelled on the basis of the following key parameters:

(i) the thermal conductivity of the ground (λ),

(ii) the thermal resistance of the borehole heat exchanger (R_b),

(iii) the undisturbed ground temperature (T_0), and,

(iv) the injection (or extraction) of heat ratio (thermal power input) (q) (that depends on flow rate and temperature gap of working fluid).

The (effective) borehole resistance (R_b) should be as low as possible since it has direct relationship with the thermal efficiency of the heat exchange. The higher borehole thermal resistance, the lower heat transferred between the heat carrier fluid and the ground. Hence, by increasing the borehole thermal efficiency (a smaller borehole thermal resistance, R_b), the average working fluid temperature under the same thermal power ratio is decreased. Therefore, by improving the thermal efficiency of the borehole, either the number of drilling meters can be reduced (while maintaining the thermal efficiency of the heat pump) or the average working fluid temperature of the borehole can be improved (while improving the thermal efficiency of the heat pump, maximising the system efficiency). This parameter, R_b, should consequently be optimised to the lowest possible value.

The thermal resistance of the borehole is mainly affected by the following key parameters:

- Properties and flow rate of the fluid through the heat exchanger,
- Diameter of the geothermal borehole,

– Geometry and materials of the heat exchanger pipe, and,
– Grouting material.

Most of these key parameters depend on borehole design. However, the flow rate can be to a certain degree controlled during the operation phase taking into account that the pumping requirements of a Ground Source Heat Pump (GSHP) should be kept as low as possible to minimise losses. It should be noted that, these hydraulic losses may be significant (between 4% to 21% of total system consumption [89], especially at high flow rates), increasing electricity consumption, and, substantially penalising the overall performance. On the other hand, borehole heat resistance depends on the fluid flow rate and, thus, borehole thermal resistance and pumping losses are interrelated. Hence, to seek a compromise between increasing of the thermal efficiency of the borehole and reducing of the hydraulic losses in the GSHP system is reasonable.

There are numerous publications dealing with the thermal resistance of borehole heat exchangers [12] either using finite element numerical techniques [13, 14] or based on analytical solutions of the heat exchange problem with different more or less realistic simplifying assumptions [15, 16, 17]. The latter are easily applied but can only to a limited type of pipe geometries and under certain conditions. These studies show that factors such as an increased thermal conductivity of the fluid conducting pipes and grout material or a closer distance of these pipes to the borehole wall will improve the thermal performance [90]. In [18] this claims were subsequently demonstrated in several field tests. Other studies focused on the impact of the heat carrier fluid flow rate on the borehole resistance (showing a strong decrease with decreasing flow rate [19]), on the thermo-hydraulic performance of a specific geometry GHE [20] or of a particular installation [21].]. Even [22] proposes an analytical solution basing an entropy minimisation technique in order to calculate the optimal flow rate but this analysis do not consider the heat pump operation.

The evaluation of GSHP investment cost has been carried out in several studies for specific buildings or facilities, mainly comparing with other renewable energies or HVAC technologies. For example, in [91] is carried out an energetic and economic analysis comparing the traditional system (boilers, chimneys and split system air conditioners) with innovative systems: GSHP, GSHP coupled with thermal solar collector, hybrid boiler-GSHP, GSHP coupled with photovoltaic cells. Operating costs are analysed in bibliography by comparison with other systems, mainly economic evaluation of a GSHP system versus an air source heat pump [92] or evaluation of strategies to minimize costs in hybrid systems [93]. Studies show that improving GSHP system efficiency is

usually done by oversizing the BHE field [94] but it is also possible to increase the efficiency decreasing the borehole thermal resistance as described above. In this context, the studies analysed show how to improve the efficiency of the system by comparing different BHE configurations [95, 96]. The aim of this work is not to characterize the best BHE configuration but to analyze the impact of working fluid flow rate on total costs (execution and operation expenditures).

Despite the background described, no studies have been found such this holistic sensitivity analysis of the impact of the heat carrier fluid flow rate on the thermal efficiency of the borehole and its reflection in the execution and operation costs. By means of a reliable analytical tool, previously validated by experimental results, an extensive fluid flow rate evaluation on the thermal efficiency of the borehole is carried out, under different design parameters (conductivity of the borehole materials, pipe and grout).

The validation of the analytical tool from experimental data has been done by means of Thermal Response Tests or TRTs [97, 50], a widely accepted method [37, 98] to determine the main parameters that define the thermal behavior of a borehole: the thermal resistance of the borehole (R_b) and the thermal conductivity of the ground (λ).

A scenario is then presented to evaluate this thermal efficiency impact considering the economic constraints, both in execution (length of borehole required due to thermal resistance of the borehole) and in operation (pumping requirements and geothermal heat pump performance). The study is focused on a single U-tube configuration, first analysing the influence of the flow rate on the thermal borehole resistance and the pressure losses and then conducting a quantification of the impact of the flow rate on drilling and operation costs in a borehole field of 9 single U-tube in two scenarios: constant length and constant efficiency of the BHEs.

5.1.2 Methodology

As explained in [99], the theoretical basis for the thermal calculation of BHEs was established long ago (see [11] for the most comprehensive treatment of the subject so far).

In broad terms, the total thermal resistance (R_{tot}) between the pipe and the ground at a large distance from the pipe centre, mediates the relation between the heat flow q (W/m) and the temperature difference between the fluid inside the pipe (T_f) and the temperature in the surrounding soil (T_g):

$$R_{tot} = \frac{(T_f - T_g)}{q}, \tag{5.1}$$

When the steady flow (or steady flux) conditions are established - after some time - the total heat resistance can be split up into two terms given by:

$$R_{tot} = R_s + R_b, \tag{5.2}$$

where R_s is the soil resistance, mainly related to the ground thermal conductivity (λ) and other soil-related factors and R_b is the – constant – borehole resistance, given mainly by borehole characteristic parameters.

At long enough time, R_s can be well approximated by simple formulas like the line, cylinder or finite line approximations – as discussed [11, 38] -, while R_b is a complex function depending on its geometric features, material properties, internal flow conditions and composite region (grout) conductivity conditions, more difficult to calculate.

5.1.2.1 Analytical tool to evaluate thermal efficiency of BHE according to hydro-geological conditions, geometric characteristics and material properties

According to the established theoretical methodology, heat transfer across borehole pipe is divided into different components which can be treated separately to model the local, steady-state heat conduction problem between the heat carrier fluid in the pipes and the adjacent surrounding ground. All these equations have been integrated into a comprehensive analytical tool that assesses the effective thermal resistance of the borehole. This work is focused on the component of the tool that allows to isolate the influence of fluid flow on heat transfer and pressure losses in a given geometrical configuration (single U-tube). The results are subsequently compared to the experimental results of our TRT tests to asses the validity of the model.

Following [11], this assessment can be characterised by means of the *effective* borehole resistance ($R_{b_{eff}}$) defined as the thermal resistance between the wall borehole temperature and the average temperature inside the borehole heat exchanger. The average temperature is defined as the average between the inlet and outlet temperature at borehole. This effective borehole heat resistance is exactly what a Thermal Response Test (TRT) seeks to determine experimentally from a given real borehole.

More precisely, the effective borehole resistance is defined as:

$$R_{b_{eff}} = \frac{\overline{T} - T_b}{\bar{q}} \tag{5.3}$$

Here it is important to note that $\overline{T}$ represents the *average* fluid temperature inside the BHE, T_b denotes the temperature in the ground at the distance corresponding to the borehole radius and $\bar{q}$ is the average thermal power heat ratio during the thermal test.

The analysis carried out by the tool to calculate the effective borehole resistance is done considering a simplified model for the counter-flow heat exchange between the downward and upward flows and solving the corresponding coupled equation system that involves the z-evolution of the temperatures in both legs (the thermal evolution along the pipe (z axis) of single U-tube for each of the two "legs" (pipes) that compose it).

5.1.2.1.1 Heat transfer assessment

The pipe resistance (R_p) is usually split into three parts [11]:

$$R_p = R_{p,wall} + R_{contact} + R_{fluid} \tag{5.4}$$

The first term ($R_{p,wall}$) relates with the resistance to heat transfer due to the conductivity of the material from which the pipe wall is made of. For a cylindrical wall with inner radius r_p and outer radius r_{po} the relation is given by:

$$R_{p,wall} = \frac{ln(\frac{r_{po}}{r_p})}{2\ \pi\ \lambda_p} \tag{5.5}$$

Note that here λ_p is now the conductivity of the *pipe material*. In the case of conventional polyethylene 100 (PE100) plastic pipes its value is around 0.4 $W/(mK)$ (see new edition of guideline VDI 4640-2[1], published in May 2015).

The $R_{contact}$ *resistance* term quantifies the resistance to heat transfer caused by a non-ideal contact between the outer pipe wall and the surrounding grout. Some authors [11, 100, 101] have discussed what could be reasonable values for $R_{contact}$, but there is no general formulation for this term. In most BHE studies, $R_{contact}$ is not considered and just included as one of the many sources of uncertainty in the analysis of thermal resistances.

[1]VDI 4640 is a widely respected industry standard in Germany and neighbouring countries, first published in 1998, and now comprising 5 parts for different aspects of shallow geothermal energy.

Finally, the R_{fluid} term is given by the heat transfer conditions due to the forced convective process between the fluid at a temperature T_f and the internal wall of the pipe. This process is conventionally represented by the non-dimensional Nusselt number, for which many correlations and studies have been made since long ([102, 103]). The relationship between the resistance and the Nusselt number is given by:

$$R_{fluid} = \frac{1}{\pi \ \lambda_f \ Nu} \tag{5.6}$$

being λ_f the thermal conductivity of the heat transfer fluid (usually water or a glycol and water mixture).

The Nusselt number (Nu) itself depends on different factors. According to the most accepted correlations, mainly on the Reynolds number (Re), the Prandlt number (Pr) and the inner radius of the pipe to borehole deep ratio of the borehole (r_p/H), hence:

$$Nu = f(Re, Pr, r_p/H)$$

$$where \quad Pr = \frac{\mu_f \ c_{p_f}}{\lambda_f} \quad and \quad Re = \frac{4 \ \rho_f \ q_f}{2 \ \pi \ \mu_f \ r_p}$$

For long depth boreholes ($H >> r_p$), r_p/H is close to zero and does not have influence on the process. The quantities appearing in the correlation are hence the basic fluid properties (viscosity, μ_f, heat capacity, c_{p_f}, and density, ρ_f, which are temperature and pressure dependent) and the volume flow, q_f.

For the present analysis, the correlations and fluid property functions were taken from reference [104], the VDI atlas published in 2010. Figure 5.1 summarises the resulting Nusselt number as a function of Reynolds number and a Prandlt number of 5.43 (which corresponds to water at atmospheric pressure and temperature of 30ºC), for circular section pipes with different internal radius to deep ratios according to the implementation of the correlations recommended by VDI Heat Atlas [104]. Each curve is representative for a different diameter, d, to length, l, ratio (in our case, it can be assimilated to inner pipe radius to borehole deep ratio), being the red curve the one that represents the long pipe scenario $r_p/H \approx 0$. As can be seen, in this case the Nusselt number in the laminar flow condition ($Re < 2300$) is basically constant. There is a steep increase of Nu in the transition regime (Re between 2300 and around 10^4) and finally an increase with a constant slope (in logarithmic

representation) is found within the turbulent flow regime ($Re > 10^4$). The blue curve would correspond to a "very short pipe" scenario with a radius to H relation of 1, whilst the red curve at the bottom depicts the result for a very long pipe, were r_p/H is about zero.

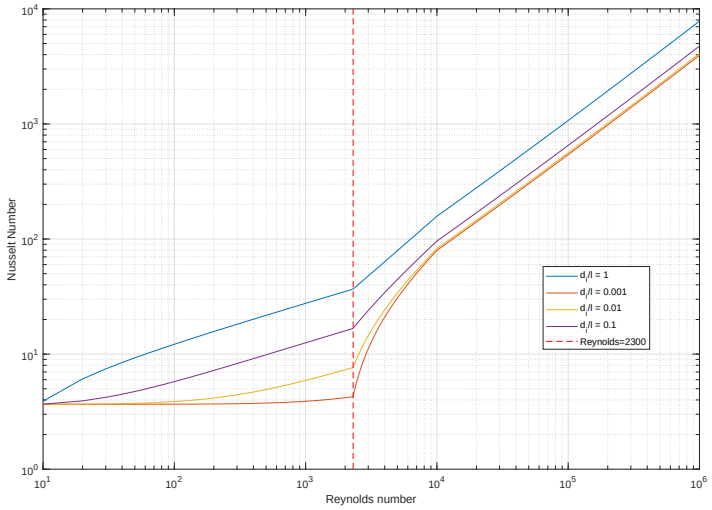

Figure 5.1: Nusselt number as a function of Reynolds number

5.1.2.1.2 Hydraulic assessment

In this analytical tool, within a framework for pressure losses calculation in arbitrary geometries, the calculation of pressure loss caused by a given flow in a circular section unit pipe (based on the Darcy law) using the Gnielinski algorithm have been implemented (as published in [104], chapter L).

Following the traditional Darcy-Weisbach analysis, the pressure loss through a pipe of a given length L, is given by:

$$\Delta P = \xi \frac{L}{d_p} \frac{\rho_f \omega^2}{2} \tag{5.7}$$

where $\omega = \frac{q_f}{\pi r_p{}^2}$ is the mean cross-section fluid velocity in the circular section pipe under consideration, d_p the inner diameter of the pipe and ξ is generally

known as the drag or friction coefficient, which depends on several factors such as the Reynolds number of the flow, the geometry of the flowing channel and the internal surface roughness characteristics.

It is important to state that – to standardise and be able to compare different design solutions – our analysis will be referred to the pipe unit length (L) and thus:

$$\delta p = \frac{\Delta P}{L} = \xi \frac{1}{d_p} \frac{\rho_f \ \omega^2}{2} \tag{5.8}$$

is the pressure drop per unit length of BHE (δp). From this, the ideal hydraulic power per unit of pipe length spent to meet the pumping needs, can be calculated in an easy way:

$$P_h = q_f \cdot \delta p \ , \tag{5.9}$$

where,

P_h is the hydraulic power per unit of length (W/m),

q_f is the volume flow (m^3/s), and,

δp is the differential pressure (Pa/m) [from equation 5.8]

5.1.2.1.3 Friction coefficient and pumping losses calculation

In the case of a circular pipe, the correlation recommended in the VDI atlas [104] and valid for smooth pipes establishes that the friction factor (ξ):

$$Laminar flow \ \ (Re < 2300): \quad \xi = \frac{64}{Re} \tag{5.10}$$

$$Turbulent flow \ \ (2300 < Re < 10^4): \quad \xi = \frac{0.3164}{\sqrt[4]{Re}} \tag{5.11}$$

And the Reynolds number:

$$Re = \frac{\rho_f \ \omega \ d_H}{\mu_f} = \frac{2 \ \rho_f \ q_f}{\pi \ r_p \ \mu_f} \tag{5.12}$$

being, $d_H = d_p$ and $\omega = \frac{q_f}{A_p} = \frac{q_f}{\pi \ {r_p}^2}$.

5.1.2.2 Capital and operating costs

Costs related to ground source heat pump installation can be classified into three main groups: investment costs, operating costs and decommissioning and disposal costs. First group refers to how much it cost to install the geothermal system, that is the cost of drilling, trenching, installing pipes, hydraulic components, circulation pump and heat pump. Operating costs are the annual costs incurred during operation such as electricity bills or maintenance work. Finally, decommissioning costs include scrapping of heat pump, disposal of refrigerants or restoration of land due to the boreholes.

In this article, the installation costs of drilling and equipping the geothermal borehole at designed depth and the energy operating costs (the electricity consumption of the heat pump during its operating time and the electricity consumption of the circulation pump necessary to overcome hydraulic losses) are analysed for different scenarios in a typical geothermal installation.

According [105], the Capital Expenditures (CAPEX) [€/year] can be calculated using the following expression:

$$CAPEX = \frac{C_1 \cdot n \cdot L}{N}, \tag{5.13}$$

where,

C_1 is the total cost of a equipped borehole per drilled meter (€/m),

n is the number of boreholes,

L is the borehole depth (m), and,

N is installation amortisation period (years).

In this case, only the capital expenditures related to the borehole field are taken into account as these are the only ones affected by the thermal efficiency of the borehole.

And, the Annual Energy Operating Costs (OPEX) [€/year]:

$$OPEX = AOC_{HP} + AOC_{CP} = C_{HP} \cdot h \cdot C_e + C_{CP} \cdot h \cdot C_e \ , \tag{5.14}$$

where,

AOC_{HP} is the Annual energy Operating Cost of Heat Pump (€/year)

AOC_{CP} is the Annual energy Operating Cost of Circulating Pump (€/year)

C_{HP} is the Heat Pump electrical hourly consumption (kW),

C_{CP} is the Circulation Pump electrical hourly consumption (kW),

h is the number of operating hours per year, and,

C_e is the electricity cost (€/kWh).

To quantify these costs, hydraulic losses must be calculated based on the characteristics of the BHE using an analysis tool that allows a thermal and hydraulic evaluation of the borehole.

5.1.3 Experimental validation

In order to validate the tool and the conclusions obtained from the analytical study, several thermal tests (called Thermal Response Test, or TRT) were performed with a constant and controlled heat injection at different flow rates to allow the thermal transfer in the borehole to be characterised.

The methodology used in these thermal tests is described in [35] and highlights the importance of a strict thermal heat injection control (by means of a PID). In this way, more precise results are obtained than in the traditional methodology, in which no control of thermal injection is carried out, being limited only to the generation of a constant heat pulse that does not take into account thermal losses of the connecting pipes and the thermal influence of the fluctuating outdoor temperatures.

The experimental validation was carried out by means of 3 thermal tests (TRTs) on a single U-tube borehole heat exchanger installed at Universitat Politècnica de València (see Figure 5.2 that shows the position of the temperature sensors at inlet and outlet of the borehole).

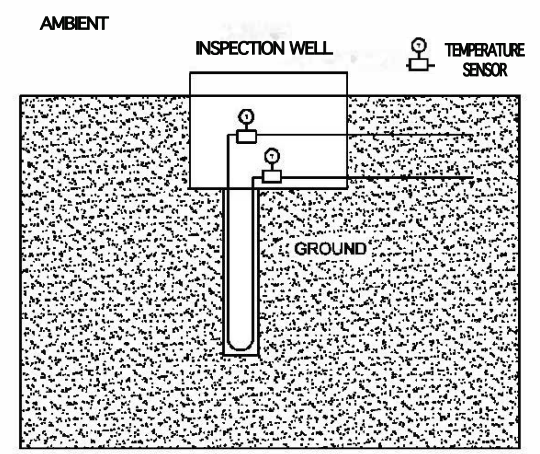

Figure 5.2: Scheme of the single U-tube borehole with temperature sensors position

5.1.3.1 Experimental data

Borehole characteristics are 15 meters deep and diameter of iron casing 126/101 mm equipped with a PE-Xa probe, 32 mm of diameter and 2.9 mm thick, and filled with a commercial thermal grout. Table 5.1 summarises all technical parameters of the borehole, which are then used as input parameters to the analytical tool.

Table 5.1: Parameters of single U-tube borehole

Borehole type	single U-tube	**Borehole probe**	RAUGEO PE-Xa green
Borehole deep	15 m	**Effective borehole length**	14.6 m
Borehole diameter	126 mm	**Casing thickness**	12.5 mm
Outer diameter	32 mm	**Inner diameter**	26.2 mm
Pipe thickness	2.9 mm	**Distance between centers**	75 mm
Pipe thermal conductivity	0.41 W/mK	**Grout Thermal conductivity**	1.2 W/mK

The thermal tests were performed at the geothermal laboratory test site located inside the Universitat Politècnica de València campus. All the information on the description of the installation is provided in Chapter 2.1 of Reference [35]. TRTs were carried out with different thermal power rate and fluid flow rate and their main parameters are indicated in Table 5.2.

Table 5.2: Main test parameters

Test #	**Flow** ($l\ s^{-1}$)	**Reynolds number** [1]	**Thermal power injected** ($W\ m^{-1}$)
1	0.022	1625	40
2	0.044	3249	80
3	0.083	5908	60

[1] water properties at 40^{o}C: density 992.3 kg/m^3 viscosity 0.000653 $kg/(ms)$

The thermal test duration was variable but longer than 100 hours. Test were performed, for three different Reynols numbers: Test 1 under laminar flow conditions, Test 2 in the boundary between laminar and turbulent flow and Test 3 under turbulent flow in order to analysed Reynolds influence in borehole thermal resistance. Both the installation for carrying out the thermal tests and its procedure are thoroughly described in [106].

The raw temperature data logged during the thermal test (average temperature between borehole inlet and outlet sensors - see Figure 5.2 - and thermal power injection) of each TRT carried out is shown in Figure 5.3.

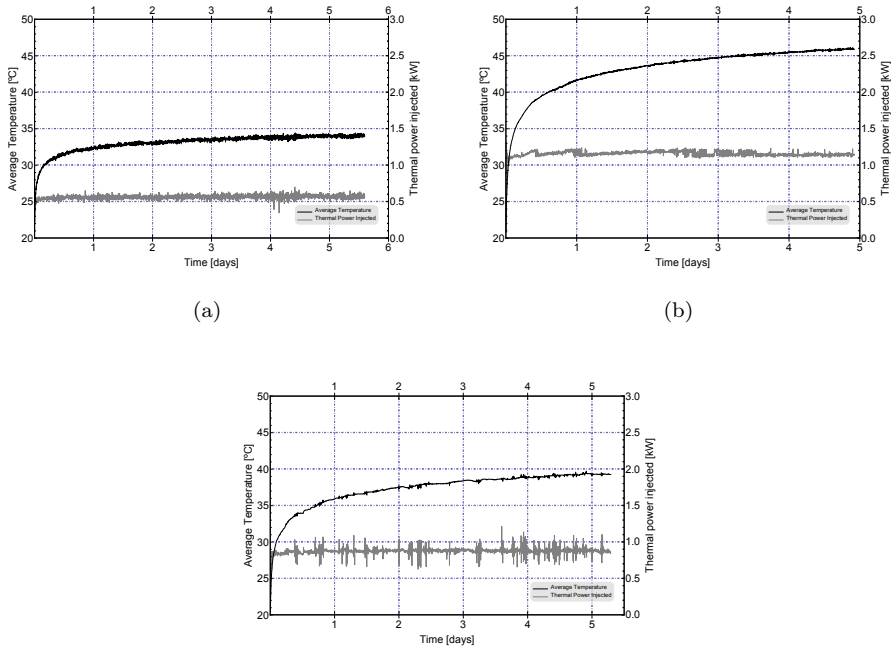

(a) (b)

(c)

Figure 5.3: Average temperature (black) and thermal power injected (grey)
(a) Test 1 (b) Test 2 (c) Test 3

5.1.3.2 Comparing results

The procedure used for the analysis of the TRTs is explained in detail in [42] and the parameters thermal conductivity of the ground (λ), borehole thermal resistance (R_b), undisturbed ground temperature (T_0) and ground thermal diffusivity (α) are drawn by means of a method of adjustment (emplsqurvefit) to the main models (Infinite Line Source Model -ILSm-, Finite Line Source Model -FLSm- and Finite Cylindric Source Model -FCSm-), using the *Levemberg-Marquardt* algorithm implemented in Matlab©.

The geological setting of the borehole field corresponds to continental alluvial sediments like sands, silts, conglomerates, peat deposits, etc, (Quaternary deposits). Sediments are related to the activity of major river (Turia) and small ravines that have influenced the geomorphology of the Valencian region during the Quaternary [107]. The hydrogeological regime in this area was

described in [42]. The area has been characterized with a low estimated Peclet number [42]. For this reason, the possible influence of the groundwater flow has not being considered in the models applied.

The comparison between the experimental results and the model data is presented below, by selecting in each experiment the model (ILSm, FLSm or FCsm) that yields the least Mean Squared Error (see Figures 5.4, 5.5 and 5.6). As can be seen, in the case of the cylindrical model, no adjustment was obtained with the lowest Mean Squared Error.

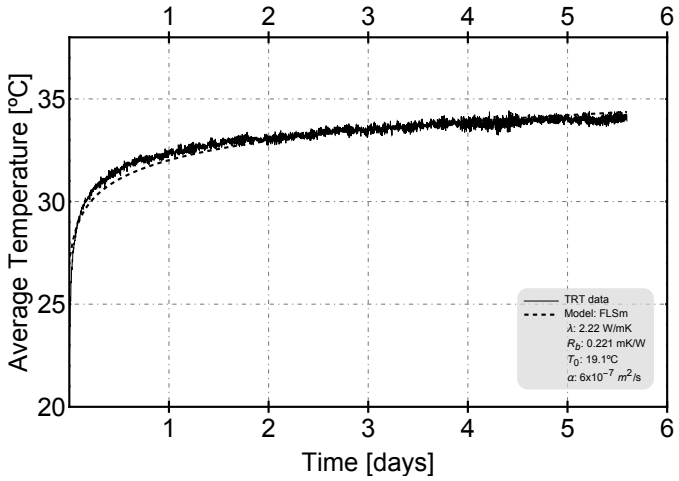

Figure 5.4: Fitting model of Test 1

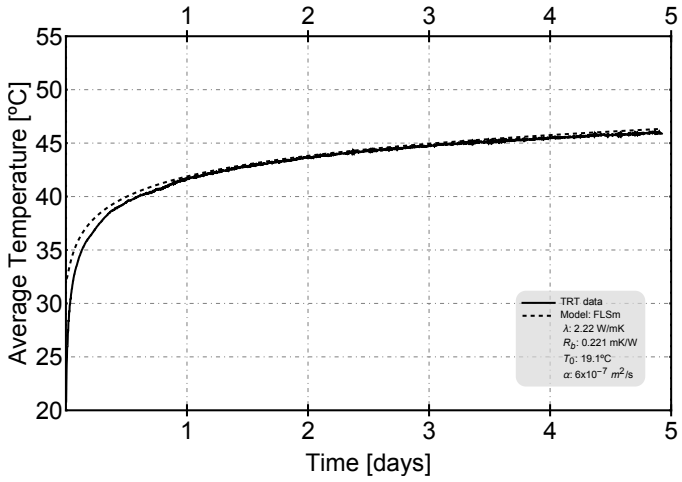

Figure 5.5: Fitting model of Test 2

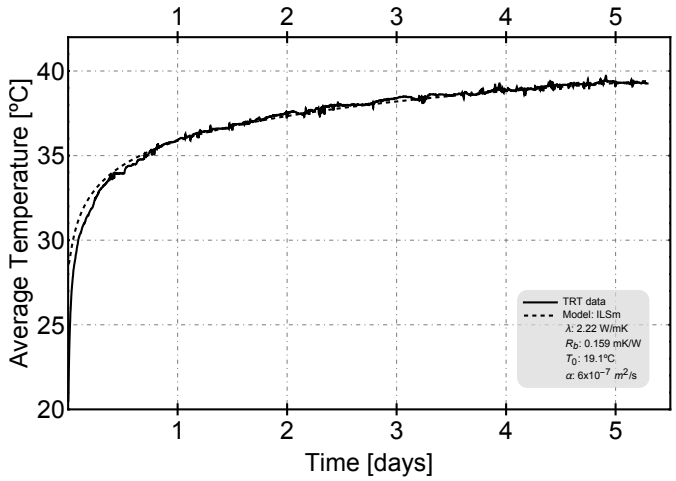

Figure 5.6: Fitting model of Test 3

On the other hand, to build the analytical tool, the analytical formulas described in the previous subsection were implemented as a collection of Mathematica© [108] functions that allow a flexible and general access to a variety of tools to analyse and visualise results. The resulting graphs for the optimisation analysis of single U-tube are shown in the next chapter.

Figure 5.7 shows the good correlation between the experimentally determined borehole resistances and the predicted values. The results correspond to the standard PE-100 plastic pipe single U-tube BHE of our facility at UPV measured at three different volume flows (ranging from laminar to highly turbulent). The individual dots (∘) represent the experimental data (from TRT tests) whilst the continuous curve represents the calculated values at any flow rate.

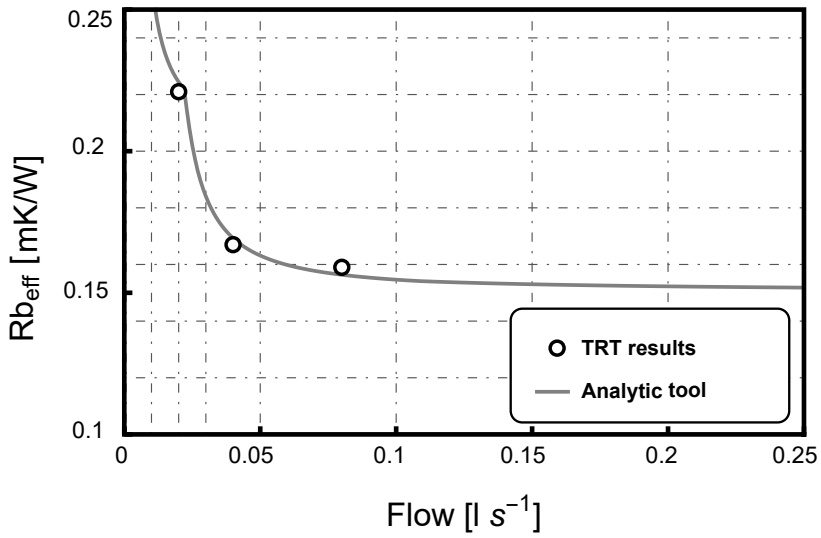

Figure 5.7: Flow influence on thermal borehole resistance (Rb) [analytical and experimental data]

Table 5.3: TRT results and comparison

Test #	TRT Results				Analytical tool	
	λ (W/mK)	R_b (mK/W)	Ad. R-Squared	Mean Squared Error	R_b (mK/W)	Error (%)
1	2.22	0.221	0.89 (FLSm)	$1.92x10^{-2}$ (FLSm)	0.224	1.36
2	2.23	0.167	0.99 (FLSm)	$2.21x10^{-3}$ (FLSm)	0.166	-0.60
3	2.22	0.159	0.97 (ILSm)	$8.77x10^{-3}$ (ILSm)	0.157	-1.26

Table 5.3 shows the results of the experimental tests (from adjustments shown in Figures 5.4, 5.5 and 5.6) and compares them with the results obtained by the analytical tool for the same characteristics of each thermal experiment. As it can be observed, the values of borehole thermal resistance obtained by means of the analytical tool predict with considerable accuracy the values obtained by the experimental analysis, which justifies the robustness of the results obtained with the analytical tool for the optimization analysis detailed in the following chapter.

5.1.4 Optimization assessment

The methodology explained in Section §5.1.2 was implemented in the framework of European projects GEOCOND[2] and GEO4CIVHIC[3] to allow a general setting for the optimisation of materials and geometrical configurations of BHEs. This methodology is used here to calculate the effective borehole thermal resistance ($R_{b_{eff}}$) and the hydraulic parameters (pressure losses) in a single U-tube borehole configuration to characterise the installation's operating costs analysing their mutual influence. Firstly, the influence of the flow rate on the thermal borehole resistance and the pressure losses in a single U-tube borehole are studied analytically through the tool. This analysis is then extended to a combined study of the influence of the conductivity of the materials (pipes and grout). Subsequently, a case study of a typical geothermal installation is carried out to quantify the impact of the flow rate on drilling and the operating costs (based on the electricity consumption of the heat pump and the circulation pump) in two limiting scenarios, constant length and constant efficiency of the BHEs.

[2]Further information at https://geocond-project.eu/
[3]Further information at https://geo4civhic.eu/

5.1.4.1 Thermal resistance and pressure losses analysis by means of analytic calculations

Once the results obtained by means of the analytical tool have been validated experimentally, the following analysis has been carried out: the influence of the fluid flow rate on pressure losses per meter of borehole has been calculated by the tool in order to subsequently show the relevant correlation between the pressure drop in the borehole and the thermal efficiency of the borehole.

In Figure 5.8, the flow rates analysed are shown reflecting the pressure drop resulting from each unit of borehole length (Pascal per meter). As expected, hydraulic losses in the borehole increase exponentially as the flow rate of fluid through it increases.

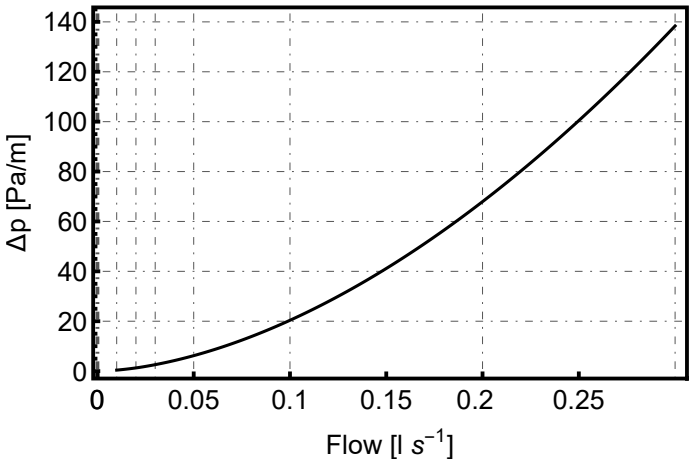

Figure 5.8: Flow influence on Pressure Drop per borehole length

Combining Figures 5.7 and 5.8 results Figure 5.9, which shows the significant relationship between the thermal resistance of the borehole and the pressure losses produced.

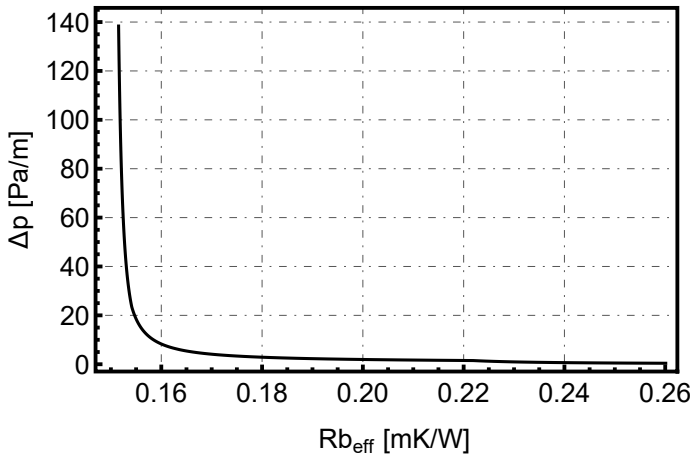

Figure 5.9: Pressure drop vs. effective borehole resistance ($R_{b_{eff}}$)

It can be observed that to obtain very low values of borehole thermal resistance, a very high energy expenditure in pumping is required; and, conversely, to obtain low pressure losses, the thermal efficiency of the borehole has to be penalized. But, as it can be observed in the graph, in each configuration and properties of the borehole, there is an optimal point that minimizes those two values (the closest value to the origin). In our case, the optimal point would be approximately for a flow rate of 0.08 l/s ($R_b : 0.152\ mK/W, \Delta p : 12\ Pa/m$).

5.1.4.2 Multi-parameter analysis

The combined influence of pipe conductivity, grouting material conductivity and fluid flow rate on the efficiency of the borehole thermal resistance has also been analysed given the robustness of the analytical tool developed.

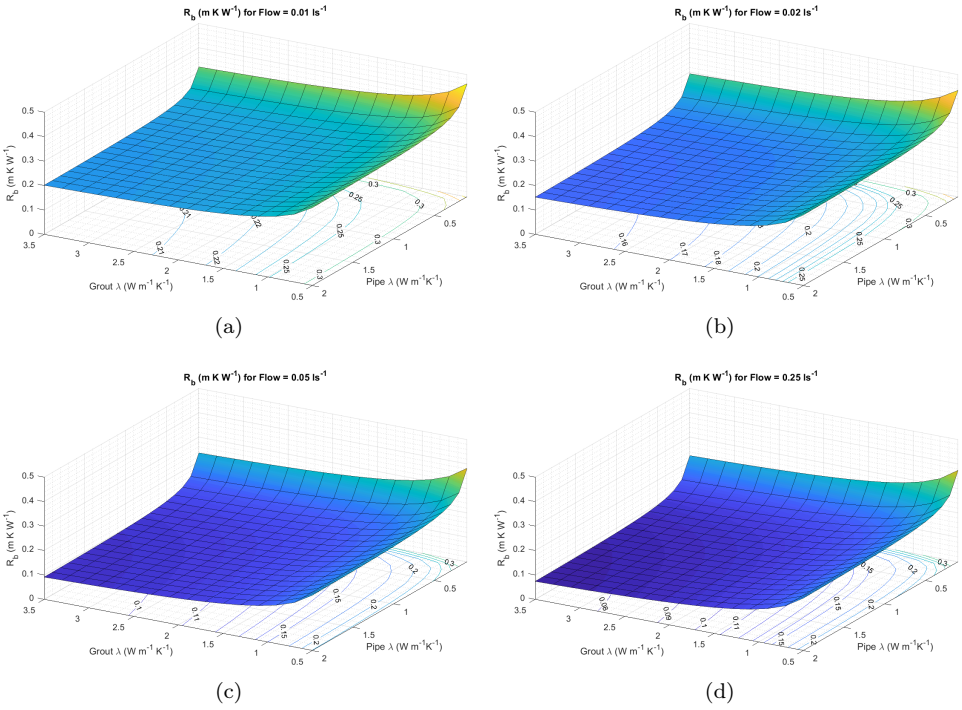

Figure 5.10: R_b surfaces for different flow values (in l/s): (a) 0.01, (b) 0.02, (c) 0.05 and (d) 0.25

This was performed by calculating the thermal resistance of the borehole with different input parameters of pipe conductivity, grouting material conductivity and heat carrier fluid flow rate. In Figure 5.10, different R_b surfaces can be seen depending on these material conductivities for 4 reference flow rate values.

Figure 5.11 shows iso-R_b surfaces: combinations of pipe conductivity, grout conductivity, and flow rate where the same borehole resistance value is obtained (the same thermal efficiency at the borehole heat exchanger).

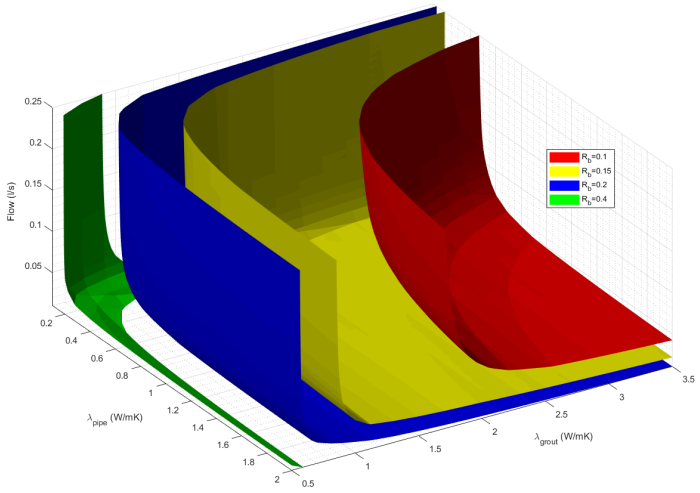

Figure 5.11:]
Iso-surfaces for selected values of R_b: 0.1, 0.15, 0.2 and 0.4 mK/W

The above Figures show the importance of the impact of not only optimal flow values, but also of the added effect of improved conductivity values of the pipe and grout, which can, conjointly, significantly improve the thermal efficiency of the borehole.

5.1.4.3 Scenario analysis

For a more detailed study of the influence on execution and operating costs, a case study is performed defining the characteristics of a geothermal installation. The installation under study is a 420 m^2 residential building located in a continental climate (Csb according to Köppen climate classification) and due to the mild summer, the it only requires a heating system, supplied by a geothermal heat pump with power capacity of 28 kW. The building complies with the Spanish construction standard (Technical Building Normative, 2013 [109]) that implies the following thermal transmittance U-values in the envelope elements: 0.6 W/Km^2 in the facade, 0.4 W/Km^2 in the floor and ceiling and 2.7 W/Km^2 in windows and external doors with a maximum of air permeability of 27 m^3h/m^2. Building hourly thermal demand (there is not heating thermal load during the summertime) is showed in Figure 5.12 (yearly heating thermal load of the building is 171.94 kWh/m^2)

and the main installation characteristics are collected in Table 5.4. This scenario was analysed using the DesignBuilder software, EED (Earth Energy Designer) [110], by carrying out hourly simulations of the thermal behaviour of the geothermal heat exchanger field.

The borehole field consists of 9 single U-tube boreholes of same characteristics of Table 5.1 with 90 depth and 6 meters separation between them.

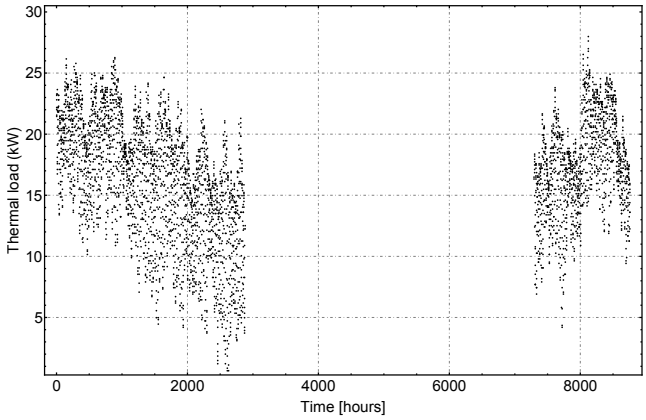

Figure 5.12: Hourly thermal demand (heating) of case study

Table 5.4: Parameters of scenario

Borehole field			
Borehole type	single U-tube	**Borehole parameters**	See Table 5.1
Borehole field	9x90 m	**Borehole separation**	6 m
Ground properties			
Undisturbed ground temperature [1]	18 $°C$	**Ground conductivity**	2.3 W/mK
Pipe properties [2]			
Installation properties			
Heat Pump	GMSW 28 HK [3]	**Pipe distance from borehole to Heat Pump**	2x35 m
Common pressure losses (filter, heat pump heat exchanger, fittings,..)			90 kPa

[1] Average ground temperature of heat exchange between the ground and the borehole

[2] single U-tube borehole of same characteristics of Table 5.1

[3] See Figure 5.13 for technical data

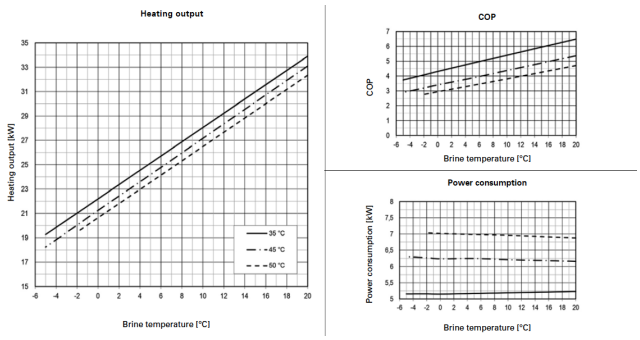

Figure 5.13: Performance curves of GMSW 28 HK Heat Pump depending on supply temperature of heating system [111]

5.1.4.3.1 Same borehole field

In the following assessment, a geothermal drilling field of the same length - 9 boreholes of 90 meters depth - for all flow rates is analysed to determine the influence of the flow on the overall cost of the geothermal system (drilling and operation costs).

The results are listed in Table 5.5.

Table 5.5: Results of same borehole field scenario

Case #	Flow	Borehole	CAPEX	OPEX						Total
	($l\ s^{-1}$)	field	Cost [1]	SPF [2]	h [3]	AOC_{HP} [4]	ΔP_b [5]	CP [6]	AOC_{CP} [7]	Costs
1	0.033	9x90m	2106€/year	3.88	2980h	2429.65€/year	0.8kPa	64.2W	24.88€/year	4560.53€/year
2	0.044	9x90m	2106€/year	4.02	2882h	2337.81€/year	1.32kPa	86.1W	32.26€/year	4476.07€/year
3	0.064	9x90m	2106€/year	4.30	2701h	2183.70€/year	2.54kPa	126.9W	44.56€/year	4334.26€/year
4	0.083	9x90m	2106€/year	4.37	2660h	2148.04€/year	4.01kPa	167.2W	57.82€/year	4311.86€/year
5	0.100	9x90m	2106€/year	4.41	2637h	2128.11€/year	5.56kPa	204.8W	70.20€/year	4304.31€/year
6	0.150	9x90m	2106€/year	4.48	2600h	2096.65€/year	11.30kPa	325.6W	110.06€/year	4312.71€/year
7	0.200	9x90m	2106€/year	4.51	2582h	2081.48€/year	18.70kPa	465.8W	156.37€/year	4343.85€/year
8	0.250	9x90m	2106€/year	4.53	2571h	2072.25€/year	27.63kPa	630.2W	210.62€/year	4388.87€/year

[1] $C_1 = 65$ €/m and $N = 25$ years

[2] See Appendices A-H

[3] Operating hours

[4] $C_2 = 13$ c€/kWh_{elect}

[5] Borehole pressure losses

[6] Circulation pump power capacity

[7] $C_{CP} = P_h \cdot \eta_{pump} \cdot \eta_{elect} \cdot L, \quad \eta_{pump} = 0.6, \quad \eta_{elect} = 0.7, \quad L = 250m, \quad C_2 = 13$ c€/kWh_{elect}

Following Figure 5.14 shows the total costs per year depending on the flow rate. Very low working fluid flow rate results in higher total costs, due to the increased electricity consumption of the heat pump operation [AOC_{HP}] because of the low thermal efficiency of the borehole (higher working

temperatures in the borehole field, as can be found in the Appendices). As the fluid flow rate increases, these total costs are reduced (higher thermal efficiency of the borehole), but after a certain point (in this case study, approximately 0.1 l/s), the pumping costs [AOC_{CP}] start to play a bigger role, increasing the total costs.

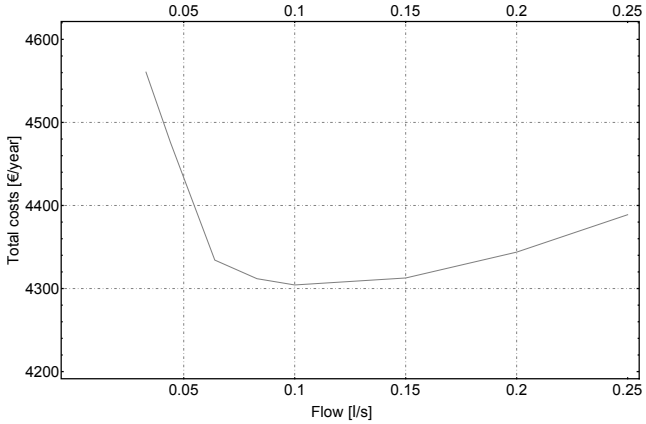

Figure 5.14: Total costs per year depending on flow rate in same borehole field scenario

The additional data from the simulations performed for each case can be seen in the Appendices A to H. For each case it is shown:

- The annual evolution of the inlet and outlet temperatures of the heat transfer fluid, which depend on the thermal performance of the borehole (R_b).
- The hourly thermal capacity of the heat pump and the rate of heat injected to the borehole throughout the year.
- The electric consumption of the heat pump and its efficiency (Coefficient of Performance -COP-) calculated based on the heat pump rating. The value of the SPF indicated in the analysis is the COP annual average.

5.1.4.3.2 Same heat pump efficiency

By means of the Energy Earth Design (EED) software, taking as a reference the operating temperatures in the borehole field in Case #3, the total length of the geothermal field has been modified to equal those temperatures (see Figure C1), and therefore, obtain the same electrical efficiency - SPF - in the heat pump. Consequently, in cases where low flow rates penalise the thermal efficiency of the borehole, the necessary length of the geothermal field increases,

and in cases of high flow rates, as there is a better thermal efficiency, a shorter length of the borehole field is required.

The simulation results are listed in Table 5.6.

Table 5.6: Results of same heat pump efficiency scenario

Case #	Flow ($l\ s^{-1}$)	Borehole field	CAPEX Cost [1]	OPEX SPF	h [2]	AOC_{HP} [3]	ΔP_b [4]	CP [5]	AOC_{CP} [6]	Total Costs
1	0.033	1215m	3159.00€/year	4.30	2701h	2183.70€/year	0.8kPa	64.2W	24.88€/year	5367.58€/year
2	0.044	990m	2574.00€/year	4.30	2701h	2183.70€/year	1.32kPa	86.1W	32.26€/year	4789.96€/year
3	0.064	810m	2106.00€/year	4.30	2701h	2183.70€/year	2.54kPa	126.9W	44.56€/year	4334.26€/year
4	0.083	738m	1918.80€/year	4.30	2701h	2183.70€/year	4.01kPa	167.2W	57.82€/year	4160.32€/year
5	0.100	702m	1825.20€/year	4.30	2701h	2183.70€/year	5.56kPa	204.8W	70.20€/year	4079.10€/year
6	0.150	657m	1708.20€/year	4.30	2701h	2183.70€/year	11.30kPa	325.6W	110.06€/year	4001.96€/year
7	0.200	630m	1638.00€/year	4.30	2701h	2183.70€/year	18.70kPa	465.8W	156.37€/year	3978.07€/year
8	0.250	617m	1604.20€/year	4.30	2701h	2183.70€/year	27.63kPa	630.2W	210.62€/year	3998.52€/year

[1] $C_1 = 65$ €/m and $N = 25$ years

[2] Operating hours

[3] $C_2 = 13$ c€/kWh_{elect}

[4] Borehole pressure losses

[5] Circulation pump power capacity

[6] $C_{CP} = P_h \cdot \eta_{pump} \cdot \eta_{elect} \cdot L, \quad \eta_{pump} = 0.6, \quad \eta_{elect} = 0.7, \quad L = 250m, \quad C_2 = 13$ c€/kWh_{elect}

Following Figure 5.15 shows the total costs per year depending on the flow rate. At very low working fluid flows, very high total costs are observed, strongly penalized by the elevated drilling costs [CAPEX], due to the longer length of the borehole heat exchanger required to obtain the same thermal efficiency in the heat pump (same working temperatures in the borehole field). As the fluid flow rate increases, these total costs are reduced (lower drilling costs), but after a certain point (in this case study, approximately 0.15 l/s), the pumping costs [AOC_{CP}] start to play a bigger role, increasing the total costs. However, in the analyzed flow rates these pumping costs [AOC_{CP}] do not exceed the savings in drilling costs (although they are expected to do so at higher flows).

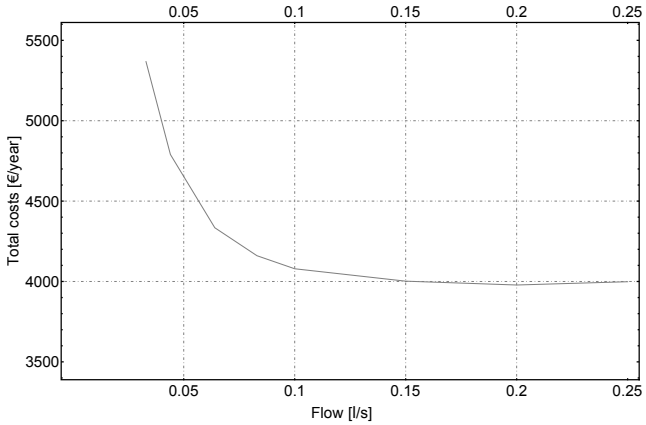

Figure 5.15: Total costs per year depending on flow rate in same heat pump efficiency scenario

5.1.5 Conclusions

This work has analysed the investment and operating costs of a typical BHE configuration taking into account the relationship between its thermal efficiency and hydraulic losses at different fluid flow rates. An extensive theoretical and numerical tool was developed to filter, refine and finally select optimal borehole configuration meeting the required criteria arising from the installation and conductivity material and evaluating the correlation between borehole thermal efficiency ($R_{b_{eff}}$) and borehole pressure losses depending on the fluid flow rate. This tool has been experimentally validated with results from thermal tests (TRTs) at three different flow rates, obtaining errors between the calculated and the experimental values of less than 1.5%.

The following results can be concluded:

- As expected, the borehole thermal resistance value significantly depends on the flow rate (see Figure 5.7). Within laminar flow (below 0.04 l/s), borehole thermal resistance is rapidly increasing with small flow rate decreases, whereas in turbulent flow, a further increase in the flow rate produces only a marginal decrease in the borehole thermal resistance.
- Since pressure losses in the borehole heat exchanger are correlated with the value of the thermal resistance (see Figure 5.8), an optimum value is observed where the pressure losses have already decreased considerably, reducing the electrical pumping costs.

– For the same flow rate value and hydraulic losses, the borehole characteristic that most penalises borehole thermal efficiency is the low thermal conductivity of the pipe material (Figure 5.10), having more influence on the borehole thermal efficiency than the value of the grout thermal conductivity.

– The difference obtained in borehole thermal efficiency values between the lowest pipe thermal conductivity and the highest for the same grout conductivity is about 0.2 mK/W for all values of flow rates analysed. This relevant result, which is not a main objective of this article, opens an interesting field to analyse in future works.

To complete this theoretical analysis, hourly numerical simulations by EED program of a case scenario were carried out to check the influence of working fluid flow rate on the total costs of the installation (drilling and operating costs). As can be seen from both the analysis with the analytical tool and the scenario simulations, the flow rate affects both the efficiency of the borehole (and therefore the efficiency of the heat pump - SPF), and the pumping costs. Working at low flow rates will result in lower borehole efficiency, with a cost overrun on heat pump consumption. On the other hand, operating at too high flows will increase the cost of pumping.

The conclusions that can be drawn are as follows:

– As shown in Table 5.5, for the same increase in circulating flow, the improvement in the energy consumption of the heat pump is higher at low flow rates. For example, the running cost of the heat pump is reduced 4% with a flow increase from 0.033 to 0.044 l/s, but the reduction is about 0.4% in the range between 0.2 and 0.25 l/s.

– When the flow rate exceeds a certain value, the penalty in the pumping operating costs are higher than the decrease in electricity consumption due the improved heat pump performance. An optimum flow rate that optimises the total costs of a certain BHE can be determined according to the scenario characteristics. In the case studied, this optimum is at a value of 0.1 l/s (Figure 5.14) representing 70% of nominal design flow rate.

– If the design objective is to set the performance of the heat pump, there is a carrier flow threshold value from which a decrease in the total costs of the installation is not very significant (Figure 5.15).

– In both cases, for the scenario analysed, it is observed that operating the installation with an inadequate fluid flow rate can produce an increase in

the total electricity consumption of the geothermal installation of between 4 and 10% (see Figures 5.14 and 5.15).

To conclude, the extensive analysis carried out in this article shows that the thermal efficiency of a BHE increases as pumping losses increase, existing, depending on borehole typology and characteristics, an optimal design point that minimises both. What this highlights is the importance, when designing a geothermal installation, of carrying out a hydraulic assessment to evaluate the influence of the fluid flow in the borehole on both the thermal efficiency of the borehole and the electrical expenditure on the circulation pump, and therefore, a compromise must be reached between both, mainly taking into account that both have impact on the operating cost of a ground source heat pump system. This optimal value can be determined for each specific installation following the methodology described in this work.

It has to be considered that, according to the theoretical analysis, only part of the pressure losses were included (related with the friction within the pipes). A more complete picture would need to account for additional losses caused by other system elements such as bends, valves or other singularities present in the system. On the other hand, another future work would be the evaluation with more complex thermal models that consider the groundwater flow.

5.2 Thermal borehole performance assessment of coaxial borehole according to working fluid flow rate

5.2.1 Heat transfer process in coaxial heat exchanger geometry

The study of the internal heat exchange process in the so called "annular passage" of a coaxial borehole is much more involved and less well characterized than in the case of a circular pipe as discussed above. This is since the thermal contact involves two surfaces with different radii and heat transfer conditions. The heat transfer process depends on many more factors: internal and external radius, flow velocities at both sides, distance from the entrance. One further complication is that the Nusselt number depends on the relationship between the heat transfer rates at both side (there are different characteristic configurations in this regard). This implies that in a coaxial arrangement the problem is highly coupled and should be tackled iteratively. There is a vast theoretical and experimental literature on this subject (see [102, 103]).

Moreover, the transition flow regime in annular passages is much less well known than in the circular pipes case and in coaxial BHEs, the Reynolds number is different in the upward and downward channels. This fact further

difficult the analysis and increases the uncertainty in the Nusselt number estimation.

Like in the case of the circular pipes, for the purpose of this analysis we have chosen the approach used in the VDI 2010 Heat Transfer Atlas [104], using the Gnielinsky correlations as a reference. This approach uses basically similar functions such as used in the circular duct case but utilizing a modified version of the Reynolds number. According to [104], this approach offers the best correspondence with a vast number of experimental researches on the topic available at that time, although new experiments have done added since then. A similar approach is used to estimate the friction coefficients for the pressure loss calculation in an annular duct. The modification of the Reynolds number introduced by Gnielinsky and supported by the VDI guide is given by:

$$Re^* = Re\ \frac{(1+a^2)\ ln[a] + (1-a^2)}{(1-a)^2\ ln[a]} \tag{5.15}$$

with $a = r_i/r_o$ the ratio of the radii of the internal and external surfaces of the annular passage (see Figure 5.16).

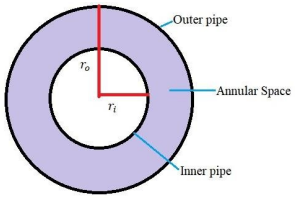

Figure 5.16: Coaxial annular passage scheme, with r_i and r_o definition

5.2.2 Pressure losses in coaxial heat exchanger geometry

In the case of a coaxial geometry (see Figure 5.16), the downward and upward legs have different Reynolds numbers (Re_1 and Re_2). In the annular duct, we follow the recommended correlation in the VDI atlas, based on the Gnielinsky correlations:

$$Re_1 = \frac{2\ V_f\ \rho_f}{r_o\ \pi\ \mu_f\ (1+a)} \frac{(1+a^2)\ ln[a] + (1-a^2)}{(1-a)^2\ ln[a]} \tag{5.16}$$

In this scheme, the correlation for the drag coefficient is the same as for the circular section pipe but based on the modified value of the Reynolds number

inside the annular channel, Re_1. And r_o is the outer radius of the annular passage.

For the returning circular pipe, the calculation is the same as a circular section pipe (see equation 5.12), with the Reynolds number given by:

$$Re_2 = \frac{2\ \rho_f\ V_f}{\pi\ r_i\ \mu_f} \tag{5.17}$$

while now r_i is the internal radius of the upward (internal) pipe.

Based on these correlations (equations 5.16 and 5.17) it is possible to calculate the pressure loss of a coaxial BHE unit length as:

$$\delta p = \delta p_1 + \delta p_2 = \xi \frac{1}{d_H} \frac{\rho_f\ \omega_1^2}{2} + \xi \frac{1}{d_i} \frac{\rho_f\ \omega_2^2}{2} \tag{5.18}$$

and the pumping loss per unit length can be found as ($\delta W_p = \delta p\ V_f$). It is important to note that the reference diameter for the Darcy equation in the case of an annular passage is the hydraulic equivalent diameter given by $d_H = d_o - d_i = 2\ (r_o - r_i)$.

An important question that arises in the case of coaxial heat exchanger is the pressure loss balance between the downward and upward legs, i.e. to ensure that the pressure losses in both legs are not very distinct, in order to avoid problems in the hydraulic balance of the system.

5.2.3 Thermal borehole performance assessment of coaxial borehole according to working fluid flow rate

The optimum diameter configuration has been analyzed, considering the assembly needs, the grouting process and the difference in thermal conductivity of the pipes (external and internal). The objective is twofold; on the one hand, to reduce the thermal resistance of the borehole as much as possible, and on the other hand, to obtain the minimum hydraulic losses due to friction in the pipe as previously discussed.

In this sense, it was decided to fix the maximum outer diameter of the outer pipe at 80 mm because the standard drilling diameter is about 110 mm and the constraint to keep some additional space available to introduce the "trimie" pipe for grouting. Moreover, the industrial conventional dimensions for PE-100 pipes with pressure resistance of at least 16 bars is 75 mm, outer diameter and 6.8 mm wall thickness. Considering these constraints, the external pipe diameter selected for testing is the 75 mm. For the inner pipes, considering the

different solutions in the market, external diameters of 40 and 50 mm are the two feasible options that will be studied.

The methodology employed was as follows: the two most realistic configurations for the coaxial heat exchanger have been selected from the commercial diameters currently on the market, according to the diameter of the drilling rig. Therefore, the external pipe analyzed is a plastic pipe with an external pipe diameter of 75 mm, an internal diameter of 61.4 mm, a thickness of 6.8 mmand a conductivity of 1.1 W/mK. Two cases have been studied for the inner pipe: plastic inner pipe with an outer diameter of 50mm, an inner diameter of 40.8 mm, a thickness of 4.6 mm and a conductivity of 0.1 W/mK or plastic inner pipe with an outer diameter of 40 mm, an inner diameter of 32.6 mm, a thickness of 3.7 mm and a conductivity of 0.1 W/mK.

One of the major issues when dealing with coaxial geometries are the high pressure drops that appear in some configurations or depending on the volume flows. One question that can be asked to the theoretical analysis is to highlight how pressure drop and borehole resistances depend on certain geometric choices. Given the constraints, with a fixed external pipe diameter of 75, the analytical tool was asked to calculate borehole resistances and pressure drops in a continuous range of internal pipe diameters ranging from less than 20 mm to 60 mm. Two internal pipe thicknesses were considered corresponding to the 75/50 and 75/40 real pipe configurations.

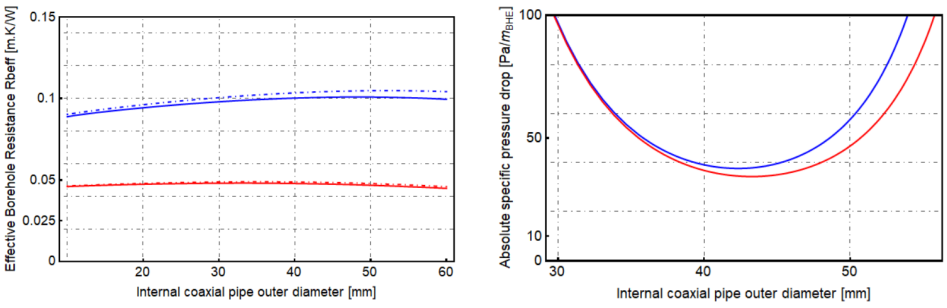

(a) (b)

Figure 5.17: Effective borehole resistance R_b vs. Absolute specific pressure drop for varying internal pipe dimensions

Figure 5.17 (a) shows effective borehole resistance R_b of a coaxial plastic arrangement for varying internal pipe dimensions and fixed external pipe diameter of 75 mm. The blue curves correspond to solutions in which both

(internal and external tubes) are made off standard PE-100 ducts, whilst the red curves correspond to solutions in which the external tube is made off highly conductive plastic and the internal one is composed of a low conductivity plastic material. Full curves show the 75/40 configurations, while dash-dotted curves show the results of the 75/50 configurations, considering the thicknesses as explained in the text.

Figure 5.17 (b) shows absolute specific pressure drop of a coaxial plastic arrangement for varying internal pipe dimensions and fixed external pipe diameter of 75 mm. The blue curve corresponds to the 75/40 configuration with internal pipe thickness of 3.7 mm, while the red curve shows the results of the 75/50 configuration with thickness of 4.6 mm. The type of material does not substantially affect the result in this case.

To complete the picture, it is important to analytically explore the substantial influence of volume flow in the heat exchange process (see Figure 5.18).

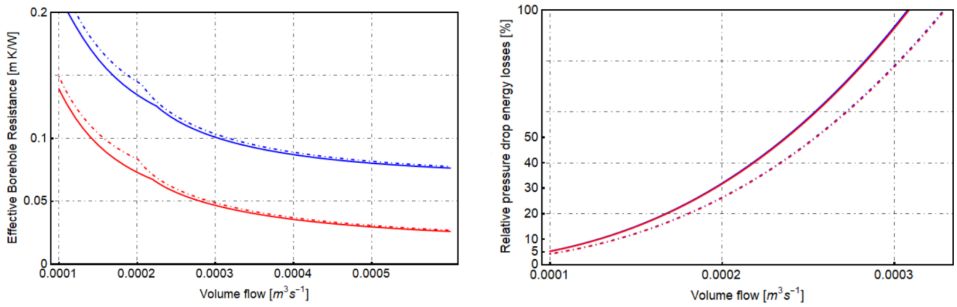

(a) (b)

Figure 5.18: Effective borehole resistance R_b vs. Absolute specific pressure drop for varying volume flows

Figure 5.18 (a) shows effective borehole resistance R_b of the different coaxial plastic arrangements for varying volume flows. The meaning of the curves is the same than in the previous graph. Figure 5.18 (b) shows pumping power relative to the heat exchange rate [in %] for the different coaxial plastic arrangements for varying volume flows.

Complementary to the analytical evaluation, several detailed simulations of different geometries were decided upon for further optimization of the influence of different thermal conductivities, both in the pipe and in the fill.

One widely accepted choice is to use an implementation of the multipole heat transfer methodology embedded in the software tool Earth Energy Designer (EED), currently in version 4. EED has been extensively used to perform design of BHE systems and there are several references comparing simulation and measurement results. It is thus a flexible and powerful tool to calculate thermal efficiencies allowing to change the basic geometrical and thermal parameters of interest.

The study of the thermal performance of the borehole was carried out with the software EED v2.0. The specifications of a house with a 12/10 kW geothermal system (heating/cooling) were simulated with the different types of configuration of geothermal heat exchanger, comparing with standard pipes. The results obtained can be seen in Table 5.7.

Table 5.7: Results of the thermal assessment

Borehole type	**Effective borehole thermal resistance** [1] $K/(mW)$	**Length** [12]	
		Total length (m)	**Reduction (%)**
Coaxial 75/40 standard	0.0944	305.5	0.0
Coaxial 75/40 high conduct.	0.0426	237.2	22.2
Coaxial 75/50 standard	0.0928	303.4	0.7
Coaxial 75/40 high conduct.	0.0246	227.0	25.7

[1] Simulations by EED v2.0 for a 12/10kW building
[2] Required borehole length for same thermal efficiency

From the results, very close to those obtained in the general theoretical analysis, it can be seen that high conductivity pipes have a significantly better thermal performance than standard pipes. Compared to the two configurations analyzed, the coaxial 75/50 high conductivity configuration has a slightly better thermal performance.

On the other hand, an analysis has also been performed of the hydraulic losses associated with each pipe configuration. The results obtained can be seen in Table 5.8. Here, higher hydraulic losses can be observed in the 75/50 coaxial pipe configuration.

Table 5.8: Results of the hydraulic assessment

Borehole type		**Flow rate** (m^3/s)	**Velocity** (m/s)	**Reynolds number**	**Hydraulic losses** ($kPA/100m$)	
Coaxial 75/40	Inner pipe	0.0003	0.36	13112	5.84	**9.07**
	Outer pipe	0.0003	0.18	4215	3.23	
Coaxial 75/50	Inner pipe	0.0003	0.23	10477	2.01	**20.43**
	Outer pipe	0.0003	0.30	3827	18.42	

Chapter 6

Discussion

Although throughout the previous chapters – or articles – (since the thesis corresponds to an article compendium) the main results obtained from the research have already been discussed, the most important ones are summarized in the diagram in the Figure 6.1.

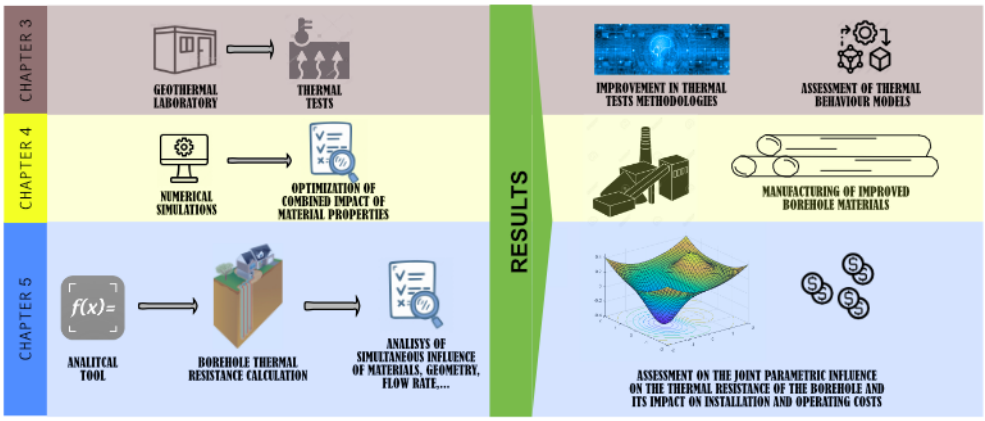

Figure 6.1: Diagram of the main results of the Doctoral Thesis

6.1 Geothermal laboratory and thermal test assessment

The geothermal laboratory at the UPV (Figure 6.2) has been designed with special emphasis on the importance of an optimum control system that ensures the injection/extraction of constant thermal power during a thermal test.

Figure 6.2: General view of the test site room

Moreover, the laboratory is challenged to measure the constant thermal power not at the source of thermal generation, but at the actual injection/extraction of heat into the borehole. This ensures a high quality of data for later analysis. The goal is to keep the rate of heat injection into the ground as stable as possible during a TRT. For this purpose, a PID controller has been implemented in the PLC to control the the openness degree of a 3-way valve and thus modulate the thermal power generated by an electrical resistance or by a heat pump. The reference is the thermal power that is injected into the borehole, taking into account the temperature difference at the inlet and outlet of the borehole and the water flow rate. The Figure 6.3 shows the quality of the data obtained during a thermal test, without observing thermal disturbances due to the outside temperature.

An important result is that thermal tests performed using PID control showed not only a better stability, but also a significant improvement in the correspondence between the experimental data and the different theoretical models used for parameter adjustment and estimation. In FLS model a slightly better least square error (LSQ) was observed and therefore allows a better parameter estimation. On the other hand, the values of ground thermal conductivity and borehole thermal resistance found were in a similar range when using ILSm or FLSm.

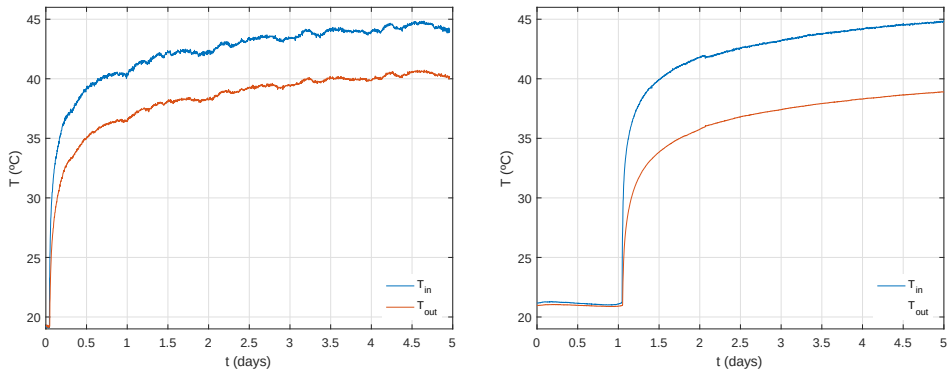

Figure 6.3: Left: inlet and outlet temperatures with no control (standard TRT). Right: inlet and outlet temperatures with PID control

Instead of the traditional TRT analysis performed by means of a parameter estimation from a logarithmic line, the data analysis performed in this research consists of an adjustment to a non-linear function of the average temperature data resulting from the thermal experiment with any of the models analyzed (ILSm, FLSm CSm). The best-fit method used for this thermal assessment is by *Levemberg-Marquardt* algorithm (Least-Squares Model Fitting Algorithms) implemented in Matlab v12.1 package, which consists of a set of functions to find the parameters that best fit a theorical model with a given dataset. Like other fitting tools, it finds the combination of parameters (in our case the thermal conductivity of the ground, λ, and the borehole thermal resistance, R_b) that minimizes the LSQ between a theoretical model prediction and the experimental data.

For a more in-depth assessment of model fitting, Figure 6.4 shows the evolution of residuals (difference error between therorical model predicted and experimental measured data) over time for FLS model fit. For non-PID controlled thermal tests (Figure 6.4 (a)) the residual curve reflects the noisy pattern of the T_{amb} curves. This ambient temperature disturbance may hide other effects or errors highly hinders the process of parameter identification. Clearly, the implementation of a PID control reduces the residuals (Figure 6.4 (b)) and removes the ambient temperature influence. Although there seems to be general pattern appears that can only be attributed

to some systematic inaccuracy (particularly in the early stages – short-term –of TRT) of the traditional employed.

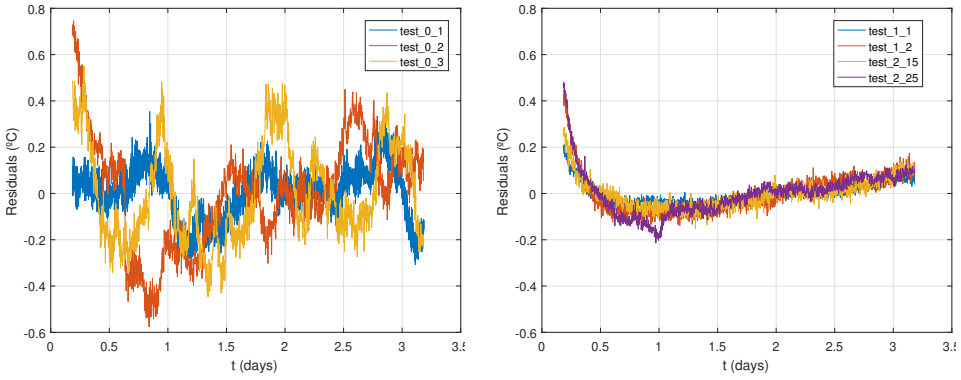

(a) (b)

Figure 6.4: Temperature residuals versus time for: (a) tests with traditional setup and (b) tests with controlled heat injection rate.

Another important consideration is the strongly dependency on the time window of experimental data selected for parameter extraction. Figure 6.5 (a) presents a TRT performed on a single-U tube borehole. The grey curve shows the experimentally measured evolution of the temperatures inside the single–U tube BHE. The red and blue dotted curves are the two best theoretical model fits based on the ILSm but taking data from different time windows. *ILS 12_48* takes only into account data starting 12h after test start up to 48h (2 days), whilst *ILS 24_118* accounts for the information from 24h of test start to the full duration of 118h. As can be seen from the graph, the red line does not represent the short-term behaviour of the single-U tube borehole properly and vice versa. Furthermore, the parameter values (λ and R_b) extracted from the best fit are different in both cases. When only shorter-term data are considered, (like in *ILS 12_48*) the estimated ground conductivity tends to larger values as well as the borehole resistance compared to when long-term data are included in the analysis.

A better understanding of this relationship is found by systematically changing the time window and observing the trends in parameter estimation (Figure 6.5 (b)). Each dot represents a parameter estimation based on a different time window, where in each case the upper time limit was fixed at 118h and the lower limit has been varying, where the closely correlation between λ

and R_b can be found. Figure 6.5 (c)) notices that not all solutions represent experimental results with the same accuracy. The least square error (LSQ) shows an abrupt increase for values of the ground conductivity estimation that are below 2.5 in the case of the ILSM and 2.3 in the case of FLSm and CLSm. This behavior indicates that, when this behavior is intended to be incorporated in the short term in the analysis, the theoretical models begin to fail representing the experimental result, as previously mentioned. Meaning, in turn, that the parameters extracted are less close to reality.

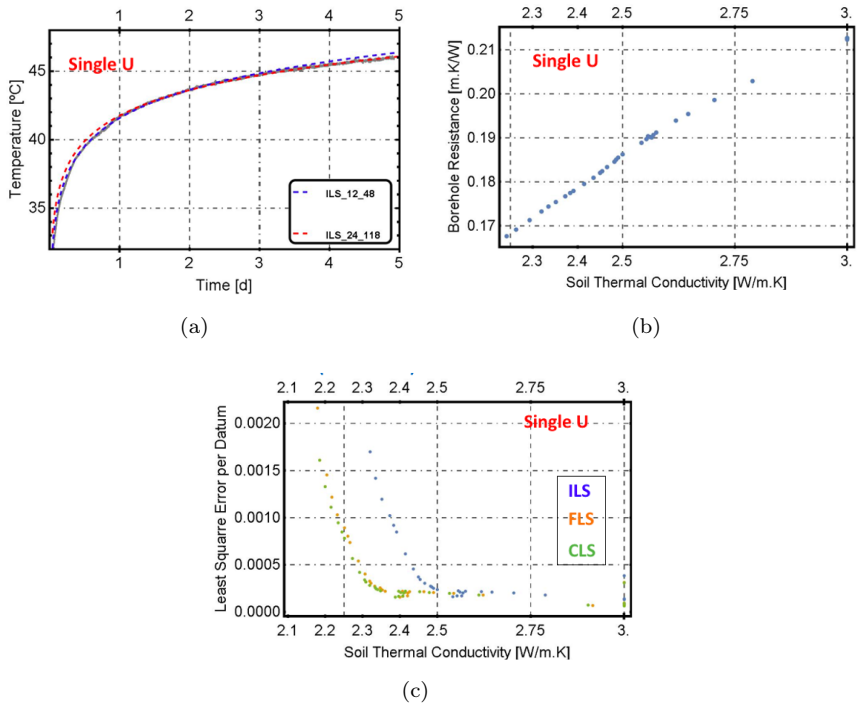

Figure 6.5: Influence of the time window

6.2 Development of advanced materials guided by numerical simulations

A detailed parameter study through numerical simulations has been developed as a valuable design guidance tool for the range of improved material specifications for subsequent composition and manufacture. The influence of the joint effect of grouting and pipe conductivity has been considered for optimization of borehole thermal efficiency in two different geometries: single-U tube and coaxial configurations.

6.2.1 Single-U tube configuration

For a single-U tube borehole[1], as shown in the Figure 6.6 (a), the findings show that the optimal area, in terms of borehole thermal resistance, corresponds to pipe conductivity between 1.2-1.5 W/(mK) and grouting conductivity between 2.1 and 2.9 W/(mK). The explanation for higher values of the thermal conductivity of the grout material being counterproductive is because it enhances the thermal short-circuiting between inlet and outlet pipes. The simulation results show (see Figure 6.6 (b)) that a considerable reduction of the required borehole length may be achieved through the use of optimally designed materials (pipe conductivity = 2 W/(mK), grouting conductivity = 2.4 W/(mK), required borehole length = 885.5 m) instead of a standard PE geothermal pipe with a standard grout material (pipe conductivity = 0.42 W/(mK), grouting conductivity = 2.0 W/(mK), required borehole length = 1003.7 m).

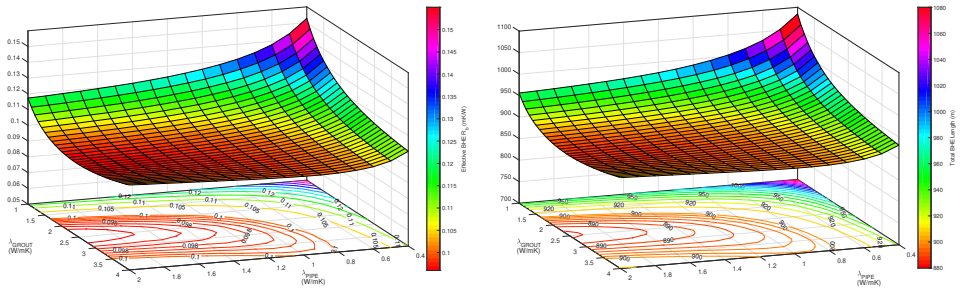

(a) (b)

Figure 6.6: Simultaneous effect of varying the λ_{PIPE} and λ_{GROUT} in the borehole thermal resistance

[1]The Figures have been placed again because they are necessary for better understanding and it would not be comfortable for the reader to have to have to return to the previous chapter.

Regarding the influence the ground typology on the borehole thermal resistance (Figure 4.16), the shape pattern of the three surfaces corresponding to different ground type is similar, although for the surface corresponding to high conductive ground, a higher influence on borehole thermal resistance is shown. While in terms of the influence of the climate on the borehole thermal resistance (Figure 4.18), nearly same surface area of borehole thermal resistance is obtained for both climates, although for hot climate surface, higher sensitivity to "thermal short-circuit" above mentioned is found.

6.2.2 Coaxial borehole configuration

The simulation results for the coaxial borehole configuration show that a substantial improvement of the borehole thermal efficiency can be achieved by employing in the outer pipe and inner pipes different thermal conductivities (see Figure 4.14). The resulting lower thermal resistance of the borehole is highly significant and would have a high impact on drilling costs, dropping from a borehole field length of 917 m in a standard polyethylene coaxial pipe to 670 m in a coaxial pipe with values of thermal conductivity of 0.1 W/(mK) for inner pipe and 2 W/(mK) for outer pipe, according to the characteristics of the scenario. The optimum configuration therefore corresponds to large differences in the thermal conductivity between the inner and outer pipes of a coaxial heat exchanger (Figure 4.14).

6.3 Effect of working fluid flow rate on the borehole thermal efficiency and pressure losses according to different pipe and grout materials

In geothermal heat pump systems, the borehole thermal efficiency is affected by different design and operating factors that impact the overall thermal performance of the system and its operating costs. An under-explored aspect is the correlation between the flow rate of the working fluid, the borehole thermal resistance and pumping energy cost. Therefore, Figure 5.9 shows the important interaction between the borehole thermal resistance and the pressure losses. As can be seen, to achieve low values of borehole thermal resistance, a high energy pumping consumption is required; and, conversely, to reach low pressure losses, the borehole thermal efficiency has to be penalized. However, this graph shows that there is an optimum spot for each configuration and borehole properties that minimizes those two values (the value closest to the origin).

The simultaneous effect of pipe conductivity, grout material conductivity and flow rate of the working fluid on the borehole thermal resistance has also been examined. For this purpose, the borehole thermal resistance was calculated using the analytical tool with different input parameters of the pipe

conductivity, the grout material conductivity and fluid flow rate. In Figure 5.10, different surfaces of borehole thermal resistance can be observed depending on these material conductivities for four fluid flow rate values. This evaluation has highlighted the significant impact of not only optimal flow values, but also of the added effect of improved conductivity values of the pipe and grouting, which together can significantly improve the thermal efficiency of the borehole.

6.3.1 Single-U tube configuration

Figure 5.14 illustrates the yearly total costs depending on the flow rate for same borehole length scenario. Low working fluid flow rates result in higher overall costs, due to the higher electricity consumption for operation of the heat pump [AOC_{HP}] due to the low thermal performance of the borehole (high working fluid temperatures in the borehole field). As the fluid flow rate is increased, these expenses are reduced (higher thermal efficiency of the borehole), but after a certain value, the pumping costs start to have a greater weigh, increasing the total expenditures.

Figure 5.15 shows the yearly total costs depending on the flow rate for same heat pump efficiency scenario. At very low working fluid flow rates, high overall costs are observed, strongly penalized by the high drilling costs, since a longer length of borehole field required to obtain the same thermal heat pump performance (same fluid temperatures in the borehole field). As the fluid flow is increased, these total expenses are reduced (lower drilling costs), but after a certain value, the pumping costs start to have a greater weigh, increasing the total expenditures. At the range of fluid flows analyzed, however, these pumping costs do not overcome the savings in drilling costs (although they are expected to happen at higher flows).

As observed in Table 5.5, for the same increment of fluid flow rate, the improvement in the energy consumption of the heat pump is higher at low flows. For instance, the operating cost of the heat pump is reduced 4% when flow increases from 0.033 to 0.044 l/s, while the decrease is about 0.4% in the range between 0.2 and 0.25 l/s. Above a certain value of fluid flow rate, the penalization in the pumping costs are higher than the decrease in electricity consumption due the improved thermal performance of the heat pump. An optimum flow rate that optimises the overall costs of a borehole configuration can be determined according to the scenario characteristics. In the case analyzed, this optimum is at a value of 0.1 l/s (Figure 5.14) representing 70% of nominal design flow rate. It is seen that operating the installation with an inadequate fluid flow can produce an increase in the total electricity consumption of the geothermal system of between 4 and 10% (see Figures 5.14 and 5.15).

6.3.2 Coaxial borehole configuration

The result of the analytic study shows, on one hand, that the improved material configurations show a substantially lower borehole thermal resistance at equivalent pressure drop conditions, validating the initial assumption that an enhanced plastic configuration will have a noticeable positive impact on the system performance.

Regarding the pressure drop, the curve show how sensitive pressure losses are to the correct choice of the internal pipe diameters. The best configuration, corresponding to the minimum or valley of the curves (i.e. between 40 and 50 mm). In terms of pressure drop, the 40/75 configuration offers a somewhat better result, while effective borehole thermal resistances are quite similar.

Chapter 7

Conclusions

The main objective of the research of this Doctoral Thesis has been to allow a holistic view of the problem of the optimization of the thermal resistance of a borehole heat exchanger through the evaluation of the combined effect of the main parameters that have impact on it. The significant improvement of the overall performance of a GSHP system by improving the borehole thermal resistance has a direct impact on the reduction of execution and operating costs, pushing forward the economic benefits of shallow geothermal technology.

Through the integration of the well-known equations that govern the heat exchange in a borehole into a single analytical tool, it has been possible to observe the weight of each parameter in the final calculation of the thermal resistance of the borehole. The results of the analytical tool have been evaluated and validated by means of experimental tests carried out in a high level geothermal laboratory. By means of three thermal tests at different flow rates (different Reynolds number and regimes – laminar, transition and turbulent –) R_b results provided by the analytical tool have been validated against the real results of experimental tests.

With the pursuit of obtaining the optimal specifications for the manufacture of new borehole materials, numerical simulations have been performed in different scenarios to allow the product developers to manufacture the new products under optimal conditions. These new developed products would achieve a shorter required borehole length and, therefore, a reduction of the

installation costs with the same efficiency of the system. The expected results obtained using these new materials have been compared with the materials currently on the market to calculate the economic impact and to assess the benefits associated with the expected improvements. In the studied scenarios (combining different types of buildings, types of ground and types of climates), the joint improvement of the thermal conductivity of pipes and products can result in a significant reduction of the total borehole length required for the installation, obtaining in the simulations of some scenarios a reduction of the required length of the borehole heat exchanger of up to 22%.

Furthermore, the results have shown that the optimum combination of thermal conductivity of the pipes and the grout should not always be the highest possible value, but should be in accordance with the thermal characteristics of the ground. In this way, it has been shown that the thermal properties of the grouting products must be adapted to the soil conditions (geological environment) of the location where the geothermal installation will be located. The results show that the application of the improved products in the actual installation could result in a reduction of the total length of the borehole field or an increase in the efficiency of the geothermal system if the total length is maintained.

Therefore, the results obtained in this research constitute a guidance document for the product developers. Finally, for production, technical, economic and optimisation reasons, it was decided to produce a geothermal plastic pipe with a conductivity of 1.1 W/(mK) and a grout with a conductivity of 2.9 W/(mK). If the results of the thermal tests are satisfactory, these products could soon be on the market, achieving important reductions in the total length to be drilled, which would result in more economical and competitive geothermal installations.

This research has also analysed the investment and operating costs of case study of a geothermal system means of a comprehensive analytical tool developed to evaluate the correlation between borehole thermal efficiency and borehole hydraulic pressure losses at different fluid flows. This tool has been experimentally validated by thermal tests (TRTs) at three different flow rates, obtaining differences between the values calculated by the tool and the experimental values below 1.5%. As expected, the borehole thermal resistance has been found to be significantly dependent on the flow rate. In laminar flow, borehole thermal resistance increases rapidly with small decreases in flow rate, while in turbulent flow, a increase in the flow rate produces only a marginal decrease in the thermal resistance of the borehole. To supplement this theoretical assessment, hourly numerical simulations by EED software of a

case scenario were performed to evaluate the influence of flow rate of working fluid on the overall costs of the geothermal system (drilling and operation costs). As can be noted from both analytical tool and the scenario simulations, the fluid flow rate impacts both the borehole thermal resistance (and therefore the heat pump performance – SPF–) and the pumping costs. Working at low flow rates will result in lower efficiency of the borehole, resulting higher heat pump consumption. On the other hand, operating with too high flow rates will increase the cost of pumping.

To conclude, the exhaustive assessment carried out in this research illustrates that the thermal efficiency of the borehole increases as pumping pressure losses increase, there being, depending on borehole typology and characteristics, an optimal design value that minimises them. The results obtained by this Ph. Doctoral Thesis highlight the importance, when designing a geothermal system, of performing a hydraulic assessment in order to evaluate the effect of the fluid flow rate on both the borehole thermal efficiency and the electrical expenditure of the circulation pump. Thus, a compromise between both will be reached, taking into account that both have impact on the overall operating cost of a ground source heat pump system. This optimal value can be determined for each specific installation following the methodology described in this research.

7.1 Future work

Regarding main open research paths that this Thesis leads to:

- As discussed in previous section, despite having high quality experimental data, there is a lot of inaccuracy in the analytical models that predict the thermal behavior, especially in the short-time, of a TRT. It is necessary to deepen in more complex models that eliminate these uncertainties.
- Only part of the pressure losses of a geothermal system were assessed (related with the friction losses in the pipes). In order to have a more complete view, additional pressure losses produced by other elements of the system(such as bends, valves or other singularities) should be taken into account.
- The effect of the borehole thermal resistance on the electrical consumption of the geothermal heat pump through analytical terms (in this research solved by computer simulations). This would allow an even more versatile analysis. And this would also allow, on the other hand, the incorporation of costs, both of materials and of operation, turning the analytical tool into a much more compact and powerful parameter optimizer.

- The new designed materials are currently in process of development and there are no real values of their cost increase with respect to the costs of the current materials. It also required a sophisticated assessment on the transition from experimental costs to commercial costs in order to be able to compare them with the current market and draw coherent conclusions. This is an important factor to consider but it has not been possible to incorporate it into the thesis.
- The research has focused on the typology of common geothermal installation in Spain (southern Europe) where the heat-carrying fluid in terms of efficiency and cost, and since the working temperatures allow it, is water. The use of glycols to prevent water freezing has a negative impact both on the efficiency of the borehole heat exchanger (lower thermal conductivity of the water) and on pumping costs (higher viscosity, higher energy costs of pumping)

Appendices

A Case 1: Flow 0.033 l/s

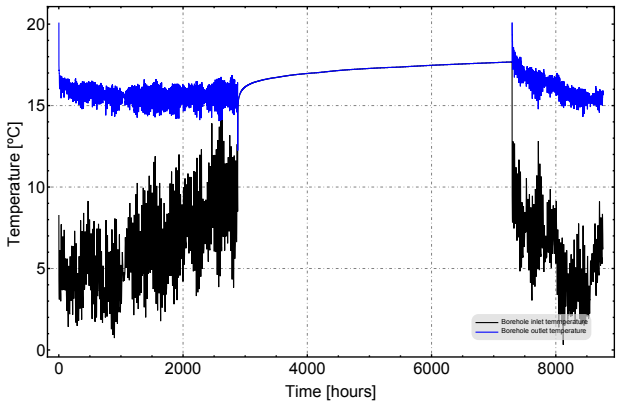

Figure A1: Inlet and Outlet temperature at borehole

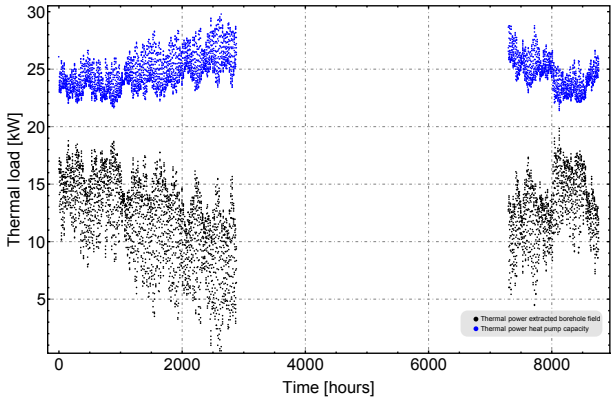

Figure A2: Thermal power extracted from the borehole field and Thermal power capacity of the heat pump

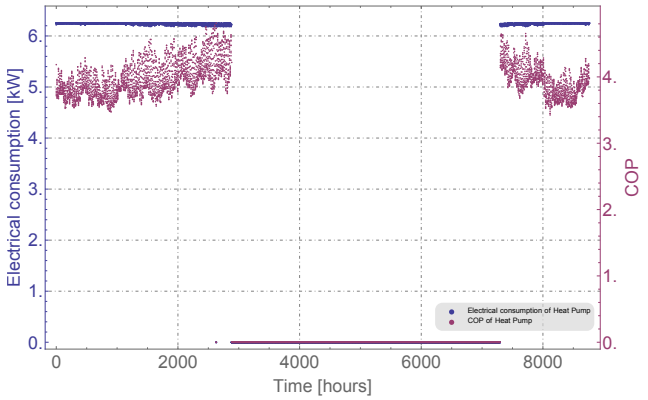

Figure A3: COP and Electrical consumption of the heat pump

B Case 2: Flow 0.044 l/s

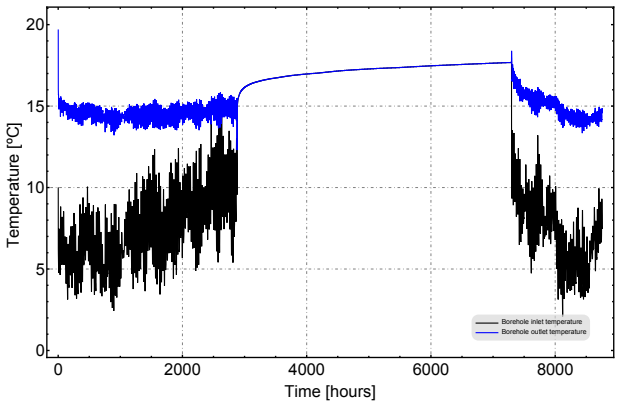

Figure B1: Inlet and Outlet temperature at borehole

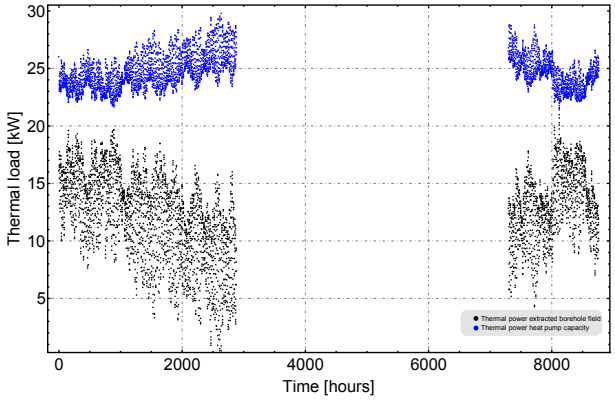

Figure B2: Thermal power extracted from the borehole field and Thermal power capacity of the heat pump

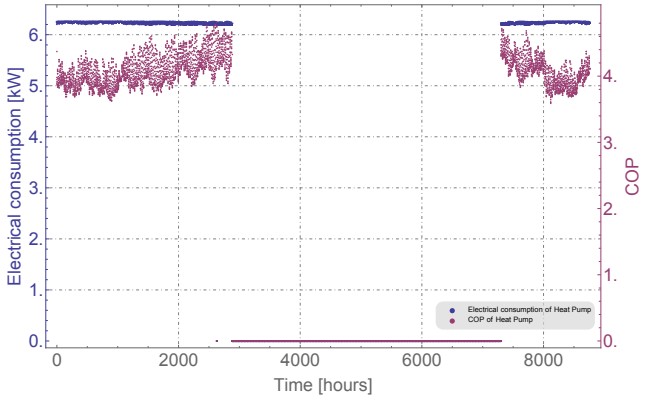

Figure B3: COP and Electrical consumption of the heat pump

C Case 3: Flow 0.064 l/s

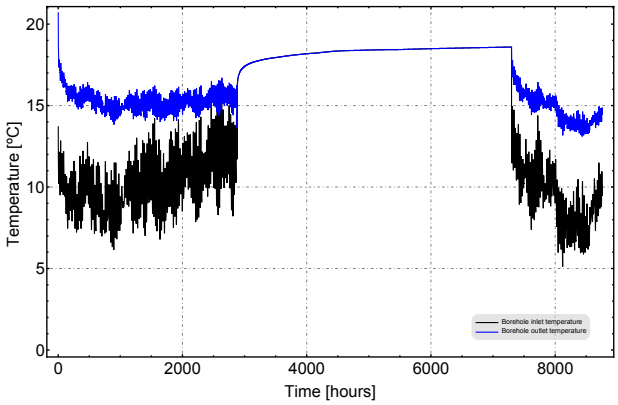

Figure C1: Inlet and Outlet temperature at borehole

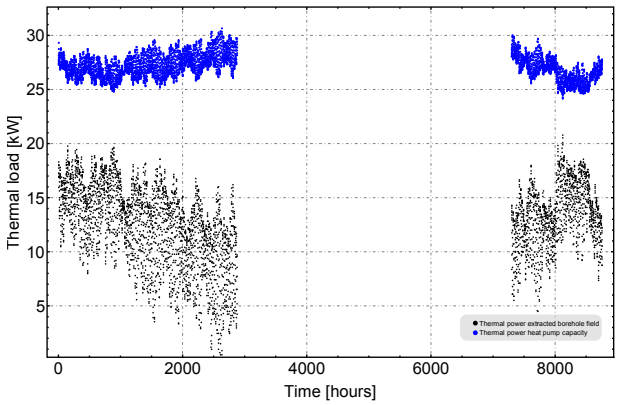

Figure C2: Thermal power extracted from the borehole field and Thermal power capacity of the heat pump

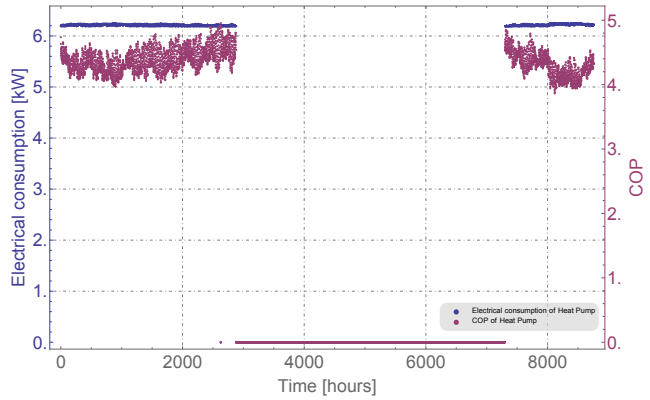

Figure C3: COP and Electrical consumption of the heat pump

D Case 4: Flow 0.083 l/s

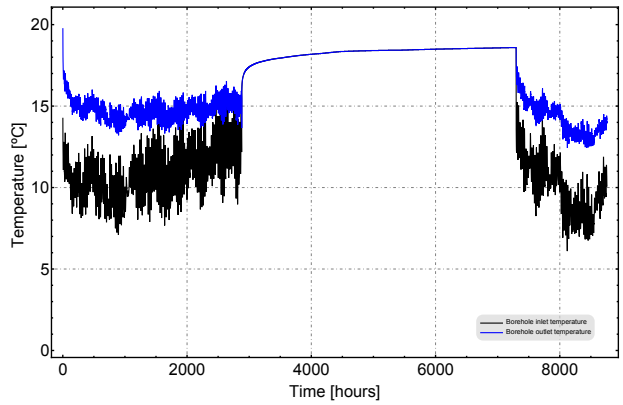

Figure D1: Inlet and Outlet temperature at borehole

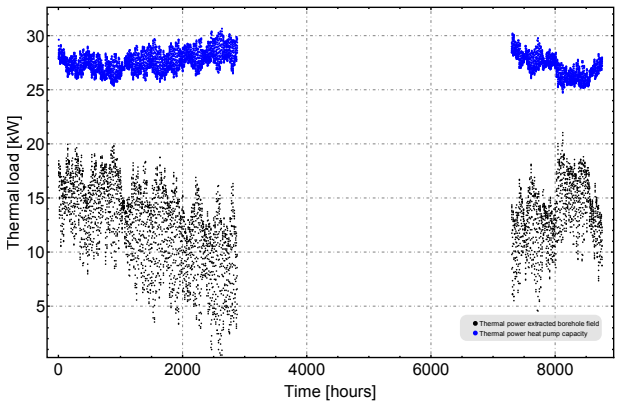

Figure D2: Thermal power extracted from the borehole field and Thermal power capacity of the heat pump

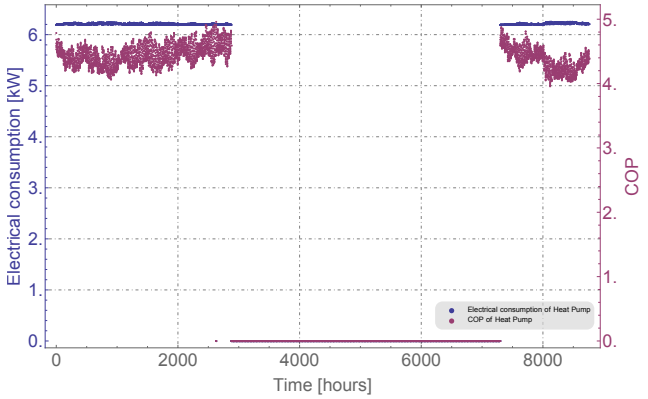

Figure D3: COP and Electrical consumption of the heat pump

E Case 5: Flow 0.1 l/s

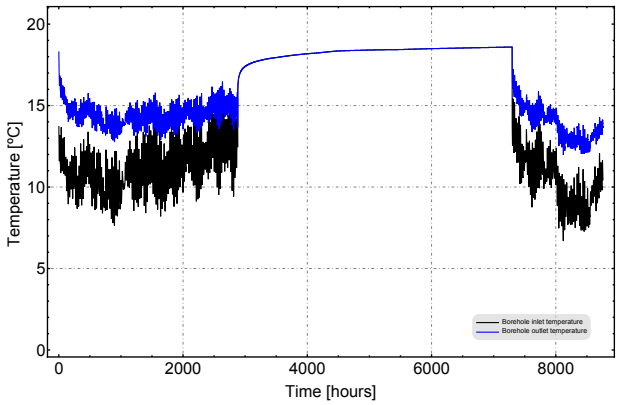

Figure E1: Inlet and Outlet temperature at borehole

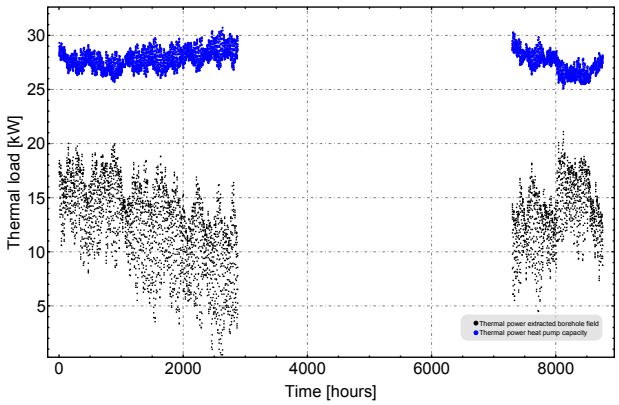

Figure E2: Thermal power extracted from the borehole field and Thermal power capacity of the heat pump

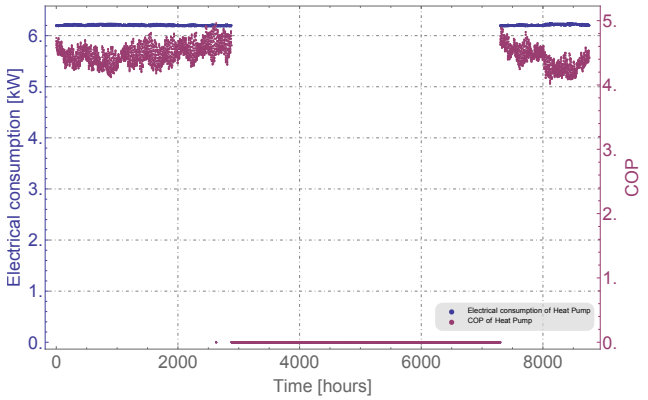

Figure E3: COP and Electrical consumption of the heat pump

F Case 6: Flow 0.15 l/s

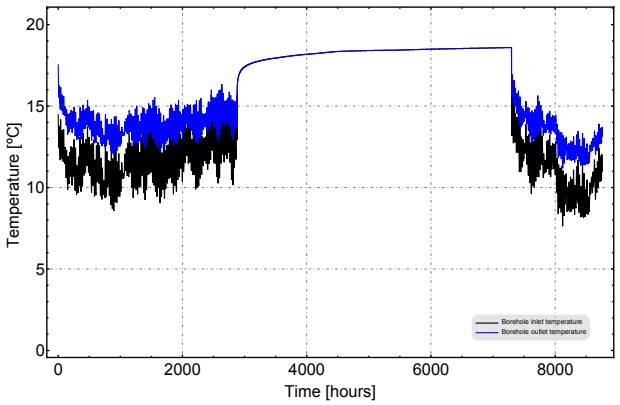

Figure F1: Inlet and Outlet temperature at borehole

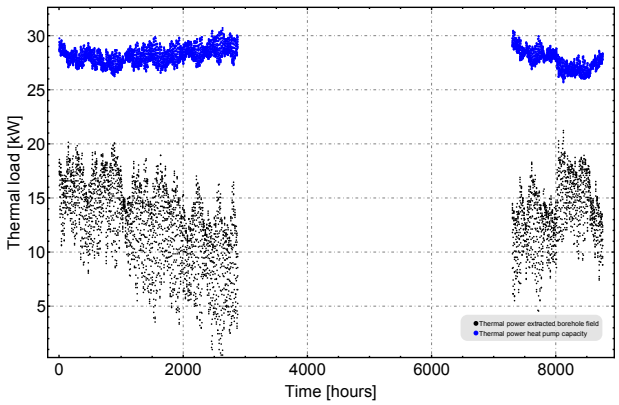

Figure F2: Thermal power extracted from the borehole field and Thermal power capacity of the heat pump

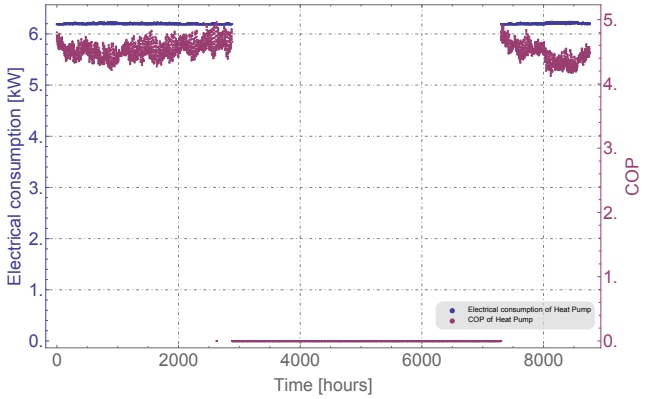

Figure F3: COP and Electrical consumption of the heat pump

G Case 7: Flow 0.2 l/s

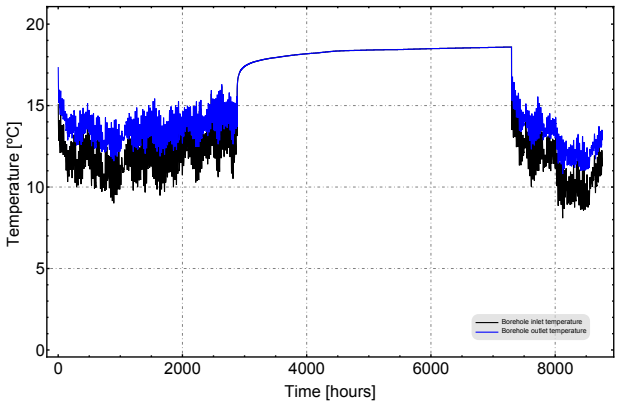

Figure G1: Inlet and Outlet temperature at borehole

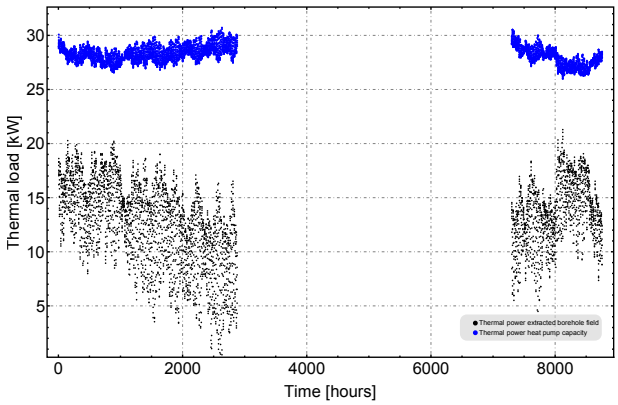

Figure G2: Thermal power extracted from the borehole field and Thermal power capacity of the heat pump

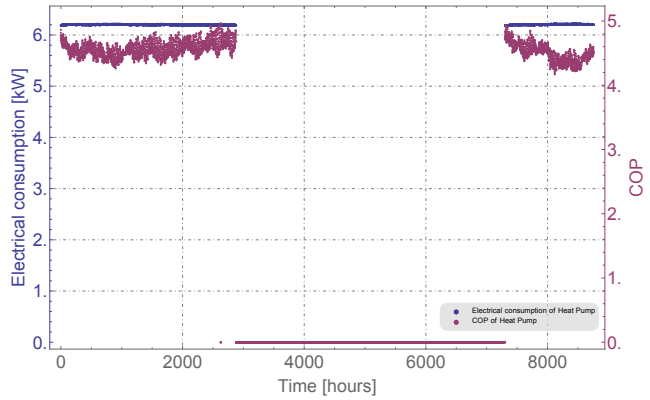

Figure G3: COP and Electrical consumption of the heat pump

H Case 8: Flow 0.25 l/s

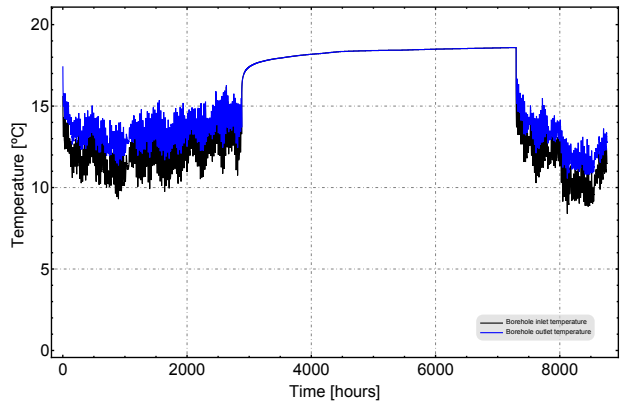

Figure H1: Inlet and Outlet temperature at borehole

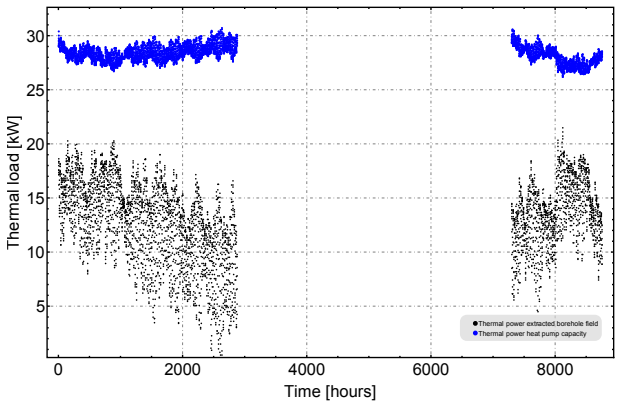

Figure H2: Thermal power extracted from the borehole field and Thermal power capacity of the heat pump

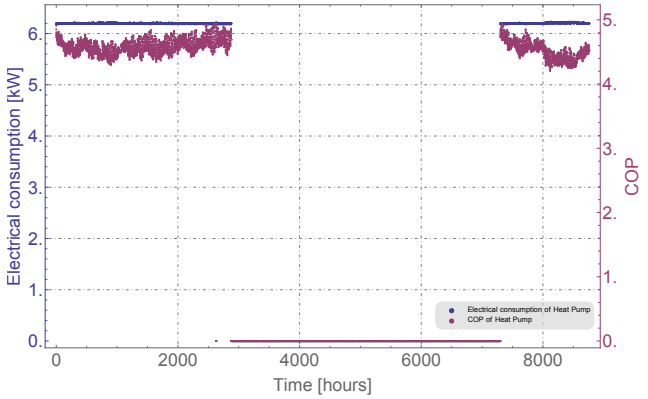

Figure H3: COP and Electrical consumption of the heat pump

Nomenclature

ΔP	Pressure drop $[Pa]$
δp	Pressure drop per unit length of BHE $[Pa/m]$
λ	Ground thermal conductivity $[W/mK]$
λ_f	Fluid thermal conductivity $[W/mK]$
AOC_{CP}	Annual energy Operating Cost of Circulating Pump [€/year]
AOC_{HP}	Annual energy Operating Cost of Heat Pump [€/year]
H	Borehole deep $[m]$
Nu	Nusselt number
Pr	Prandlt number
q	Thermal power heat ratio $[W/m]$
R_b or $R_{b_{eff}}$	Borehole (effective) thermal resistance $[mK/W]$
r_i	Inner radius of outer pipe in a coaxial borehole $[m]$
r_o	Outer radius of inner pipe in a coaxial borehole $[m]$
r_p	Inner radius of the pipe $[m]$
r_{po}	Outer radius of the pipe $[m]$

R_{tot}	Total borehole resistance $[mK/W]$
Re	Reynolds number
T_0	Undisturbed ground temperature $[°C]$
T_f	Fluid temperature $[°C]$
T_g	Surrounding ground temperature $[°C]$
ATES	Aquifer Thermal Energy Storage
BHE	Borehole Heat Exchanger
BTES	Borehole Thermal Energy Storage
CAPEX	Capital Expenses
COP	Coefficient of Performance
CSm	Cylinder Source model
EED	Earth Energy Designer (PC-program)
FLSm	Finite Line Source model
GHE	Ground Heat Exchanger
GSHP	Ground Source Heat Pump
HVAC	Heating, Ventilation and Air Conditioning
ILSm	Infinite Line Source model
LSQ	Least Square Error
OPEX	Operating Expenses
PB	Polybutylene
PCM	Phase Changing Materials
PE-pipe	Polyethylene pipe
PID	Proportional Integral Derivative (PID) Control
SGES	Shallow Geothermal Energy Systems

SPF	Seasonal Performance Factor
TRT	Thermal Response Test
UTES	Underground Thermal Energy Storage

Bibliography

[1] *Heating Market Report 2020.* http://www.ehi.eu/fileadmin/user_upload/user_upload/Heating_Market_Report_2020.pdf. European Heating Industry (EHI), October 2020 (cit. on p. 1).

[2] *Energy, transport and environment statistics, 2019 edition.* http://www.ehi.eu/fileadmin/user_upload/user_upload/Heating_Market_Report_2020.pdf. Eurostats, 2020 (cit. on p. 1).

[3] *Strategy report for future energy planning and management concepts to foster the use of shallow geothermal methods.* https://www.interreg-central.eu/Content.Node/GeoPLASMA-CE/CE177-GeoPLASMA-CE-D.T.4.4.1-Joint-strategy-report-final-Eng.pdf. GEOPLASMA European project. Deliverable D.T4.4.1. LP-GBA, 2019 (cit. on p. 2).

[4] *Heat Pumps.* https://www.iea.org/reports/heat-pumps. International Energy Agency (IEA), 2020 (cit. on p. 2).

[5] *Strategic research innovation agenda for geothermal technologies.* https://www.egec.org/wp-content/uploads/2020/09/Geothermal-SRIA-2020-v.3-FINAL.pdf. Renewable Heating and Cooling Platform, August 2020 (cit. on p. 3).

[6] Iñigo Arrizabalaga, Margarita De Gregorio, Cristina De Santiago, Celestino García de la Noceda, Paloma Pérez and Javier F. Urchueguía.

"Geothermal Energy Use, Country Update for Spain". In: *Proceedings of the European Geothermal Congress 2019*. 2019 (cit. on p. 3).

[7] *El sector de la geotermia prevé triplicar el número de instalaciones en España a 2025, hasta más de 20.000*. https://www.europapress.es/economia/noticia-sector-geotermia-preve-triplicar-numero-instalaciones-espana-2025-mas-20000-20180601115925.html. Accessed: 2020-08-30 (cit. on p. 3).

[8] Javier F. Urchueguia, Eija Alakangas, Inga Berre, Luisa F. Cabeza, Grammelis Panagiotis, Walter Haslinger, Roland Hellmer, Daniel Mugnier, Philippe Papillon, Gerhard Stryi-Hipp, Wim Helden, Christian Engel, Rainer Janssen, Dominik Rutz, Thomas Nowak, Burkhard Sanner, W. Sparber, Claes Tullin, Werner Weiss and Pedro Dias. *Common Implementation Roadmap for Renewable Heating and Cooling Technologies*. June 2014. DOI: 10.13140/2.1.1309.4082 (cit. on p. 4).

[9] "Geothermal Heating and Cooling". In: *Energy Efficient Buildings with Solar and Geothermal Resources*. John Wiley & Sons, Ltd, 2014. Chap. 6, pp. 419–458. ISBN: 9781118707050. DOI: 10.1002/9781118707050.ch6. eprint: https://onlinelibrary.wiley.com/doi/pdf/10.1002/9781118707050.ch6 (cit. on p. 4).

[10] Per Eskilson. "Thermal Analysis of Heat Extraction Boreholes". PhD thesis. Lund University, 1987, p. 222. ISBN: 9179002986 (cit. on pp. 5, 10, 11, 70).

[11] G. Hellström. "Ground heat storage: Thermal analyses of duct storage systems". PhD thesis. Lund University, 1991, p. 310. ISBN: 9789162802905; 9162802909 (cit. on pp. 5, 10, 70, 72–74).

[12] Cristina Sáez Blázquez, Laura Piedelobo, Jesús Fernández-Hernández, Ignacio Martín Nieto, Arturo Farfán Martín, Susana Lagüela and Diego González-Aguilera. "Novel Experimental Device to Monitor the Ground Thermal Exchange in a Borehole Heat Exchanger". In: *Energies* 13.5 (2020). ISSN: 1996-1073. DOI: 10.3390/en13051270 (cit. on pp. 5, 71).

[13] Sang Mu Bae, Yujin Nam and Byoung Ohan Shim. "Feasibility Study of Ground Source Heat Pump System Considering Underground Thermal

Properties". In: *Energies* 11.7 (2018). ISSN: 1996-1073. DOI: 10.3390/en11071786 (cit. on pp. 5, 71).

[14] Tena Bilić, Sara Raos, Perica Ilak, Ivan Rajšl and Robert Pašičko. "Assessment of Geothermal Fields in the South Pannonian Basin System Using a Multi-Criteria Decision-Making Tool". In: *Energies* 13.5 (2020). ISSN: 1996-1073. DOI: 10.3390/en13051026 (cit. on pp. 5, 71).

[15] Y. Gu and Dennis O'Neal. "Development of an equivalent diameter expression for vertical U-Tubes used in ground-coupled heat pumps". In: *ASHRAE Transactions* 104 (Jan. 1998), pp. 347–355 (cit. on pp. 5, 11, 71).

[16] M. Philippe, M. Bernier and D. Marchio. "Sizing Calculation Spreadsheet Vertical Geothermal Borefields". In: *ASHRAE Journal* 52, no. 7 (July 2010) (cit. on pp. 5, 11, 71).

[17] Louis Lamarche, Jasmin Raymond and Claude Hugo Koubikana Pambou. "Evaluation of the Internal and Borehole Resistances during Thermal Response Tests and Impact on Ground Heat Exchanger Design". In: *Energies* 11.1 (2018). ISSN: 1996-1073. DOI: 10.3390/en11010038 (cit. on pp. 5, 71).

[18] R.A. Beier and G.N. Ewbank. "In-situ thermal response test interpretations: OG&E ground source heat exchange study". In: *IGSHPA,OKSU* (2012) (cit. on pp. 6, 11, 71).

[19] S. Javed and J.D. Spitler. "3 - Calculation of borehole thermal resistance". In: *Advances in Ground-Source Heat Pump Systems*. Ed. by Simon J. Rees. Woodhead Publishing, 2016, pp. 63 –95. ISBN: 978-0-08-100311-4. DOI: https://doi.org/10.1016/B978-0-08-100311-4.00003-0 (cit. on pp. 6, 71).

[20] Ahmed A. Serageldin, Yoshitaka Sakata, Takao Katsura and Katsunori Nagano. "Thermo-hydraulic performance of the U-tube borehole heat exchanger with a novel oval cross-section: Numerical approach". In: *Energy Conversion and Management* 177 (2018), pp. 406 –415. ISSN: 0196-8904. DOI: https://doi.org/10.1016/j.enconman.2018.09.081 (cit. on pp. 6, 71).

[21] Gaoyang Hou, Hessam Taherian, Longjun Li, Jordan Fuse and Lee Moradi. "System performance analysis of a hybrid ground source heat pump with optimal control strategies based on numerical simulations". In: *Geothermics* 86 (2020), p. 101849. ISSN: 0375-6505. DOI: https://doi.org/10.1016/j.geothermics.2020.101849 (cit. on pp. 6, 71).

[22] Min Li and Alvin C.K. Lai. "Thermodynamic optimization of ground heat exchangers with single U-tube by entropy generation minimization method". In: *Energy Conversion and Management* 65 (2013). Global Conference on Renewable energy and Energy Efficiency for Desert Regions 2011, GCREEDER 2011, pp. 133 –139. ISSN: 0196-8904. DOI: https://doi.org/10.1016/j.enconman.2012.07.013 (cit. on pp. 6, 71).

[23] Henk Witte. "A parametric sensitivity study into borehole performance design parameters". In: *Proceedings of the 12th International Conference on Energy Storage, Lleida, Spain.* 2012, pp. 16–18 (cit. on p. 6).

[24] Henrik Holmberg, José Acuña, Erling Næss and Otto K. Sønju. "Thermal evaluation of coaxial deep borehole heat exchangers". In: *Renewable Energy* 97 (2016), pp. 65 –76. ISSN: 0960-1481. DOI: https://doi.org/10.1016/j.renene.2016.05.048 (cit. on p. 6).

[25] H.J.L. Witte. "The GEOTHEX geothermal heat exchanger, characterisation of a novel high efficiency heat exchanger design. The 12th International conference on Energy Storage (INNOSTOCK, Lleida)." In: May 2012 (cit. on p. 6).

[26] Francesco Tinti, Roberto Bruno and Sara Focaccia. "Thermal response test for shallow geothermal applications: a probabilistic analysis approach". In: *Geothermal Energy* 3.1 (2015), p. 6. ISSN: 2195-9706. DOI: 10.1186/s40517-015-0025-5 (cit. on p. 6).

[27] Richard A. Beier. "Insights into parameter estimation for thermal response tests on borehole heat exchangers". In: *Science and Technology for the Built Environment* 25.8 (2019), pp. 947–962. DOI: 10.1080/23744731.2019.1634969. eprint: https://doi.org/10.1080/23744731.2019.1634969 (cit. on p. 6).

[28] Sara Focaccia. "Thermal response test numerical modeling using a dynamic simulator". In: *Geothermal Energy* 1 (Sept. 2013), pp. 3–14. DOI: 10.1186/2195-9706-1-3 (cit. on p. 6).

[29] H. Witte and Groenholland Geo-Energysystems. "Error Analysis of Thermal Response Tests (Extended Version)". In: 2012 (cit. on p. 6).

[30] A.J. Van Gelder, H.J.L. Witte, S. Kalma, A. Snijders and R.G.A. Wennekes. "In-situ Messungen der thermische Eigenschaften des Untergrunds durch Wärmeentzug." In: *Seminar "Erdgekoppelte Warmepumpen zum heizen und Klimatisieren von Gebauden.* 1999, 109 pp (cit. on p. 6).

[31] H.J.G. Diersch, D. Bauer, W. Heidemann, Wolfram Rühaak and Peter Schätzl. "Finite element formulation for borehole heat exchangers in modeling geothermal heating systems by FEFLOW". In: *WASY Software FEFLOW White Paper* 5 (Jan. 2010), pp. 5–96 (cit. on p. 11).

[32] R. Al-Khoury and P. Bonnier. "Efficient finite element formulation for geothermal heating systems. Part II: Transient". In: *International Journal for Numerical Methods in Engineering* 67 (July 2006), pp. 725 –745. DOI: 10.1002/nme.1662 (cit. on p. 11).

[33] Angelo Zarrella, Michele De Carli and Antonio Galgaro. "Thermal performance of two types of energy foundation pile: Helical pipe and triple U-tube". In: *Applied Thermal Engineering* 61.2 (2013), pp. 301 –310. ISSN: 1359-4311. DOI: https://doi.org/10.1016/j.applthermaleng.2013.08.011 (cit. on p. 11).

[34] Borja Badenes, Teresa Magraner, Cristina de Santiago, Fernando Pardo de Santayana and Javier F. Urchueguía. "Thermal Behaviour under Service Loads of a Thermo-Active Precast Pile". In: *Energies* 10.9 (2017). ISSN: 1996-1073 (cit. on p. 12).

[35] Borja Badenes, Á. Miguel Mateo Pla, G. Lenin Lemus-Zúñiga, Begoña Sáiz Mauleón and Javier F. Urchueguía. "On the Influence of Operational and Control Parameters in Thermal Response Testing of Borehole Heat Exchangers". In: *Energies* 10.9 (2017). ISSN: 1996-1073. DOI: 10.3390/en10091328 (cit. on pp. 12, 14, 23, 26, 79, 80).

[36] Marc Sauer, Burkhard Sanner, Erich Mands, Edgar Grundmann and Alfredo Fernández. "Thermal Response Test: Practical experience and extended range of application". In: *Proceedings of the Innostock 2012 (12th International Conference on Energy Storage)*. 2012 (cit. on p. 14).

[37] Burkhard Sanner, Göran Hellström, Jeffrey D Spitler and Signhild Gehlin. "More than 15 years of mobile Thermal Response Test – a summary of experiences and prospects". In: *Proceedings of the European Geothermal Congress 2013*. 2013 (cit. on pp. 14, 72).

[38] Tatyana V. Bandos, Álvaro Montero, Esther Fernández, Juan Luis G. Santander, José María Isidro, Jezabel Pérez, Pedro J. Fernández de Córdoba and Javier F. Urchueguía. "Finite line-source model for borehole heat exchangers: effect of vertical temperature variations". In: *Geothermics* 38.2 (2009), pp. 263 –270. ISSN: 0375-6505. DOI: 10.1016/j.geothermics.2009.01.003 (cit. on pp. 14, 73).

[39] Álvaro Montero, Javier F. Urchueguía, Julio Martos and Borja Badenes. "Ground temperature recovery time after BHE insertion". In: *Proceedings of the European Geothermal Congress 2013*. 2013, pp. 1–6 (cit. on p. 14).

[40] María de Groot, Cristina de Santiago, Fernando Pardo, José Luis Arcos, Francisco Martín, Javier F. Urchueguía and Borja Badenes. "Heating and cooling an energy pile under working load in Valencia". In: *Proceedings of the European Geothermal Congress 2013*. 2013 (cit. on p. 19).

[41] Borja Badenes, Marco Belliardi, Adriana Bernardi, Michele De Carli, Maria Di Tuccio, Giuseppe Emmi, Antonio Galgaro, Samantha Graci, Luc Pockele, Arianna Vivarelli, Sebastian Pera, Javier F. Urchueguía and Angelo Zarrella. "Definition of Standardized Energy Profiles for Heating and Cooling of Buildings". In: *CLIMA 2016 - proceedings of the 12th REHVA World Congress: volume 6. Aalborg: Aalborg University, Department of Civil Engineering*. 2016 (cit. on p. 19).

[42] Javier F. Urchueguía, Lenin-Guillermo Lemus-Zúñiga, Jose-Vicente Oliver-Villanueva, Borja Badenes, Miguel A. Mateo Pla and José Manuel Cuevas. "How Reliable Are Standard Thermal Response Tests? An Assessment Based on Long-Term Thermal Response Tests Under

Different Operational Conditions". In: *Energies* 11.12 (2018). ISSN: 1996-1073. DOI: 10.3390/en11123347 (cit. on pp. 22, 26, 82, 83).

[43] Guruprasad Alva, Yaxue Lin and Guiyin Fang. "An overview of thermal energy storage systems". In: *Energy* 144 (2018), pp. 341 –378. ISSN: 0360-5442. DOI: https://doi.org/10.1016/j.energy.2017.12.037 (cit. on p. 34).

[44] Huai Li, Wei Xu, Zhen Yu, Jianlin Wu and Zhifeng Sun. "Application analyze of a ground source heat pump system in a nearly zero energy building in China". In: *Energy* 125 (2017), pp. 140 –151. ISSN: 0360-5442. DOI: https://doi.org/10.1016/j.energy.2017.02.108 (cit. on p. 34).

[45] Onder Ozgener. "Use of solar assisted geothermal heat pump and small wind turbine systems for heating agricultural and residential buildings". In: *Energy* 35.1 (2010), pp. 262 –268. ISSN: 0360-5442. DOI: https://doi.org/10.1016/j.energy.2009.09.018 (cit. on p. 34).

[46] Jonas K. Jensen, Torben Ommen, Wiebke B. Markussen and Brian Elmegaard. "Design of serially connected district heating heat pumps utilising a geothermal heat source". In: *Energy* 137 (2017), pp. 865 –877. ISSN: 0360-5442. DOI: https://doi.org/10.1016/j.energy.2017.03.164 (cit. on p. 34).

[47] B Sanner. "Ground Source Heat Pumps – history, development, current status, and future prospects." In: *Proceedings of 12th IEA Heat Pump Conference (paper K.2.9.1, 14p). Rotterdam.* 2017 (cit. on p. 34).

[48] A. C. Crandall. "House Heating with Earth Heat Pump". In: *Electrical World, 126/19, 94-95.* (1946) (cit. on p. 34).

[49] E. N. Kemler. "Methods of Earth Heat Recovery for the Heat Pump". In: *Heating and Ventilating, 9/1947, 69-72.* (1947) (cit. on p. 35).

[50] Burkhard Sanner, Göran Hellström, Jeff Spitler and Signhild Gehlin. "Thermal Response Test – Current Status and World-Wide Application". In: *Proceedings of the World Geothermal Congress 2005.* 2005 (cit. on pp. 35, 72).

[51] Eric Moegle. "Erd- und gebäudeseitige Rahmenbedingungen eines 1974 in Schönaich (Kreis Böblingen) errichteten Erdwärmesondenfeldes mit fünf Koaxialsonden? ein Beitrag zur Geschichte der oberflächennahen Geothermie in Europa". In: *Jahresberichte und Mitteilungen des Oberrheinischen Geologischen Vereins* 91 (Apr. 2009), pp. 31–35 (cit. on p. 35).

[52] *WTA (1981). Wärmepumpen-Energiequellen in Theorie und Praxis, Worms: WTA company brochure* (cit. on p. 35).

[53] B. Sanner. "Schwalbach Ground Coupled Heat Pump Research Station". In: *Newsletter IEA Heat Pump Centre, 4/4, 8-10.* (1986) (cit. on p. 36).

[54] K. Hess. "Ground-Coupled Heat Pumps". In: *Proceedings WS on GSHP Albany (Report HPC-WR-2, 209-217). Karlsruhe.* 1987 (cit. on p. 36).

[55] Bo Nordell. "Borehole heat store design optimization". PhD thesis. Lulea University of Technology, Architecture and Water, 1994, p. 196 (cit. on pp. 36, 37).

[56] M. Lundh and J.-O. Dalenbäck. "Swedish solar heated residential area with seasonal storage in rock: Initial evaluation". In: *Renewable Energy* 33.4 (2008), pp. 703 –711. ISSN: 0960-1481 (cit. on p. 36).

[57] B. Sanner and K. Knoblich. "In-Situ Corrosion Test for Ground Heat Exchanger Materials in Schwalbach GCHP Research Station". In: *Newsletter IEA Heat Pump Centre, 9/3, 27-29* (1991) (cit. on p. 37).

[58] D. Mendrinos, S. Katsantonis and C. Karytsas. "Review of Alternative Pipe Materials for Exploiting Shallow Geothermal Energy". In: *Innovations in Corrosion and Materials Science 2017/7, 13-29.* (2017) (cit. on p. 37).

[59] "VDI 4640-2 (2015), Thermische Nutzung des Untergrunds, Erdgekoppelte Wärmepumpenanlagen. Düsseldorf/Berlin: VDI guideline draft (published 05-2015)." In: (2015) (cit. on pp. 38, 65).

[60] "Ground coupled heat pumps of high technology - GROUNDHIT". In: *Funded by FP6-SUSTDEV - Sustainable Development, Global Change and Ecosystems: thematic priority 6 under the Focusing and Integrating Community Research programme 2002-2006. Project ID: 503063* (2004-2008) (cit. on p. 39).

[61] B. Sanner, C. Karytsas, M. Abry, L. Coelho, J. Goldbrunner and D. Mendrinos. "GROUNDHIT – Advancement in ground source heat pumps through EU support". In: *Proceedings of EGC 2007 (paper 121, 6p). Unterhaching* (cit. on p. 39).

[62] *AWP T1 (1992). Wärmepumpenheizungsanlagen mit Erdwärmesonden. Zurich: AWP guideline.* (Cit. on p. 40).

[63] "VDI 4640-2 (1998), Thermische Nutzung des Untergrunds, Erdgekoppelte Wärmepumpenanlagen. Düsseldorf/Berlin: VDI guideline draft (published 02-1998)." In: (1998) (cit. on pp. 40, 43).

[64] "VDI 4640-2 (2001) , Thermische Nutzung des Untergrunds, Erdgekoppelte Wärmepumpenanlagen. Düsseldorf/Berlin: VDI guideline draft(published 09-2001)." In: (2001) (cit. on p. 40).

[65] Charles P. Remund and James T. Lund. "Thermal enhancement of bentonite grouts for vertical GSHP systems". In: *ASME, Vol. 29, 95-106.* 29 (Jan. 1993), pp. 95–106 (cit. on p. 40).

[66] M. L. Allan and A.J. Philippacopoulos. "Properties and performance of cement-based grouts for geothermal heat pump applications". In: *Office of Geothermal Technologies* (1999) (cit. on p. 40).

[67] *VDI 4640-4 (2016) – draft: Thermal use of the underground - Direct uses.* (Cit. on pp. 40, 65).

[68] Gyu-Hyun Go, Seung-Rae Lee, Seok Yoon, Hyunku Park and SKhan Park. "Estimation and experimental validation of borehole thermal resistance". In: *KSCE Journal of Civil Engineering* 18.4 (May 2014), pp. 992–1000. ISSN: 1976-3808 (cit. on p. 41).

[69] Shikun Zhang, Zhongwei Huang, Gensheng Li, Xiaoguang Wu, Chi Peng and Wenping Zhang. "Numerical analysis of transient conjugate heat transfer and thermal stress distribution in geothermal drilling with high-pressure liquid nitrogen jet". In: *Applied Thermal Engineering* 129 (2018), pp. 1348 –1357. ISSN: 1359-4311. DOI: https://doi.org/10.1016/j.applthermaleng.2017.10.042 (cit. on p. 41).

[70] Marco Fossa and Fabio Minchio. "The effect of borefield geometry and ground thermal load profile on hourly thermal response of geothermal heat pump systems". In: *Energy* 51 (2013), pp. 323 –329. ISSN: 0360-5442. DOI: https://doi.org/10.1016/j.energy.2012.12.043 (cit. on p. 41).

[71] Hellström G. and Sanner B. "Earth energy designer: software for dimensioning of deep boreholes for heat extraction. Version 2.0. https://buildingphysics.com/eed-2/". In: (2000) (cit. on p. 41).

[72] G. Hellström and B. Sanner. "PC-programs and modelling for borehole heat exchanger design". In: *Paper from International Geothermal Days Germany 2001, Bad Urach (organised by ISS, Skopje, Macedonia)* () (cit. on p. 42).

[73] D. Bohne, M. Wohlfahrt, G. Harhausen, B. Sanner, E. Mands, M. Sauer and E. Grundmann. "Results and lessons learned from geothermal monitoring of eight non-residential buildings with heat and cold production in Germany." In: *Proceedings of European Geothermal Congress 2013, Pisa (Italy)* () (cit. on p. 42).

[74] B. Sanner, F. Bockelmann, L. Kühl and E. s. Mands. "System optimisation of ground-coupled heat- and cold supply for office building". In: *Proceedings of European Geothermal Congress 2016, Strasbourg (France)* () (cit. on p. 42).

[75] P Mogensen. "Fluid to Duct Wall Heat Transfer in Duct System Heat Storages". In: *Stockholm: The International Conference on Subsurface Heat Storage in Theory and Practice*. 1983 (cit. on pp. 50, 70).

[76] *SPIN-PET, Via R. Piaggio, 32, 56025, Pontedera ,Italy.* http://www.spinpet.it//. [Online; accessed 12-December-2019] (cit. on p. 62).

[77] *SILMA, Via Lombardia 97/00/101, Poggio a Caiano, Italy.* `http://www.spinpet.it//`. [Online; accessed 12-December-2019] (cit. on p. 62).

[78] *AIMPLAS, Plastics Technology Centre.* `https://www.aimplas.net/aimplas/`. [Online; accessed 12-December-2019] (cit. on p. 63).

[79] *CAUDAL - Extruline Systems, Puerto Lumbreras (Murcia), Spain.* `https://www.caudal.es/index.php/en/`. [Online; accessed 12-December-2019] (cit. on p. 64).

[80] *ASTM C 666: Standard Test Method for Resistance of Concrete to Rapid Freezing and Thawing.* (Cit. on p. 65).

[81] *ASTM C 531-85: Standard Test Method for Linear Shrinkage and Coefficient of Thermal Expansion of Chemical-Resistant Mortars, Grouts, Monolithic Surfacings, and Polymer Concretes* (cit. on p. 65).

[82] *EN 197-1: Cement - Part 1: Composition, specifications and conformity criteria for common cements.* (Cit. on p. 65).

[83] *EN 445: Grout for prestressing tendons - Test methods.* (Cit. on p. 65).

[84] *GSHVBS Vertical Borehole Standard, published by the Ground Source Heat Pump Association (GSHPA), UK 2017* (cit. on p. 65).

[85] *SS 137540 (2008): Concrete testing – Cement mortar – Bleeding and volume change.* (Cit. on p. 65).

[86] *SS 137244: Concrete testing – Hardened concrete – Scaling at freezing* (cit. on p. 65).

[87] *UNE 100715-1 (2014): Guide for the design, implementation and monitoring of a geothermal system. Part 1: Vertical closed circuit systems.* (Cit. on p. 65).

[88] *RISE Research Institutes of Sweden, Division Samhällsbyggnad – Infrastructure and Concrete Construction, Stockholm, Sweden.* `https://www.ri.se/sv`. [Online; accessed 12-December-2019] (cit. on p. 65).

[89] *ASHRAE. (2007). AHSRAE Handbook HVAC Application, Chap 32, Geothermal Energy. American Society of Heating, Refrigerating and Air Conditioning Engineers, Atlanta.* (Cit. on p. 71).

[90] Christopher Vella, Simon Paul Borg and Daniel Micallef. "The Effect of Shank-Space on the Thermal Performance of Shallow Vertical U-Tube Ground Heat Exchangers". In: *Energies* 13.3 (2020). ISSN: 1996-1073. DOI: 10.3390/en13030602 (cit. on p. 71).

[91] Michele De Carli, Antonio Galgaro, Michele Pasqualetto and Angelo Zarrella. "Energetic and economic aspects of a heating and cooling district in a mild climate based on closed loop ground source heat pump". In: *Applied Thermal Engineering* 71 (Feb. 2014). DOI: 10.1016/j.applthermaleng.2014.01.064 (cit. on p. 71).

[92] Qi Lu, Guillermo Narsilio, Gregorius Aditya and Ian Johnston. "Economic analysis of vertical ground source heat pump systems in Melbourne". In: *Energy* 125 (Feb. 2017). DOI: 10.1016/j.energy.2017.02.082 (cit. on p. 71).

[93] Hiep Nguyen, Ying Law, Masih Alavy, Philip Walsh, Wey Leong and S. Dworkin. "An analysis of the factors affecting hybrid ground-source heat pump installation potential in North America". In: *Applied Energy* 125 (July 2014), 28–38. DOI: 10.1016/j.apenergy.2014.03.044 (cit. on p. 71).

[94] Denis Garber, R. Choudhary and Kenichi Soga. "Risk based lifetime costs assessment of a ground source heat pump (GSHP) system design: Methodology and case study". In: *Building and Environment* 60 (Feb. 2013), 66–80. DOI: 10.1016/j.buildenv.2012.11.011 (cit. on p. 72).

[95] Seok Yoon, S.-R Lee, Jianfeng Xue, Kai Zosseder, Gyu Go and Hyunku Park. "Evaluation of the thermal efficiency and a cost analysis of different types of ground heat exchangers in energy piles". In: *Energy Conversion and Management* 105 (Aug. 2015), pp. 393–402. DOI: 10.1016/j.enconman.2015.08.002 (cit. on p. 72).

[96] Giuseppe Emmi, Angelo Zarrella, Michele De Carli, Mirco Dona and Antonio Galgaro. "Energy performance and cost analysis of some borehole heat exchanger configurations with different heat-carrier fluids

in mild climates". In: *Geothermics* 65 (Jan. 2017), pp. 158–169. DOI: 10.1016/j.geothermics.2016.09.006 (cit. on p. 72).

[97] S.E Gehlin. "Thermal response test - Method development and evaluation". PhD thesis. Department of Environmental Engineering, (Luleå University of Technology.) Sweden., 2002 (cit. on p. 72).

[98] Jeffrey Spitler and Signhild Gehlin. "Thermal response testing for ground source heat pump systems—An historical review". In: *Renewable and Sustainable Energy Reviews* 50 (Oct. 2015), pp. 1125–1137. DOI: 10.1016/j.rser.2015.05.061 (cit. on p. 72).

[99] Borja Badenes, Miguel A. Mateo, Jose M. Cuevas, Lenin G. Lemus, Jose V. Oliver and Javier F. Urchueguia. "Optimization methodology of borehole heat exchangers (BHEs) according geometric characteristics, material properties and installation and operation costs". In: *Proceedings of Alternative Energy Sources, Materials & Technologies (AESMT'19) Congress*. 2019 (cit. on p. 72).

[100] Nairen Diao, Ping Cui and Zhaohong Fang. "The thermal resistance in a borehole of geothermal heat exchangers". In: Jan. 2002, p. 5. DOI: 10.1615/IHTC12.3050 (cit. on p. 74).

[101] H. Ali and A Tarrad. "Borehole Thermal Resistance Correlation for a Single Vertical DX U-Tube in Geothermal Energy Application". In: *American Journal of Environmental Science and Engineering. Vol. 3, No. 4, 2019, pp. 75-83.* (2019). DOI: 10.11648/j.ajese.20190304.12 (cit. on p. 74).

[102] M. Ould-Rouiss, L. Redjem-Saad and G. Lauriat. "Direct numerical simulation of turbulent heat transfer in annuli: Effect of heat flux ratio". In: *Int. Journal of Heat and Fluid Flow 30. pp. 579–589* (2009) (cit. on pp. 75, 97).

[103] R. E. Lundberg, P. A. McCuen and W. C. Reynolds. "Heat Transfer in Annular Passages. Hydrodynamically Developed Laminar Flow with Arbitrarily Prescribed Wall Temperatures or Heat Fluxes". In: *Int. J. Heat Mas: Transfer. Vol. 6, pp. 495 - 529. Pergam. Press* (1963) (cit. on pp. 75, 97).

[104] *VDI - Heat Atlas, Second Edition. VDI – Gesellschaft Verfahrenstechnick und Chemieingenieurwesen.* Tech. rep. 2010 (cit. on pp. 75–77, 98).

[105] Asociación de productores de energías renovables (APPA). "Análisis sectorial - Sector geotérmico de Baja Entalpía". In: (2010) (cit. on p. 78).

[106] Miguel A. Mateo Pla, Borja Badenes, Lenin Lemus and Javier F. Urchueguía. "Assessing the Shallow Geothermal Laboratory at Universitat Politècnica de València". In: *Proceedings of the European Geothermal Congress 2019.* 2019 (cit. on p. 81).

[107] IGME, ed. *Geological Map of Spain. Scale 1:50.000, MAGNA. Page nº722 (Valencia).* 1972 (cit. on p. 82).

[108] Wolfram Research, Inc. *Mathematica, Version 12.1.* Champaign, IL, 2020 (cit. on p. 85).

[109] *Código Técnico de la Edificación de España.* `https://www.codigotecnico.org/`. [Online; accessed 10-September-2020] (cit. on p. 90).

[110] *EED – Earth Energy Designer, v4.* `https://buildingphysics.com/eed-2/` (cit. on p. 91).

[111] *GMSW 28 HK.* `https://www.ochsner.com/en/ochsner-products/product-detail/gmsw-28-hk/`. [Online; accessed 25-August-2020] (cit. on p. 92).